P R O C E E D I N G S MPA/P12

June 2000

P R O C E E D I N G S

of the 10th Workshop on

"Nuclear Astrophysics"

Ringberg Castle, Tegernsee, Germany

March 20 – 25, 2000

Wolfgang Hillebrandt and Ewald Müller (eds.)
Max-Planck-Institut für Astrophysik
Karl-Schwarzschild-Strasse 1
85740 Garching b. München

Preface

From March 20 through 25, 2000, again one of the traditional Workshops on Nuclear Astrophysics was held at the Ringberg Castle near Munich. This workshop was the tenth in a series which began in May 1981. As on all previous occasions, nuclear physicists, astrophysicists, and astronomers met for one week at the spectacular Ringberg Castle to discuss problems and projects of common interest.

This year's workshop was attended by 38 scientists from 7 countries many of whom had participated in previous workshops. Among these, two colleagues (Hermann Beer and Franz Käppeler; and the organizers) had already participated in the first Nuclear Astrophysics workshop in 1981. This workshop was the third meeting at all to take place at the Ringberg Castle, and and at that time was organized by Dave Arnett and Richard Ward together with the two of us.

Continuing a good tradition of the series, again several students had an opportunity to present, for the fist time, their work to an international audience in a benevolently and friendly atmosphere. The workshop programme consisted of 37 talks often stimulating intensive discussions. As during all previous meetings the relaxed atmosphere of the Castle, ample time for discussions between the sessions, and the almost perfect weather including lots of fresh snow provided optimum conditions for a successful workshop.

The topics discussed in the talks covered most aspects of nuclear astrophysics including abundance determinations, reaction rate measurements, modeling specific nucleosynthetic processes and stellar evolutionary phases, simulating stellar explosions, and discussing cosmic chemical evolution. Some reaction rate measurements, the site of the neutron capture processes, and some astrophysical models discussed during the present meeting were already a hot topic at the first workshop of the series, and some of these even ever since. In these Proceedings extended abstracts of most of the contributions are collected which were presented at the Tenth Nuclear Astrophysics workshop.

The success of the workshop, of course, also depended on financial support by the Max-Planck-Gesellschaft and, needless to say, on the enormous efficiency and friendliness of Mr. Hörmann and his crew.

Garching, June 2000 Wolfgang Hillebrandt Ewald Müller

	List of Participants
Marialuisa Aliotta	Inst. f. Physik mit Ionenstrahlung, Uni Bonn, D
Bodo Baschek	Inst. f. Theoret. Astrophysik, Uni Heidelberg, D
Hermann Beer	Inst. f. Kernphysik, Karlsruhe, D
Guennadi Bisnovatyi-Kogan	Space Research Inst., Moscow, RUS
Marcus Brueggen	MPI für Astrophysik, Garching, D
Ramon Canal	Univ. Barcelona, E
Alessandro Chieffi	Instituto di Astrofisica Spaziale, I
John Cowan	Univ. of Oklahoma, Norman, USA
Pavel Denissenkov	Univ. of St. Petersburg, RUS
Roland Diehl	MPI für Extraterrestrische Physik, Garching, D
Christian Freiburghaus	Univ. Basel, CH
Bruce Fryxell	Univ. of Chicago, USA
Dieter Hartmann	Clemson Univ.
Alexander Heger	UCO/LICK, Observ. Santa Cruz, USA
Wolfgang Hillebrandt	MPI für Astrophysik, Garching, D
Jordi Isern	Inst. d'Estudis Espacials de Catalunya, E
Anatoli Iyudin	MPI für Extraterrestrische Physik, Garching, D
Thomas Janka	MPI für Astrophysik, Garching, D
Franz Kaeppler	Forschungszentrum Karlsruhe, D
Andreas Kercek	MPI für Astrophysik, Garching, D
Konstantinos Kifonidis	MPI für Astrophysik, Garching, D
Karlheinz Langanke	Univ. of Aarhus, DK
Gabriel Martinez Pinedo	Inst of Phys. and Astron.,
Ewald Müller	MPI für Astrophysik, Garching, D
Dimitrij Nadyozhin	ITEP Moscow, RUS
Roland Oechslin	Univ. Basel, CH
Igor Panov	ITEP Moscow, RUS
Luciano Piersanti	Osservatorio Astronomico di Teramo, I
Rene Reifarth	Forschungszentrum Karlsruhe, D
Martin Reinecke	MPI fr Astrophysik, Garching, D
Detlef Rogalla	Inst. f. Physik mit Ionenstrahlung, Bochum, D
Elena Sorokina	Sternberg Astron. Inst., Moscow, RUS
Oscar Straniero	Osservatorio Astronomico di Teramo, I
Jim Truran	Univ. of Chicago, USA
Rainer Wehrse	Inst. f. Theoret. Astrophysik, Univ. Heidelberg, D,
Achim Weiss	MPI fr Astrophysik, Garching, D

Contents

Diffusion of radiation in moving media

B. Baschek[1,2], *R. Wehrse*[1,2], *W. v. Waldenfels*[3,2]

[1] *Institut für Theoretische Astrophysik, Tiergartenstrasse 15, D-69121 Heidelberg*
[2] *Interdisziplinäres Zentrum für Wissenschaftliches Rechnen, Im Neuenheimer Feld 368, D-69120 Heidelberg*
[3] *Institut für Angewandte Mathematik, Im Neuenheimer Feld 294, D-69120 Heidelberg*

While the solution for the radiative flux in the diffusion limit for the static case is long known by the work of Rosseland (1924), the problem in differentially *moving* media is much more involved. After the first attempt by Karp et al. [1] to solve this problem by the concept of the expansion opacity, there have been numerous contributions ([2] and references cited therein), mainly with specific application to the calculation of supernova explosions and light curves.

Our aim is to give a rigorous derivation of the flux, the Rosseland mean, and the radiative acceleration in moving 3D media. Here we present selected results, without giving details, for the diffusion limit of radiation, i.e. for the optically thick case where the radiative transfer is particularly simple. We restrict ourselves to the expressions for the flux or, equivalently, for the generalized Rosseland mean opacity; for details see [3].

We start from the 3D comoving-frame radiative transfer equation for the intensity $I = I(s,\xi)$ in the direction $\mathbf{s}$ for small velocities $\beta = v/c$

$$\frac{dI}{d\mathbf{s}} + w\frac{\partial I}{\partial \xi} = -\chi(I-S) \quad \text{with} \quad w \simeq \mathbf{n}\cdot\nabla(\boldsymbol{\beta}\cdot\mathbf{n}) = \frac{d(\mathbf{n}\cdot\boldsymbol{\beta})}{ds}\,, \quad \mathbf{n} = \frac{\mathbf{s}}{|\mathbf{s}|}\,, \tag{1}$$

and $d/d\mathbf{s} = \mathbf{n}\cdot\nabla$. In the diffusion limit the source function is equal to the Planck function $S = B(T,\xi)$ of the local temperature T. The monochromatic extinction coefficient is written as the sum of the contributions of a continuum $\chi_{\rm c}(\xi)$ plus L spectral lines $\chi_l(\xi)$,

$$\chi(\xi) = \chi_{\rm c}(\xi) + \sum_{l=1}^{L}\chi_l(\xi)\,. \tag{2}$$

For the diffusion limit it is also characteristic that the velocity change over the mean free path of photons in the continuum is small: $|d\beta/ds|\cdot 1/\chi_{\rm c} \ll 1$ or $|w| \ll \chi_{\rm c}$. It is furthermore of advantage to use a logarithmic wavelength scale $\xi = \ln\lambda$ in which the Doppler shift is $d\xi = d\lambda/\lambda = dv/c = d\beta = w\,ds$.

¿From Eq. (1) we derive the monochromatic flux, here in the two-stream approximation $F(\xi) = I^+ - I^-$, and other radiative quantities in the diffusion limit such as the total flux and the radiative acceleration (not considered here). The motions of the medium enter the transfer equation only via the "velocity gradient" w, and hence their effects upon the radiative quantities can be expressed in terms of w.

In order to apply the analytical solution [4] of the transfer equation we take $w = \text{const}$, i.e. consider sufficiently small layers in the actual calculations. Then the monochromatic flux in the diffusion approximation is given by

$$F(\xi;w) = F_0(\xi)\cdot[1+\theta(\xi;w)] = 2g(\xi)\int_0^\infty \exp\left(-\frac{1}{w}\int_{\xi-ws}^{\xi}\chi(\zeta)d\zeta\right)ds \tag{3}$$

with $g(\xi) = (\partial B(T,\xi)/\partial T)(\partial T/\partial s)$. Here $F_0(\xi) \equiv F(\xi;0)$ is the static flux, and the effect of the motions is contained in $\theta(\xi;w)$. We note that according to [4] the essential expression occurring in the terms of the solution for I is always $\exp(-\int_{\xi-ws}^{\xi}\chi(\zeta)d\zeta/w)$ as in (3).

Since $\lim_{w\to 0}\int_{\xi-ws}^{\xi}\chi(\zeta)d\zeta/(ws) = \chi(\xi)$, we convince ourselves that from Eq. (3) in the limit $w \to 0$ the well-known static monochromatic flux

$$F_0(\xi) = 2g(\xi)\int_0^\infty \mathrm{e}^{-\chi(\xi)\cdot s}ds = 2\,\frac{g(\xi)}{\chi(\xi)}\,. \tag{4}$$

results. By integration of (3) over all wavelengths the total flux and, equivalently, the generalized Rosseland mean,

$$F(w) = \int_{-\infty}^{\infty} F(\xi;w)\,\mathrm{e}^{\xi}d\xi = F_0\cdot\Big[1+\Theta(w)\Big]\,, \qquad \frac{1}{\bar\chi_\beta(w)} = \frac{1}{\bar\chi_{\mathrm{R}}}\cdot\Big[1+\Theta(w)\Big]\,, \tag{5}$$

is derived. Here $\bar\chi_{\mathrm{R}}$ is the conventional Rosseland mean, defined by

$$\frac{1}{\bar\chi_{\mathrm{R}}} = \int_{-\infty}^{\infty}\frac{G(\xi)}{\chi(\xi)}\,d\xi \quad \text{with} \quad G(\xi) = \left(\frac{\partial B(T,\xi)}{\partial T}\Big/\frac{\partial B(T)}{\partial T}\right)\mathrm{e}^{\xi} \tag{6}$$

where $B(T)$ is the wavelength-integrated Planck function. In the static limit $w \to 0$ this expression reduces to Rosseland's result for the diffusion limit in the two-stream approximation

$$F_0 = 2\,\frac{\partial B(T)}{\partial T}\,\frac{\partial T}{\partial s}\cdot\frac{1}{\bar\chi_{\mathrm{R}}}\,. \tag{7}$$

In this contribution the "velocity correction" $\Theta(w)$ is given only for the limit of small $|w|$, i.e. if the Doppler shift is small compared to the intrinsic line width. For a Lorentz profile with damping constant γ this condition reads $|w| \ll \gamma\chi_{\mathrm{c}}$. Then

$$F(\xi;w) = F_0(\xi)\cdot\left[1 - \frac{\partial}{\partial\xi}\frac{1}{\chi(\xi)}\cdot w + \frac{1}{2}\frac{\partial^2}{\partial\xi^2}\frac{1}{\chi(\xi)^2}\cdot w^2\right]\,, \tag{8}$$

and

$$F(w) = F_0\cdot\Big[1+\eta_1\cdot w+\eta_2\cdot w^2\Big] \quad \text{or} \quad \frac{1}{\bar\chi_\beta(w)} = \frac{1}{\bar\chi_{\mathrm{R}}}\cdot\Big[1+\eta_1\cdot w+\eta_2\cdot w^2\Big] \tag{9}$$

with the coefficients

$$\eta_1 = -\frac{\bar\chi_{\mathrm{R}}}{2}\int_{-\infty}^{\infty}\frac{\partial}{\partial\xi}\left(\frac{1}{\chi(\xi)}\right)^2 G(\xi)\,d\xi\,, \quad \eta_2 = +\frac{\bar\chi_{\mathrm{R}}}{2}\int_{-\infty}^{\infty}\frac{1}{\chi(\xi)}\frac{\partial^2}{\partial\xi^2}\left(\frac{1}{\chi(\xi)}\right)^2 G(\xi)\,d\xi\,. \tag{10}$$

For example, the calculation of a single – symmetric – Lorentzian line on a continuum, whose monochromatic contributions to the flux are shown in Fig. 1., leads to $\eta_1 = 0$ and $\eta_2 < 0$, i.e. its effect is only of second order in w, and independently of the flow direction the flux is decreased (or $\bar\chi_\beta$ increased).

In the case of very *many* overlapping lines of different strength the symmetry with respect to ξ is destroyed. Then either F has to be calculated numerically or a *statistical* distribution of the lines may be assumed so that the expectation value $\langle F\rangle$ of the flux can be given.

It has been shown [5] that the *Poisson point process* is very flexible and well suited for the presentation of lists of "real" lines, in addition it allows to some extent further analytical

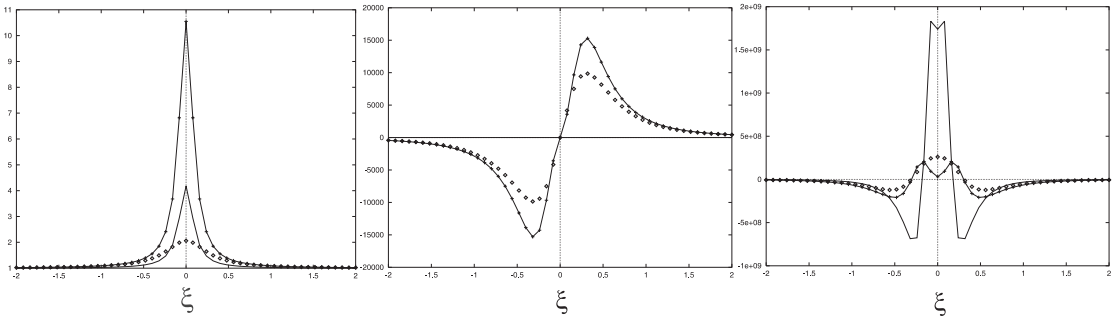

Figure 1: Extinction coefficient $\chi(\xi)$ and the derivatives of the corresponding free mean path, $\partial(1/\chi(\xi)^2)/\partial\xi$ and $\partial^2(1/\chi(\xi)^2)/\partial\xi^2/\chi(\xi)$ entering Eq. (9), as functions of ξ for a single Lorentz line $\chi_l = A/(2\pi)\cdot\gamma/((\xi-\hat{\xi})^2+(\gamma/2)^2)$ on a continuum χ_c for different strengths A and damping constants γ.

evaluation. In the Poisson point process the number L of lines is Poisson distributed, whereas the line positions $\hat{\xi}$ have an equal-probability distribution, and the line density $\varrho(\xi,\vartheta)$ – which takes the role of L – is largely arbitrary. Here ϑ is a mutidimensional variable comprising the line properties such as the strength A and the damping constant γ, and $\hat{\xi}$ and ϑ are regarded as continuous variables. We may e.g. write $\varrho(\xi,\theta)=\varrho(\xi)f(\vartheta)$; frequently the strengths are assumed to follow a power law $f\propto A^{-\alpha}$.

Instead of (3) we now have to consider the *expectation value* of the monochromatic flux

$$\Big\langle F(\xi;w)\Big\rangle = 2g(\xi)\int_0^\infty \mathrm{e}^{-\chi_c(\xi)\cdot s}\cdot \underbrace{\left\langle \exp\left(-\frac{1}{w}\sum_{l=1}^{L}\int_{\xi-ws}^{\xi}\chi(\hat{\xi}_l,\vartheta_l,\zeta-\hat{\xi}_l)d\zeta\right)\right\rangle}_{=\Omega(\xi,\xi-w;w)} ds\,. \tag{11}$$

Evaluation of the line contribution Ω to the expectation value yields [5]

$$\Omega(\xi,\xi-ws;w)=\exp\left(\int_\Theta\int_{-\infty}^{\infty}\varrho(\hat{\xi},\vartheta)\left\{\exp\left(-\frac{1}{w}\int_{\xi-ws}^{\xi}\chi(\hat{\xi},\vartheta,\zeta-\hat{\xi})d\zeta\right)-1\right\}d\hat{\xi}d\vartheta\right). \tag{12}$$

Note that in this expression the additional integration over $\hat{\xi}$ originates from the summation over the line contributions χ_l. In the limit of small $|w|$ we write

$$\Omega(\xi,\xi-ws;w)=\Omega(\xi,\xi;0)\cdot[1+\omega_1\cdot w+\tfrac{1}{2}\,\omega_2\cdot w^2] \tag{13}$$

with $\Omega(\xi,\xi;0)$ being the static expectation value. (Note that the static Ω is the Laplace transform of the opacity distribution function.)

Discussion of the coefficients ω_1 and ω_2 (given in detail by [3]) utilizing the symmetry of $\chi(\hat{\xi},\vartheta,\xi-\hat{\xi})$ with respect to ξ and $\hat{\xi}$, leads to the important result for the monochromatic flux and hence also for the total flux:

Let $\varrho(\xi)=\varrho_0+\varrho_1\xi+\varrho_2\xi^2+\ldots$ over a small piece of the spectrum, then (i) if $\varrho=\varrho_0=\mathrm{const}$ (or only even powers of ξ occur) $\omega_1=0$ and only the w^2-term is important for the flux. (ii) if there are only odd powers of ξ then the w-term is important and $\omega_2=0$.

Future work will among others comprise the evaluation of other radiative quantities such as the acceleration and the energy balance $\int_0^\infty\chi\cdot(J-B)d\lambda$, the determination of a set of

stochastic parameters for the Poisson point process by adaptation of "real" line lists, the generalization of opacity distribution functions to moving media, and, of course the astronomical application of our formalism, e.g. to supernovae, novae and accretion disks.

Acknowledgements

We are indebted to G.V. Efimov, Ph. Rosenau, G. Kanschat and G. Shaviv for many helpful discussions. This work has been supported in part by the DFG (Sonderforschungsbereich 359/C2).

References

[1] A.H. Karp, G. Lasher, K.L. Chang, and E.E. Salpeter, Ap.J. **214** (1977) 161

[2] P.A. Pinto and R.G. Eastman, Ap.J. **530** (2000) 744, 757

[3] R. Wehrse, B. Baschek, and W. v. Waldenfels, A&A (2000) in press

[4] B. Baschek, G.V. Efimov, W. v. Waldenfels, and R. Wehrse, A&A **317** (1997) 630

[5] R. Wehrse, W. v. Waldenfels, and B. Baschek, JQSRT **60** (1998) 963

Mixing through shear instabilities

M. Brüggen[1,2], *W. Hillebrandt*[1]

[1] *Max-Planck-Institut für Astrophysik, Karl-Schwarzschild-Str.1, 85740 Garching, Germany*
[2] *Churchill College, Storey's Way, Cambridge, CB3 0DS, UK*

Mixing is a fundamental process which profoundly affects the evolution of stars. One of the prominent mechanisms responsible for mixing in stars is the shear or Kelvin-Helmholtz instability. Since most stars are at least partly differentially rotating, shear mixing plays an important role in stellar evolution. We present results of numerical simulations of the Kelvin-Helmholtz instability in a stratified shear layer. The shear instability is believed to be responsible for extra mixing in differentially rotating stellar interiors and is the prime candidate to explain the abundance anomalies observed in many rotating stars [1]. All mixing prescriptions currently in use are based on phenomenological and heuristic estimates whose validity is often vague [2], [3]. Using three-dimensional numerical simulations, we study the mixing efficiency as a function of the Richardson number.

The Kelvin-Helmholtz instability occurs in chemically homogeneous, stratified shear flows when the destabilising effect of the relative motion in the different layers dominates over the stabilising effect of buoyancy. The competition between the two effects is described by the Richardson number, Ri. For non-dissipative, parallel, steady flow a simple linear stability criterion can be derived:

$$\mathrm{Ri} := \frac{N^2}{(dU/dz)^2} > \frac{1}{4}, \tag{1}$$

where N is the Brunt-Väisälä frequency, U the shear velocity and z the coordinate in the direction of gravity.

Our simulations were obtained using the ZEUS-3D code which was developed especially for problems in astrophysical hydrodynamics [4]. In our simulations we employed an ideal gas equation of state, we ignored the effects of magnetic fields, rotation, nuclear reactions and variations in radiative processes. The simulations were computed on a Cartesian grid and the computational domain was chosen to have the dimension $2 \cdot 10^8$ cm $\times$ $2 \cdot 10^8$ cm $\times$ 10^8 cm (in the x-, y- and z-direction, where gravity acts in the z-direction). It was covered by 100 $\times$ 100 $\times$ 50 grid points. A shear velocity profile was imposed on the fluid. It was chosen to have the form of a hyperbolic tangent in order to minimise the effect of the boundaries onto the shear layer. The parameters of this shear velocity profile were varied to yield a range of Richardson numbers in the shear layer.

In order to study mixing processes the ZEUS code was modified to follow the motion of 'tracer' particles which are advected with the fluid. The diffusion constant can then be defined as

$$D = \sigma^2/t, \tag{2}$$

where $\sigma^2 = \frac{1}{N}\sum_N (z - z_0)^2$, z_0 being the original height of the tracer particle and z its height after a time t. The diffusion constant for as a function of time have been plotted in Fig. 1. In Fig. 1 the Richardson number is 0.4, which is greater than 0.25 and, therefore, the flow should be stable to the shear instability according to the simple Richardson criterion. The simulations reveal that it is not, as has in fact been shown in previous simulations. One can observe that initially D rises with time before it eventually approaches a value which remains nearly constant for some time. The remaining scatter is mainly due to the stochastic nature of the turbulent mixing. Eventually, dissipation becomes noticeable and D starts to slowly decrease again. The constant value of D to which the curves are converging, is the value that is of greatest interest for the purpose of constructing stellar models. This value for D depends on the Richardson number. An understanding of the quantitative dependence of D on parameters such as the Richardson number will be useful for stellar models which treat mixing through a diffusion equation.

One objection to these kinds of direct numerical simulations is that Reynolds numbers as high as those encountered in stars are unattainable on current computers, and that therefore the results are unrealistic. But, as pointed out by Balbus, Hawley & Stone (1996), this criticism is unjustified for simulations of the shear instability. They argue, that in order to simulate the onset of instability in a laminar flow, it is merely necessary that the 'typical' wavelength of the instability is resolved by the numerical scheme and that the numerical diffusion at this wavelength is less than the growth rate. This makes the simulation of shear instabilities an easier task than the simulation of viscous instabilities where in theory one would have to resolve everything down to the viscous length scale.

The diffusion coefficient derived from the 2D simulations as a function of time is displayed as a dashed line in Fig. 1. The figures show that in 2D simulations D rises more slowly with time than in three dimensions. But it is interesting to note that eventually D converges to about the same value as obtained in the three-dimensional simulations. This is an encouraging result. Not only does this raise the trust in the credibility and self-consistency of these results, it also suggests that 2D simulations may be sufficient to determine the efficiency of shear mixing.

The results for the diffusion coefficient as a function of Richardson number as well as a discussion of these results in the light of existing mixing formalism are presented in [5]. Finally we should mention that a number of factors can inhibit or facilitate mixing such as gradients in the chemical potential of the fluid, diffusion of radiation, magnetic fields and effects pertaining to the spherical geometry. This will be studied in the near future.

1.1 Figures

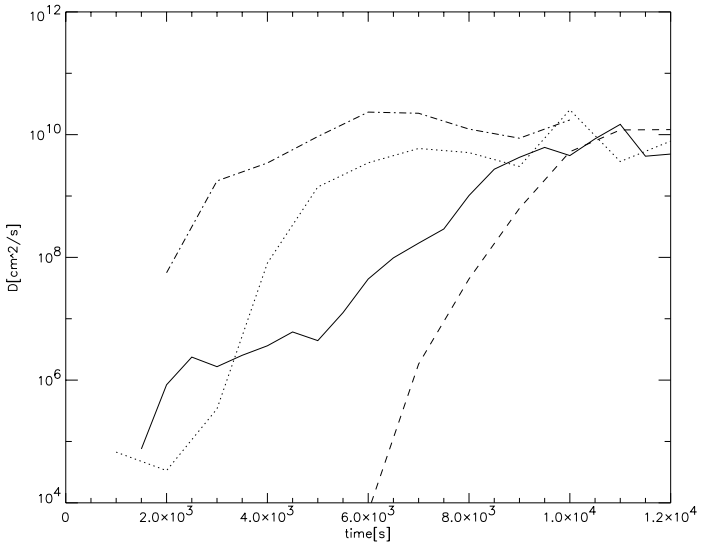

Figure 1: Diffusion coefficient as a function of time for Ri=0.4. The solid line shows the result of the 3D simulation and the dashed line the result of the 2D simulation with the same resolution. The dotted and dashed-dotted line represent results of 2D simulations of increased resolution.

Acknowledgements

A part of the simulations were performed on computers of the Rechenzentrum Garching.

References

[1] Denissenkov, P.A., Tout, C.A., 2000, MNRAS in press

[2] Maeder, A., Zahn, J.-P., 1998, A&A, 334, 1000

[3] Canuto, V.M., 1998, ApJ, 508, 767

[4] Stone, J.M., Norman, M.L., 1992a, ApJS, 80, 753

[5] Brüggen, M., Hillebrandt, H., 2000, submitted to MNRAS

Optical and UV Light Curves of Thermonuclear Supernovae

E. Sorokina[1], *S. Blinnikov*[2]

[1] *Sternberg Astronomical Institute, Moscow, Russia*
[2] *Institute for Theoretical and Experimental Physics, Moscow, Russia*

Theoretical and observational investigation of multi-color light curves of Type Ia supernovae (SNe Ia) still remains a very important subject for understanding physics of the explosion: so far we have no definite knowledge about neither the progenitors of SNe Ia, nor the burning regime during the explosion. The comparison of observations with light curves calculated for different models can put restrictions on the set of models and lead us to understanding which explosion scenario is preferred in nature. Another reason is the recent exciting result derived from observations of SNe Ia at cosmological distances that implies acceleration of expansion of the Universe. One should remember that this result was obtained by application of statistical dependences between observable parameters of nearby SNe Ia to very distant events. Even if the physics of nearby stellar explosions were clear one could not be sure that distant supernovae should be exactly the same. And if explosions in younger Universe were different we have to understand how this could change observational manifestations.

Here we present the results of our light curve calculations for 4 models from near infrared to far-ultraviolet ranges. We use for computations our hydrocode STELLA [1, 2], which solves simultaneously hydrodynamic equations and time-dependent equations for multi-group radiation energy and flux. Our models have 100–200 Lagrangean zones and up to 100 frequency bins. In the equation of state, LTE ionization and recombination are taken into account. Level population is supposed to be also in LTE.

Computations of SN Ia light curves have been performed for an extensive set of models by Höflich et al. (e.g. [4]). We present an independent calculation of similar models, and we believe that our code employs more correct physics, at least in the part which uses expansion opacity. The differences are discussed in our paper [5]. The correct approach to the treatment of expansion opacity is given in [6].

Table 1: Parameters of SN Ia models

Model	$M_{\rm WD}$	$M_{^{56}\rm Ni}$	E_{51}	$t^B_{\rm rise}$	$M^B_{\rm max}$	$t^V_{\rm rise}$	$M^V_{\rm max}$	$t^{\rm bol}_{\rm rise}$	$M^{\rm bol}_{\rm max}$	$\log L^{\rm bol}_{\rm max}$
DD4	1.3861	0.63	1.23	17.1	–18.91	22.1	–19.03	9.4	–19.36	43.23
W7	1.3775	0.60	1.20	16.0	–18.71	20.5	–18.82	8.6	–19.38	43.24
LA4	0.8678	0.47	1.15	12.8	–18.74	18.7	–18.92	8.4	–18.90	43.05
WD065	0.6500	0.05	0.56	10.3	–16.55	13.5	–17.09	12.4	–16.75	42.19

We have considered the delayed detonation model DD4 [7], the deflagration model W7 [8], the helium detonation model LA4 [9], and the low-mass model WD065 [10] with central detonation. The main parameters of the models are shown in the Table 1 as well as their maximum magnitudes and rise times to the maximum. The latter values for Chandrasekhar-mass models DD4 and W7 are in better agreement with observational data than those by Höflich et al. This allows us to believe that our code reproduces the physics correctly.

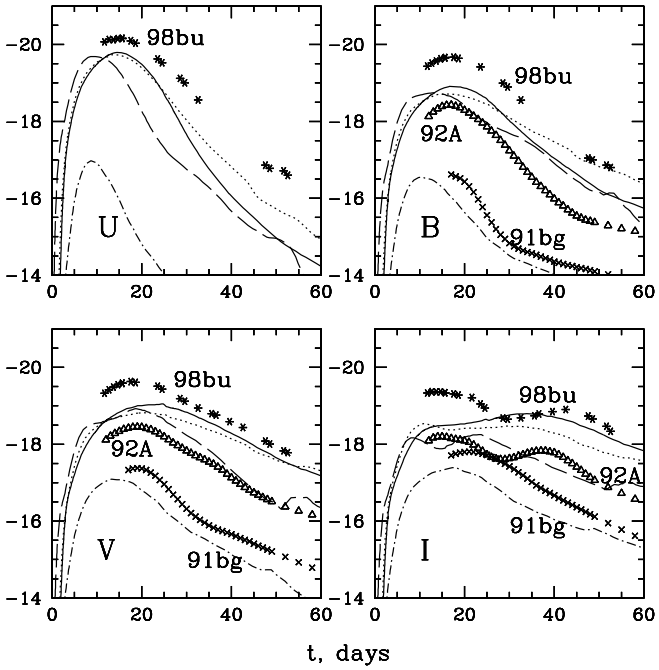

Figure 1: UBVI light curves of SNe Ia. Models DD4 (solid), W7 (dots), LA4 (dashes) and WD065 (dash–dots). Asterisks, triangles and crosses show the examples of observed supernovae.

Fig. 1 presents the resulting light curves in optical range (*UBVI* bands). First of all, it is easily seen how cautious one should be applying SNe Ia to the determination of cosmological distances: two Chandrasekhar-mass models, though having quite similar main parameters (explosion energy, ^{56}Ni production), differ significantly in their post-maximum decline rates due to slightly different distribution of chemical elements over the ejecta (in our case, it is because of different burning regimes). The delayed detonation model DD4 reproduces the slope of observed light curves of nearby SNe Ia quite well, while W7 seems to be too slow to fit them.

For cosmological purposes, the so-called Phillips relation [11] $M_{\max}(\Delta m_{15}^B)$ is usually used. Here Δm_{15}^B denotes difference between supernova magnitudes in the B band at the maximum light and 15 days after that. The brighter events show slower decline after the maximum light. This dependence is only statistical. Many individual SNe Ia deviate from it significantly. Our calculations show that the decline rate is very sensitive to the details of the models. Most probably it is the slope of the ^{56}Ni distribution over the ejecta which fixes the decline rate, so the latter could strongly depend on the mode of burning inside a white dwarf, and also on the later mixing of the burned matter. If these effects changed as the Universe evolved, and if in the past there were, for instance, more W7-like events, then the "Phillips relation" would be different for nearby and for distant SNe Ia. If despite this, one still uses the nearby "Phillips relation" for distant events, one can easily overestimate the distance up to 10–15%. The change of distance of that order would have drastic impact on the values of cosmological Λ-term.

The difference between the two Chandrasekhar-mass models after the maximum light

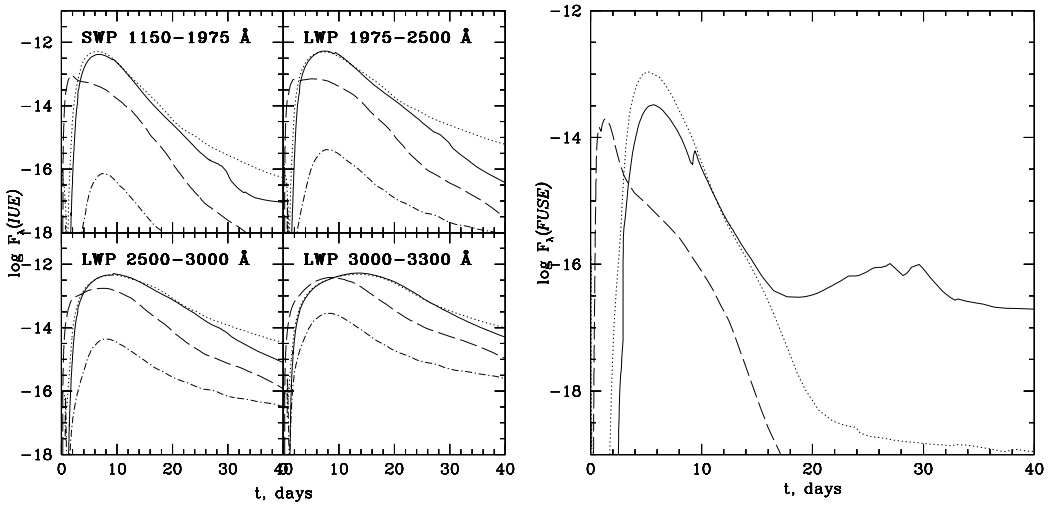

Figure 2: UV light curves of SNe Ia in the IUE wavelength range (left panel) and in the FUSE range 905–1187Å (right panel). Models are drawn with the same curves as in the Fig. 1.

becomes more pronounced in the far UV [3]. It is quite probable that more observational data will soon be available in UV from HST, and that the Far-Ultraviolet Spectroscopic Explorer (FUSE), operating at shorter wavelengths, will be able to obtain light curves and spectra of SNe Ia in the range where they were not observed so far.

In the working wavelength range of FUSE the light curves look out much more different than in the visible light (Fig. 2). This spectral range is more sensitive to the mode of explosion, since it reflects more directly the distribution of ^{56}Ni synthesized during the explosion and the conditions in the exploding star. So, if we wish to distinguish models observationally, it would be good to pay more attention to observations in UV. This seems quite feasible after launching FUSE.

Infrared is another spectral range very sensitive to physical conditions in the ejected matter. Observations reveal that light curve shapes in the I band are more different than in B and V. Most of them show clearly two-maximum structure, though the secondary maximum is not identical for each event and sometimes it is absent at all. Our preliminary investigation shows that the appearance of the secondary maximum depends strongly on the treatment of the line opacity since this determines the efficiency of the redistribution of energy from blue photons to red ones. In our calculations we force all lines to be absorptive to emulate the effect of the energy redistribution. In reality, fluorescence plays the most important role. Numerical modeling of this process could be done only in the frame of a fully NLTE code, yet recent ETLA results [12] for DD4 confirm that our approximation is very good indeed for the first two months after the SN Ia explosion. We plan to compare the results of our calculations (with LTE lines) with the ones derived from NLTE codes (which require as initial data the hydro structure and the flux on the level of photosphere that could be got from our code). Better understanding of the origin of the secondary maximum and its dependence on physical parameters would shed light on the supernova physics and put restrictions on the explosion models.

Light curves of sub-Chandrasekhar-mass models differ noticeably from the Chandrasekhar-

mass ones already in optical. UV range just brings out some new features of their emission. The model WD065 was constructed in [10] specially to explain the emission from very subluminous SN 1991bg. The chemical composition was selected so that the model fits the late spectrum of this supernova very well. Our calculation of the light curve near the maximum shows that the model is also in good agreement with multi-color observations of SN 1991bg at this time. The light curve is about 2^m fainter than those of Chandrasekhar-mass models due to an order-of-magnitude lower ^{56}Ni mass. The same factor explains very fast weakening of the emission in the UV range towards bluer wavelengths: too low number of γ-photons is produced in the decay $^{56}\mathrm{Ni} \to {}^{56}\mathrm{Co} \to {}^{56}\mathrm{Fe}$, so that they heat the gas less than it happens in ^{56}Ni-abundant Chandrasekhar-mass models. As a result, a blue edge of the spectrum of WD065 is shifted to the longer wavelengths, and the flux rises to the maximum almost simultaneously for the whole UV range. This is also in contrast with maximum light of the Chandrasekhar-mass models which is shifted progressively towards later epochs for longer wavelengths remaining almost equal in brightness.

The last model we have calculated, LA4, is the model with helium detonation in the outer layers. We confirm the widespread opinion that such models are too hot and too blue near maximum light and the time of rise to the maximum is too short when compared to observed values. In several days after the maximum the model becomes redder very quickly. The initial very fast spike of the emission in this model is clearly seen in all UV light curves. This is the main feature of the model. The origin of this spike can be easily explained by the hard emission from outer layers, since first days after the explosion we observe the emission from these layers which are heated by outer region of radioactive ^{56}Ni, and hard photons just have no time to degrade. The brightness of LA4 in the optical range is almost the same as given from Chandrasekhar-mass models, while in UV it starts to diminish. The effect is not so much as for WD065, but the reason is perhaps the same – a bit lower amount of ^{56}Ni than in the Chandrasekhar-mass models. The emission of such a supernova can be detected in far UV earlier than in visual light, yet the flux rises up and falls down so quickly that it seems to be of low probability to catch it near the maximum.

Unfortunately, the sensitivity of modern UV telescopes is not extremely high, so UV emission could be detected only from nearby SNe Ia: we estimate that they could be observed up to 300 Mpc in the near UV and up to 30 Mpc in the far UV (with HST and FUSE, respectively). Actually, we somewhat underestimate the observational possibilities here. The UV light curves of cosmological SNe Ia are shifted to the redder wavelengths where the instrumental sensitivity is higher. Yet the far-UV range, where differences between models are more pronounced, will still be shifted only to the near-UV, not to the optical (unless one observes *extremely* distant events), therefore the improvement in the detectability would not be very drastic. Perhaps, one should use the whole possible range of wavelengths to widely observe the nearby objects. And when after that we understand the physics of explosions better, this would help us to derive the properties of more distant explosions relying only on observations in the visible light.

When applying the calculations like ours to the analysis of observations, one should also have in mind that the circumstellar medium around SNe Ia can absorb radiation, especially in the UV band. In this case our predictions should be used as an input for calculations of reprocessing of UV photons to redder wavelengths.

Acknowledgements

We are grateful to E. Livne, K. Nomoto, P. Ruiz-Lapuente, and S. Woosley for providing us with SNe Ia models, to P. Lundqvist for the possibility of using the computer facilities of the Stockholm Observatory. ES would like to thank MPA for the support and especially E. Müller and W. Hillebrandt for organizing the Workshop and for the very warm atmosphere they created there.

References

[1] S. Blinnikov and O. Bartunov, Astron. Astrophys. **273** (1993) 106

[2] S. Blinnikov et al., ApJ **496** (1998) 454

[3] S. Blinnikov and E. Sorokina, Astron. Astrophys. **356** (2000) L30

[4] P. Höflich and A. Khokhlov, ApJ **457** (1996) 500

[5] E. Sorokina, S. Blinnikov, O. Bartunov, Astron. Letters **26** (2000) 67

[6] S. Blinnikov, in Thermonuclear Supernovae, eds. P. Ruiz-Lapuente et al., Dordrecht: Kluwer (1997) p.589

[7] S.E. Woosley and T.A. Weaver, in Supernovae, eds. J. Audouze et al., Amsterdam: Elsevier (1994) p.63

[8] K. Nomoto, F.-K. Thielemann, K. Yokoi, ApJ **286** (1984) 644

[9] E. Livne and D. Arnett, ApJ **452** (1995) 62

[10] P. Ruiz-Lapuente et al., Nature **365** (1993) 728

[11] M.M. Phillips, ApJ **413** (1993) L105

[12] P.A. Pinto, R.G. Eastman, ApJ **530** (2000) 757

Neutron Cross Sections of Radioactive Isotopes: Recent Measurements and Future Perspectives

C. Arlandini[1], *B. Haight*[2], *M. Heil*[1], *F. Käppeler*[1], *R. Reifarth*[1], *B. Rundberg*[2], *P. Sedyshev*[3], *J. Ullmann*[2], *J. Wilhelmy*[2]

[1] *Forschungszentrum Karlsruhe, Institut für Kernphysik, Postfach 3640, D-76021 Karlsruhe, Germany*
[2] *Los Alamos National Laboratory, Los Alamos, NM 87545, USA*
[3] *Frank Laboratory of Neutron Physics, JINR 141980 Dubna, Moscow Region, Russia*

1.1 Introduction

Models for neutron capture nucleosynthesis in Red Giant stars can be sensitively tested via characteristic abundance patterns produced by branchings in the reaction path, since these reflect the physical conditions at the stellar site. The essential nuclear physics input for such studies are the neutron capture cross sections of the involved isotopes including those of the radioactive branch point nuclei.

At traditional facilities the available neutron fluxes are too small to allow for time-of-flight (TOF) experiments on most of the relevant unstable nuclei, because the measured effect is overwhelmed by background from the radioactive decay of the sample. Therefore, only a few isotopes with very long half-lives and/or very soft decay radiation could be studied experimentally so far.

The necessary improvement in sensitivity that is required to extend such measurements to more unstable isotopes can be achieved by means of the much higher neutron fluxes obtained via spallation reactions or by using the activation technique. These two options will be outlined in the following at the example of recent measurements on ^{147}Pm and ^{171}Tm. Finally, the consequences resulting from these measurements on radioactive nuclei and the corresponding quests for more experimental data will be discussed as well.

1.2 Stellar (n,γ) cross sections of ^{147}Pm and ^{171}Tm

Activation measurements have been performed recently on the radioactive nuclei ^{147}Pm ($t_{1/2}$=2.6 yr) and ^{171}Tm ($t_{1/2}$=1.9 yr), which are relevant for analyzing the branchings at A=147/148 and at A=170/171, respectively.

The branchings in the Nd-Pm-Sm region (Fig. 1) are of great interest for probing the s-process neutron density since the β-decay rates of all three branching points ^{147}Nd, ^{147}Pm, and ^{148}Pm are practically independent of temperature and electron density [1]. Previously, the effective strength of these branchings has been well defined by accurate cross section measurements on the s-only isotopes ^{148}Sm and ^{150}Sm [2, 3, 4].

The corresponding stellar (n,γ) cross sections of the radioactive branch point nuclei have so far been adopted from statistical model calculations. However, these calculations are complicated by systematic difficulties in describing the level density of these isotopes near magic neutron number 82. Accordingly, various calculations differ by a factor two [5].

Therefore, activation measurements have been performed by irradiating a sample of only 29 ng ^{147}Pm for 2.5 and 12 days in a quasi-stellar spectrum corresponding to a thermal energy of kT = 25 keV. Neutron capture on ^{147}Pm populates ground state and isomer in ^{148}Pm with

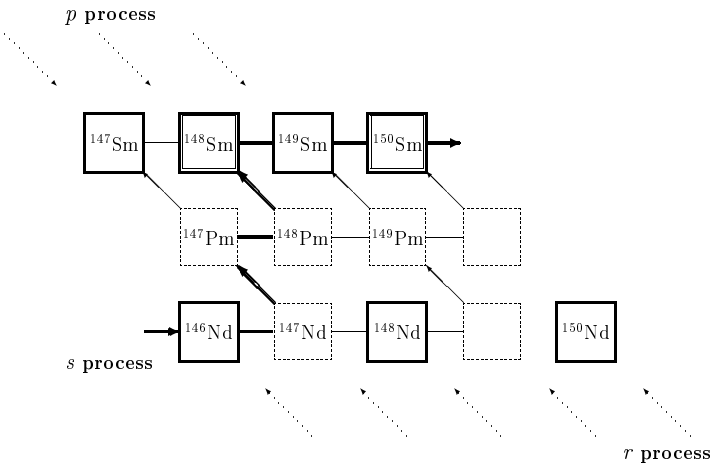

Figure 1: The s-process reaction chain between Nd and Sm with the branchings at A=147/148. (Neutron captures on ^{149}Pm can be neglected.)

half-lives of 5 d and 41 d, respectively. The γ-activity from the decay of these states was measured with an array of two Ge-Clover detectors facing each other. Fig. 2 shows two γ-spectra for illustration, a spectrum of a single Ge detector and a sum spectrum from all 8 detectors in the array including the add-back option that partly restores Compton-scattered events. Obviously, the ^{148}Pm decay is too weak to be observed, either due to the overall background or due to interfering lines.

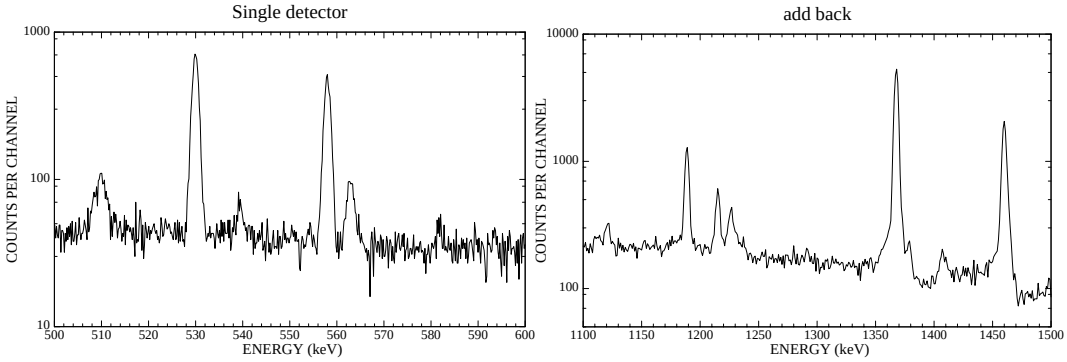

Figure 2: Gamma-ray spectra of the activated ^{147}Pm sample measured with a single Ge detector (left panel) and using all 8 detectors of both Clover arrays including the add-back option (right panel). Even the strongest transition from the ^{148}Pm decay at 550 keV can not be distinguished from the overall background and the γ-line at 1465 keV is additionally obscured by the nearby ^{40}K transition (1461 keV).

This difficulty could be solved by means of the 8-fold granularity of the Ge array, which allowed to record γ,γ coincidences with reasonable efficiency. In this way a number of γ-ray cascades in the decay of ^{148}Pm could be identified and analyzed.

The (yet preliminary) results indicate that the partial cross sections to ground state and isomer contribute almost equally to the total (n,γ) cross section of ^{147}Pm. The important implication of these data is, however, that the stellar cross section of ^{147}Pm appears to be

significantly smaller than all previous predictions obtained with statistical model calculations.

The neutron capture cross section of ^{171}Tm was first studied in a time-of-flight (TOF) experiment using the LANSCE facility at the Los Alamos spallation neutron source [6]. The enormous neutron flux available at this facility allows to perform TOF measurements even on milligram-samples, an important prerequisite to keep the background from the decay of the radioactive sample at a manageable level. In the same experiment, the cross section of the stable isotope ^{169}Tm was measured as well. Comparison with a statistical model calculation showed perfect agreement with the ^{169}Tm result, but in the neutron energy range above 10 keV the measured ^{171}Tm cross section was found to be three times larger than the theoretical data.

In order to check this discrepancy, an independent activation measurement was carried out at Karlsruhe, similar to the one described before. Irradiation of a 800 ng ^{171}Tm sample in the aforementioned quasi-stellar neutron spectrum resulted in a clear γ-ray signature from the induced ^{172}Tm activity. In this case, the cross section showed very good agreement with the calculation.

1.3 Conclusions

The consequences of these results are twofold. (i) TOF measurements using very small radioactive samples are still in their infancy. To fully exploit the potential of such advanced experiments requires further optimization. (ii) Predictions based on the statistical model are still suffering from large systematic uncertainties. This can give rise to unexpected problems as in case of ^{147}Pm, where the observed discrepancy is significantly larger than the average difference to experimental data. Obviously, such problems may occur even for nuclei with fairly large level densities in or near the stability valley.

This underlines the need for further experimental efforts, in particular with respect to more reliable extrapolations off the stability line, where such data are required for describing explosive scenarios. First successful cross section measurements on unstable isotopes have been reported, but this new class of experiments - in particular in the very high fluxes of spallation neutron sources - has to be further optimized. In this respect, the design parameters of the spallation neutron facility now under construction at CERN [7] seem to promise also interesting possibilities.

References

[1] K. Takahashi and K. Yokoi, Atomic Data Nucl. Data Tables **36**, 375 (1987).

[2] K. Wisshak *et al.*, Phys. Rev. C **48**, 1401 (1993).

[3] K. Wisshak *et al.*, Phys. Rev. C **57**, 391 (1998).

[4] K. Wisshak, F. Voss, and F. Käppeler, Phys. Rev. C **57**, 3452 (1998).

[5] Z. Bao *et al.*, Atomic Data Nucl. Data Tables, in print.

[6] R. Rundberg *et al.*, LANSCE Activity Report, LA-13547-SR, Los Alamos National Laboratory (1999).

[7] S. Abramovich *et al.*, Technical Report CERN/SPSC 99-8; SPSC/P 310, CERN (1999).

Stellar neutron capture on ^{128,129,130}Xe

René Reifarth, Franz Käppeler, Friedrich Voss, Klaus Wisshak

[1] *Forschungszentrum Karlsruhe, Institut für Kernphysik, Postfach 3640, D-76021 Karlsruhe, Germany*

1.1 Introduction

Almost all elements beyond iron are produced via neutron capture nucleosysnthesis. Rapid neutron capture () process in explosive scenarios and slow neutron capture (s) process in Red Giant stars contribute about 50% at a time to the solar mass distribution.

Starting at iron seed, the s-process mass flow follows the valley of stability. If the β-decay and neutron capture rates are comparable, the s-process path branches. The branching ratio is determined by the (possibly temperature-dependent) β-decay rate and the neutron capture rate which depends on the neutron density. Hence, it reflects the physical conditions in the He burning zone of the star, where the s process takes place.

Xenon is one of the six elements with two s-only isotopes. If one of these isotopes is partly bypassed by the s-process reaction flow, these branchings are best suited for a quantitative analysis. In contrast to all other relevant cases, the investigated branching at ^{128}I is originates only from the competition between β^- and electron capture decays (see figure 1). Hence it is completely independent of the neutron flux, a peculiarity that makes the resulting abundance pattern a sensitive test for the temperature and electron density profiles predicted by various s-process models.

1.2 Stellar (n, γ) cross sections of the Xe isotopes

The experiment was performed at the Karlsruhe 3.7 MV Van de Graaff accelerator using the time of flight technique. Neutrons were produced via the ^{7}Li$(p,n)^7$Be reaction by bombarding metallic Li targets with a pulsed proton beam. Capture events were registered with the Karlsruhe 4π Barium Fluoride Detector, consisting of 41 BaF_2 modules. Due to the high γ-ray efficiency and energy resolution of this detector ([1]) 0.5 g isotopically enriched xenon samples were sufficient to achieve an accuracy of 2% in the energy range from 3 to 225 keV (see Fig. 2). The cross sections were measured relative to the standard cross section of ^{197}Au.

The comparison with statistical model predictions [2] shows fair agreement except for the ^{129}Xe cross section, which is significantly larger than the value recommended in Ref. [2]. After these results (which represent the first experimental keV cross sections for these important s-only isotopes) are completed by the final analysis, reliable Maxwellian averaged cross sections can be determined for a quantitative discussion of the astrophysical consequences.

References

[1] K. Wisshak, K. Guber, F. Käppeler, J. Kirsch, H. Müller, G. Rupp, and F. Voss, Nucl. Instr. Methods **A292** (1990) 595.

[2] Z.Y. Bao, H. Beer, F. Käppeler, F. Voss, K. Wisshak, and T. Rauscher, Atomic Data Nuclear Data Tables (in print).

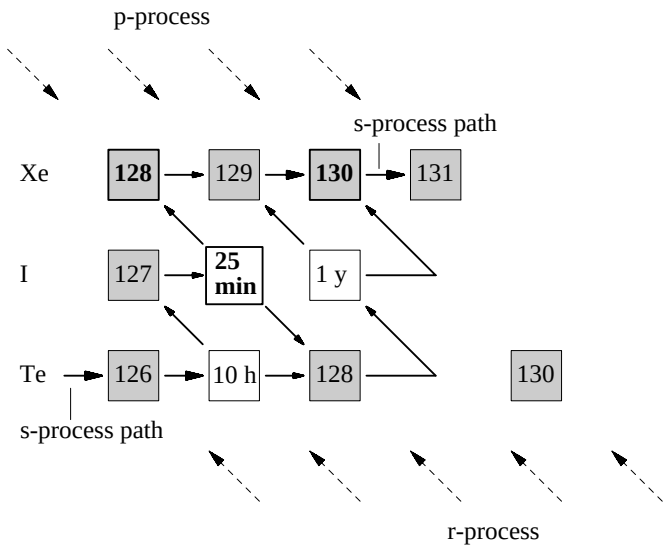

Figure 1: The s-process reaction path between Te and Xe. In contrast to ^{130}Xe, ^{128}Xe is partly bypassed due to the branching at ^{128}I. Both Xe isotopes are shielded against r-process contributions by their stable Te isobars. Note that the branching results from the competition between β^- and electron capture decays and is completely independent of the neutron flux.

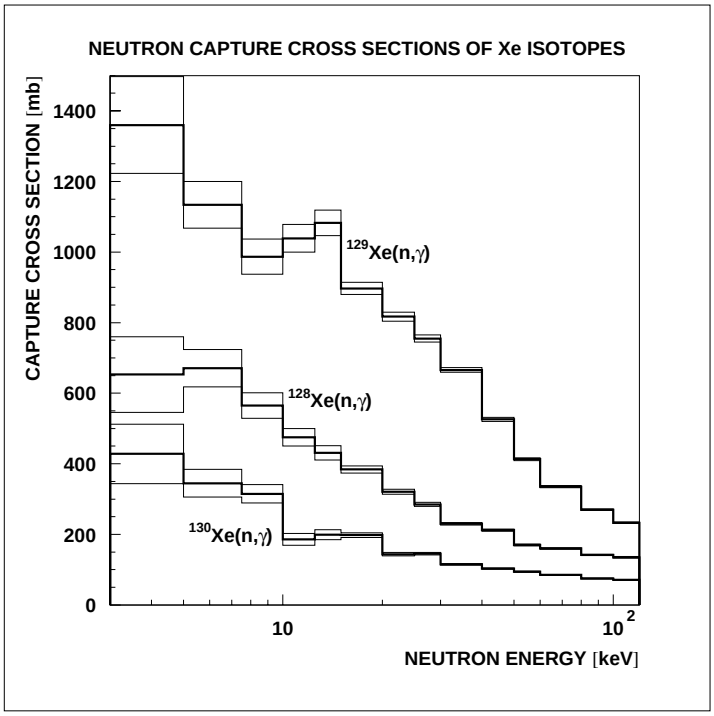

Figure 2: The neutron capture cross sections of ^{128,129,130}Xe in the keV region. Below 20 keV, the overall uncertainties (indicated by bands) are dominated by counting statistics.

s-Process Termination: A New Capture Cross Section Result of the ^{208}Pb Bottleneck

H. Beer[a], W. Rochow[b], P. Mutti[c], F. Corvi[c], K.-L. Kratz[d], B. Pfeiffer[d]

[a] *Forschungszentrum Karlsruhe, IK, Postfach 3640, 76021 Karlsruhe, Germany*
[b] *Physikalishes Institut, Universiät Tübingen, Auf der Morgenstelle 14, 72076 Tübingen, Germany*
[c] *CEC, JRC, Institute for Reference Materials and Measurements, Retieseweg, B–2440 Geel, Belgium*
[d] *Institut für Kernchemie, Universität Mainz, Fritz-Strassmann-Weg 2, D-55099 Mainz, Germany*

Abstract

The Maxwellian average neutron capture (MAC) cross section of ^{208}Pb has been measured at the Tübingen Van de Graaff accelerator with the activation technique at a thermonuclear energy of kT=52 keV. The neutrons were generated via the T(p,n) reaction at a proton energy of $E_{p,lab}$=1091 keV close to reaction theshold. The ^{209}Pb(3.253 h) β activity produced in the irradiations of samples with natural composition was counted with a $4\pi\beta$ Si(Li) spectrometer.

1.1 Introduction

The neutron capture cross section of the nucleus ^{208}Pb is in the keV energy region the smallest capture cross section of the heavy stable isotopes (A>56). Therefore, in s-process nucleosynthesis ^{208}Pb represents an extreme bottleneck, where an especially large abundance is generated. Because ^{208}Pb is double magic its resonance capture cross section is very small. Direct capture and resonance capture are of the same order of magnitude. Theoretical calculations show that direct capture is p-wave capture. The bottleneck function of the stellar ^{208}Pb capture rate is especially important for the analysis of the s–process termination at ^{209}Bi and the decomposition of the isotopic solar abundances of Pb and Bi into the s–, r–, and radiogenic contributions from U and Th [1, 2].

1.2 Measurements

The resonance capture contribution of ^{208}Pb has been measured by time-of-flight at the electron linear accelerator GELINA using 4 C_6D_6 liquid scintillation detectors [1]. Direct and resonance capture of ^{208}Pb can be investigated also by the activation technique. An activation measurement at kT=25 keV has been carried out previously at the Karlsruhe 3.75 MV Van de Graaff accelerator using the ^{7}Li(p,n) reaction [3]. In the present work a new activation measurement was performed at the Tübingen Van de Graaff accelerator to determine the MAC cross section at kT=52 keV. The neutron spectra were generated using proton energies close above the T(p,n) reaction threshold at $E_{p,lab}$=1091 keV. The ^{209}Pb(3.253 h) β activity produced in the irradiations of samples with natural composition was counted with a $4\pi\beta$ Si(Li) spectrometer.

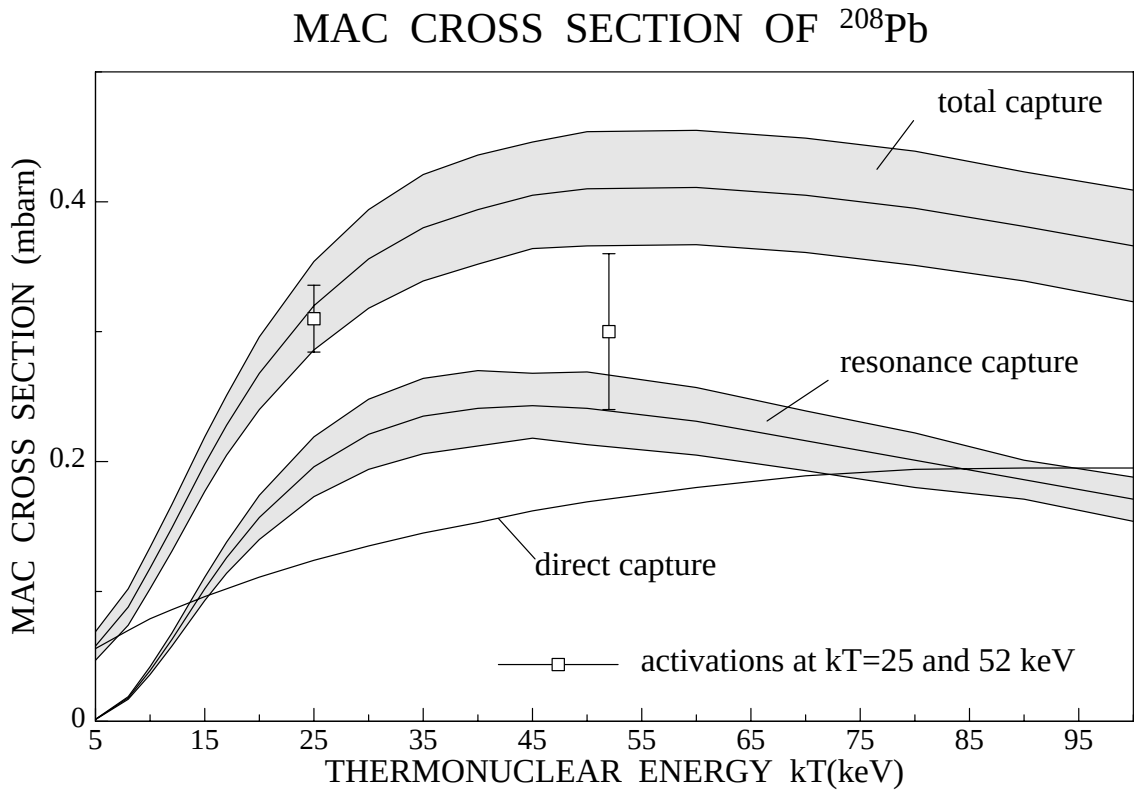

Figure 1: The Maxwellian average capture (MAC) cross section of ^{208}Pb. The data from reference [1] (resonance and total capture values) are shown as solid lines. Corresponding uncertainties are indicated as shaded areas. Open square symbols are the activation measurements at kT=25 keV [3] and 52 keV, respectively.

In Fig. 1 our measurement and the previous results are summarized. Previous results shown are, the value at kT=25 keV reported by [3] and the resonance capture data and the total capture (i.e., the sum of direct + resonance capture) from [1]. The MAC cross section at kT=52 keV was determined in this work from six individual activation runs. The runs were carried out relative to the well-known ^{197}Au standard cross section. The uncertainty is dominated by the statistical error in counting the ^{209}Pb activity.

1.3 Discussion

The present MAC cross section at kT=52 keV, still with a large uncertainty, is lower than the value predicted from the combined data (experimental resonace + theoretical direct capture) of reference [1]. This illustrates that the stellar reaction rate of ^{208}Pb is less well settled than assumed up to now. To improve the situation the statistics of the kT=52 keV data point can be increased by carrying out more runs. Additionally, activation measurements at other neutron energies can be performed. As the ^{208}Pb(n,γ) reaction has no resonances below the 43 keV p-wave resonance it was attempted to measure the direct capture contribution separately with 30 keV monoenergetic neutrons from the ^{7}Li(p,n) reaction at the reaction threshold, but because of the low neutron intensity without success. To measure directly the

direct capture contribution at higher energies in a suitable gap between two resonances is more promising because the direct capture cross section is increasing with energy.

In conclusion, the new MAC cross section result confirms the very small ^{208}Pb capture cross section which makes ^{208}Pb an extreme bottleneck so that the s-process is practically already terminated at ^{208}Pb with the consequence that the last stable isotope ^{209}Bi within s-process reach has to be mainly an r-process nucleus.

Acknowledgements

The interest and support of Prof. G.J. Wagner of the Universität Tübingen is gratefully acknowledged. We would like to thank the technician of the Tübingen Van de Graaff accelerator M. Brandt for his assistance. Support was also provided by the Volkswagen-Stiftung (Az: I/72286).

References

[1] H. Beer, F. Corvi, and P. Mutti, Ap. J. **474** (1997) 843.

[2] J.J. Cowan, B. Pfeiffer, K.-L- Kratz, F.-K. Thilemann, C. Sneden, S. Burles, D. Tyler, and T.C. Beers, Ap. J. **521** (1999) 194.

[3] U. Ratzel, Diplomarbeit 1988, unpublished.

Stellar weak interaction rates

K. Langanke and G. Martínez-Pinedo

Institute for Physics and Astronomy, University of Aarhus, Denmark

1.1 Introduction

Nuclear reactions mediated by the weak force play an essential role in many astrophysical scenarios. To improve on the current treatment of such processes, we have currently finished two large-scale projects in which we have calculated the weak-interaction rates for nuclei in the mass range $A = 45 - 65$, which are crucial for the presupernova evolution, and the neutrino-induced reaction rates for neutron-rich nuclei which are needed in simulations of the nuclear r-process under conditions with extreme neutrino fluxes. The present manuscript will briefly summarize these two projects.

1.2 Weak interaction rates in stars

The core of a massive star becomes dynamically unstable when it exhausts its nuclear fuel. If the core mass exceeds the appropriate Chandrasekhar mass (roughly 1.4 solar masses), electron degeneracy pressure cannot longer stabilize the center and it collapses. Weak-interaction processes play the essential role in the early stage of the collapse. At first, electrons are captured by nuclei which reduces the number of leptons per baryons Y_e and hence the pressure which the electron gas can stem against the collapse. As a further consequence the distribution of nuclei in the core is shifted to more neutron-rich material. Secondly, many of the nuclei present can also β decay. While this process is quite unimportant compared to electron capture for initial Y_e values around 0.5, it becomes increasingly competative for neutron-rich nuclei due to an increase in phase space related to larger Q_β values. We like to stress that the densities in the core are still low enough so that the neutrinos, produced by both electron capture and β decay, can leave the star and thus carry some energy away and cool the core. Thus, both effects (reduction of the electron fraction and energy) conspire to accelerate the collapse. The importance of electron capture for the presupernova collapse is for example discussed in [1, 2].

Presupernova models have so far employed the weak-interaction rates by Fuller, Fowler and Newman (FFN) [3] who have systematically and phenomenologically estimated rates for nuclei in the mass range $A = 45-60$. Under supernova conditions electron capture and β decay is dominated by Gamow-Teller (GT) (and Fermi) transitions. At the time, FFN did their seminal work no experimental guidance about the GT strength distribution in the electron capture direction has been available, and the FFN rates rely on the (admirable) nuclear physics knowledge and intuition of the authors. In recent years experimental information about the GT strength distributions became available indicating differences to the empirical FFN parametrizations. Most importantly the GT strength is fragmented over many nuclear states (rather than concentrated in one central resonance as assumed by FFN) caused by correlations among the nucleons introduced by a strong residual interaction. To recover these correlations, the interacting shell model is the method of choice, requiring, however, calculations in model spaces of several 10 million configurations. Very recent decisive progress in computer hardware and shell model diagonalization software make such demanding calculations feasible. We

have demonstrated recently that state-of-the-art shell model studies indeed reproduce all the necessary ingredients to calculate weak-interaction rates in supernovae [4]. In general, we have demonstrated that the shell model reproduces all measured GT_+ distributions very well (an example is given in Fig. 1) and gives a very reasonable account of the experimentally known GT_- distributions. Further, the lifetimes of the nuclei and the spectroscopy at low energies are simultaneously also well described.

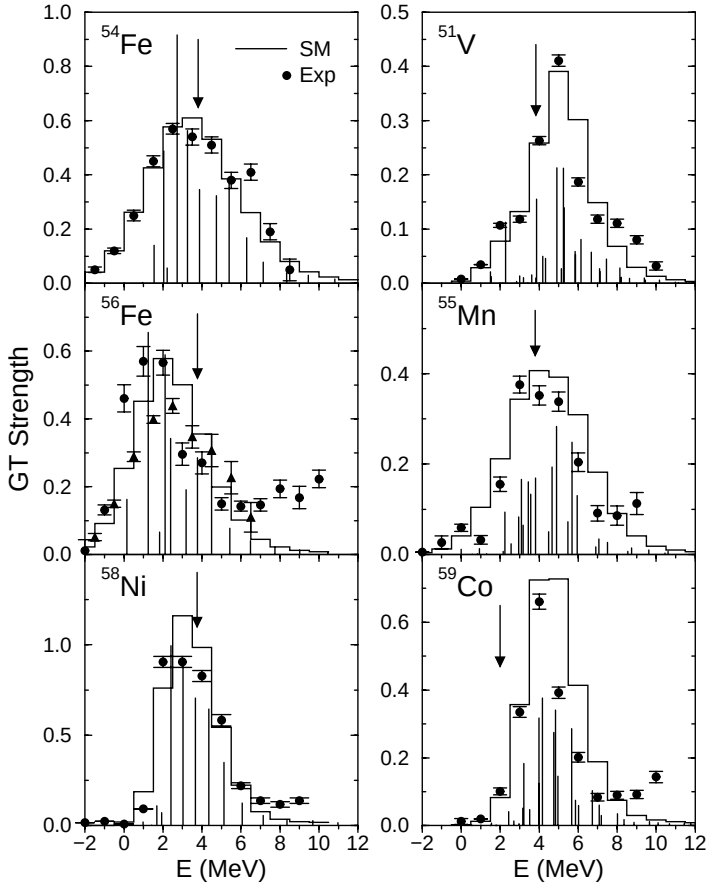

Figure 1: Comparison of the shell model GT strength distribution (histogram) with data for selected even-even and odd-A nuclei. For the comparison the calculated discrete spectrum has been folded with the experimental resolution. The positions of the GT centroids assumed in the FFN parametrization are shown by arrows.

Based on the shell model calculations and using experimental data, whenever available, we have finished the compilation of weak interaction rates on nuclei in the mass range $A = 45-65$ for supernova temperatures and densities. The shell model rates differ from the FFN rates in two important aspects [5]:

- The electron capture rates are generally significantly smaller than estimated by FFN (on average by more than an order of magnitude).
- The β decay rate exceeds the electron capture for values of $Y_e = 0.42 - 0.46$.

The consequences of the improved rates in presupernova models are currently explored. First preliminary results indicate that the Y_e values along the stellar trajectories are noticeably

larger than previously assumed, while temperature and density profiles of final presupernova models remain rather unaffected [6]. Importantly the entropy is also small with the new weak-interaction rates. Possible effects of the shell model weak-interaction rates on type Ia supernovae are discussed in [7].

A table with the new rates has been prepared using the same format as in the compilations of the FFN rates. Furthermore an electronic rate file of the rates can be obtained from the authors upon request.

1.3 Neutrino-nucleus reactions

Most of the supernova neutrinos are generated by the cooling of the nascent neutron star, which releases its gravitational binding energy by neutrino-pair production. Although pairs of all three flavors are generated with equal luminosity, due to their smaller opacities ν_μ and ν_τ neutrinos and their antiparticles decouple at smaller radii, and thus higher temperatures in the core, than ν_e and $\bar{\nu}_e$ neutrinos. As the neutrinos decouple in neutron-rich matter, which is less transparent for ν_e than for $\bar{\nu}_e$, it is expected on general grounds that the neutrino spectra after decoupling obey the temperature hierarchy, $T_{\nu_x} > T_{\bar{\nu}_e} > T_{\nu_e}$, where ν_x stands for ν_μ, ν_τ and their antiparticles, which are assumed to have identical spectra (e.g. [8]). The neutrino spectra can be approximately described by Fermi-Dirac (FD) distributions with zero chemical potential and $T_{\nu_x} = 8$ MeV, $T_{\bar{\nu}_e} = 5$ MeV, and $T_{\nu_e} = 3.5$ MeV, corresponding to average neutrino energies of $\langle E_{\nu_x} \rangle = 25$ MeV, $\langle E_{\bar{\nu}_e} \rangle = 16$ MeV, and $\langle E_{\nu_e} \rangle = 11$ MeV.

The rapid neutron capture process (short r-process) is believed to synthesize about half of the elements heavier than mass $A \sim 60$. The currently favored site for the r-process is the neutrino-driven wind just above the surface of the newly born neutron star in a supernova explosion [9]. If this site is correct, we have pointed out that neutrino-induced reactions can be important even after the r-process has ceased because the neutron fuel has all be consumed. The reason is that the r-process matter will be exposed to rather strong neutrino fluxes, which can alter the matter abundance distribution [10]. By both, ν_e-induced charged-current and ν_x-induced neutral-current reactions, neutrinos can inelastically interact with r-process nuclei. In these processes the final nucleus will be in an excited state and most likely decay by the emission of one or several neutrons, thus effecting the final r-process abundance. Furthermore, ν_e-induced charged-current reactions on nuclei can simulate β decays and might help to speed-up the matter-flow in this r-process scenario. Finally, Meyer et al. [11] have pointed out that the sensitivity of the r process to neutrino irradiation means that neutrino-capture effects can strongly help to constrain the r-process site or neutrino physics. Here it is quite exciting to speculate that, in a scenario where electron neutrinos were converted to other neutrino species by matter-enhanced processes in the region above the neutron star surface, the large flux of antineutrinos would drive protons into neutrons ensuring a large initial neutron richness.

Consistent simulations of the r-process in the neutrino-driven wind model require the knowledge of the relevant neutrino-induced reaction rates. As the neutrino reaction can excite the daughter nucleus above the neutron threshold, which are quite low for r-process nuclei, the daughter nucleus will decay by emission of one or several neutrons. We have calculated the relevant total and partial neutron spallation cross sections for r-process nuclei with neutron numbers $N = 41 - 135$. Our calculations are based on the random phase approximation and consider allowed as well as forbidden transitions. The study of the charged-current reactions are strongly faciliated by the observation that the cross sections for supernova ν_e neutrinos (due to their rather low average energy) are mainly given by allowed transitions

which are governed by sum rules which are fulfilled within the RPA approach. The calculation distinguishes between proton and neutron degrees of freedom for the particle and hole states. Furthermore, our choice of the single-particle energies in the daughter ensures the correct reproduction of the IAS state.

The cross sections have been calculated assuming a Fermi-Dirac distribution for the neutrinos with chemical potential $\alpha = 0$ and $\alpha = 3$, and for each of these values, temperatures $T = 2.75$, 3.5, 4.0, 5.0, 6.4, 8.0 and 10.0 MeV. This grid includes the currently recommended supernova neutrino spectra for all 6 different neutrino types [5]. The chosen (T, α) grid also allows one to explore the consequences of neutrino oscillations. Fig. 2 shows the systematics of total charged-current cross sections for selected isotopic chains. More results are presented in [12]. A publication of the cross sections in tabulated form and as an electronic file is currently under preparation.

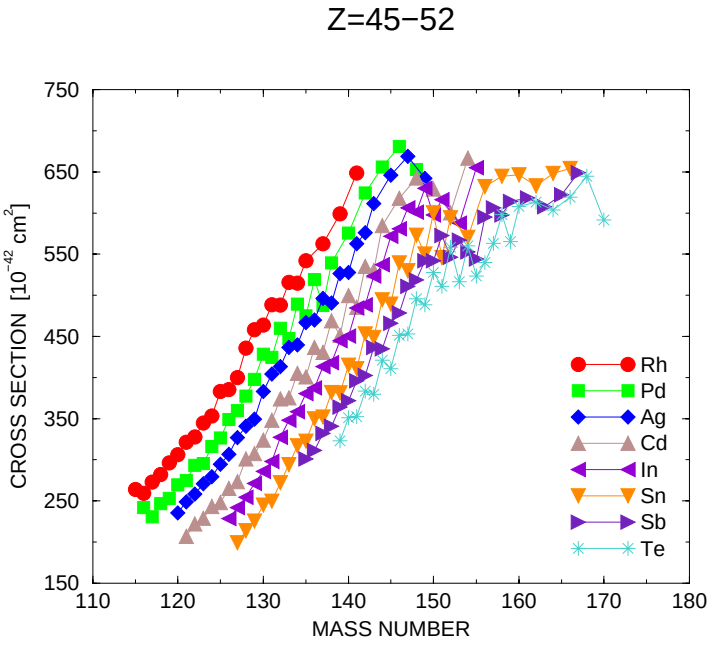

Figure 2: Total charged-current cross sections for neutron-rich nuclei with $Z = 45-52$ induced by supernova ν_e neutrinos with ($T = 4$ MeV and $\alpha = 0$.

Acknowledgements

The work has been partially supported by a grant of the Danish Research Council.

References

[1] H.A. Bethe, G.E. Brown, J. Applegate and J.M. Lattimer, Nucl. Phys. **A324** (1979) 487

[2] H.A. Bethe, Rev. Mod. Phys. **62** (1990) 801

[3] G.M. Fuller, W.A. Fowler and M.J. Newman, ApJS **42** (1980) 447; **48** (1982) 279; ApJ **252** (1982) 715; **293** (1985) 1

[4] E. Caurier, K. Langanke, G. Martinez-Pinedo and F. Nowacki, Nucl. Phys. **A653** (1999) 439

[5] K. Langanke and G. Martinez-Pinedo, Nucl. Phys. **A673** (2000) 481

[6] A. Heger, K. Langanke, G. Martinez-Pinedo and S.E. Woosley, in preparation for Phys. Rev. Lett.

[7] F. Brachwitz *et al.*, Ap.J., in print

[8] H.-T. Janka and W. Hillebrandt, Astron. Astrophys. **224** (1989) 49

[9] S.E. Woosley *et al.*, Ap.J. **433** (1994) 229; K. Takahashi, J. Witti and H.-T. Janka, Astron. Astrophys. **286** (1994) 857

[10] W.C. Haxton, K. Langanke, Y.-Z. Qian and P. Vogel, Phys. Rev. Lett. **78** (1997) 1532

[11] B.S. Meyer, G. McLaughlin and G.M. Fuller, Phys. Rev. **C58** (1998) 3696

[12] A. Hektor, E. Kolbe, K. Langanke and J. Toivanen, Phys. Rev. **C61** (2000) 055803

Shell-Model Half-Lives for r-process nuclei

G. Martínez-Pinedo, K. Langanke

Institut for Fysik og Astronomi, Århus Universitet, DK-8000 Århus C, Denmark

About half of the elements heavier than mass number $A \approx 60$ are produced in the astrophysical r process, a sequence of neutron capture and beta decay processes [1, 2, 3]. The r process is associated with an environment of relatively high temperatures ($T \approx 10^9$ K) and very high neutron densities ($> 10^{20}$ cm^{-3}) such that the intervals between neutron captures are generally much smaller than the β lifetimes, i.e., $\tau_n \ll \tau_\beta$ in the r process. The series of successive neutron captures comes to a stop when the (n, γ) capture rate for an isotope equals the rate of the destructive (γ, n) photodisintegration rate. Under the typical conditions for the r process the equilibrium is achieved at neutron separation energies, $S_n \approx 2$ MeV [4].

Simulations of the r process require a knowledge of nuclear properties far from the valley of stability. As the relevant nuclei are not experimentally accessible, theoretical predictions for the relevant quantities (i.e., neutron separation energies and half-lives) are needed. Of particular relevance is the determination of the half-lives for nuclei in the neutron shell closures at $N = 50, 82$, and 126 as they determine the abundance peaks at mass numbers $A \approx 80, 130$, and 195. Furthermore, the duration of the r process, i.e., the minimal time required to transmute, at one site, seed nuclei into nuclei around $A \approx 200$, is dominantly given by the sum of the half-lives of the r-process nuclei at the three magic neutron numbers. It appears as if the required minimal time is longer than the duration of the favorable r-process conditions in the neutrino-driven wind from type II supernovae [5], which is the currently most favored r-process site.

Here, we are concerned with the calculation of β decays of r-process nuclei at the magic neutron number $N = 82$. Previous estimates have been based on semiempirical global models, quasiparticle random phase approximation, or, very recently, the Hartree-Fock-Bogoulivov method. But the method of choice to calculate Gamow-Teller transitions is the interacting shell-model. Our shell-model calculations have been performed with the code ANTOINE developed by E. Caurier [6]. A detailed description of our calculations can be found in reference [7].

Our shell-model half-lives are compared with data and with other theoretical predictions on figure 1. For $Z = 47$–49, the half-lives are known experimentally [8, 9] and our shell-model values are slightly faster. Our shell-model half-lives show significant and important differences to those calculated in the finite range droplet model (FRDM) [10] and the extended Thomas-Fermi with Strutinsky integral (ETFSI) [11] approaches, which have been typically used in r-process simulations. Although the latter predicts a Z dependence of the half-lives very similar to the present results, the ETFSI half-lives are longer on average by factors 4–5. The FRDM half-lives show a very pronounced odd-even dependence which is predicted neither by ETFSI nor shell-model. While the FRDM half-lives for the odd-A $N = 82$ isotones agree with the shell-model results (within a factor of 2) and the experimental values for ^{131}In and ^{129}Ag, they overestimate the half-lives for even isotones by an order of magnitude. Recently, Engel *et al.* have performed half-live calculations of r-process nuclei within the Hartree-Fock-Bogoliubov (HFB) model [12]. Their study is restricted to even-even nuclei, but they obtain results wich, except for a factor 2, closely resemble the present shell-model results. Both approaches predict that the half-lives of the $N = 82$ isotones are noticeable shorter than currently assumed in r-process simulations.

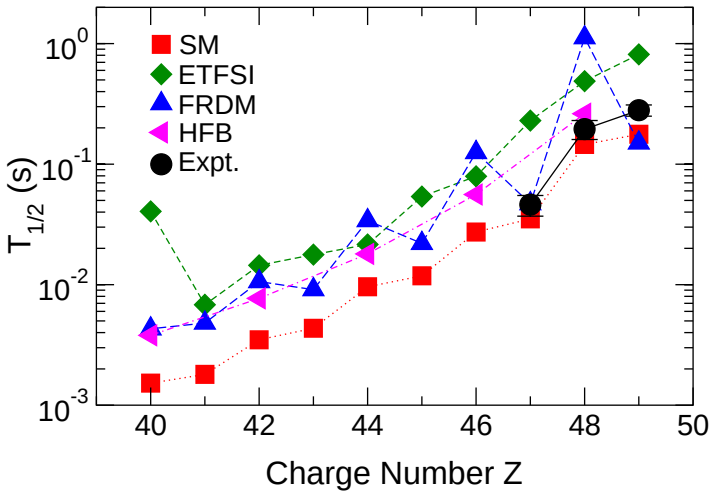

Figure 1: Comparison of half-lives of the $N = 82$ isotones as calculated in the ETFSI, FRDM, HFB, and the present shell-model approaches with data.

Odd-A nuclei in this mass range usually exhibit a low-lying $1/2^-$ isomeric state which can affect the r-process half-lives. We have calculated the energy positions and half-lives of the isomeric states within our shell-model approach. We find that the excitation energy of the isomeric state slowly decreases within the $N = 82$ isotones when moving from ^{123}Nb ($E^* = 500$ keV) to ^{131}In (375 keV) where experimentally only the isomeric state in ^{131}In is known at $E^* = 360$ keV. Our calculation predicts the half-lives of the isomeric states to be comparable to the ground state half-lives in all cases. Thus, the effective r-process half-lives will be very close to the ground state half-lives.

An interesting question is whether the r process proceeds in β-flow equilibrium also at the waiting points related to magic neutron numbers [13]. In this picture, the observed r-process abundances scale as the respective β-decay half-lives, if the former are corrected for β-delayed neutron emissions during their decays from the r-process paths towards the stable nuclei. Using the solar r-process abundances [14] and our computed values for the neutron emissions probabilities, we have determined the abundances of the $N = 82$ progenitor nuclei, that should be proportional to the corresponding half-lives if β-flow equilibrium is achieved. Figure 2 shows that β-flow equilibrium can be attained for the $N = 82$ isotones with $Z = 44$–47, but fails by more than a factor 4 for ^{130}Cd. As the systematics of neutron separation energies put ^{130}Cd on the r-process path, our results suggest that the conditions which allow one to build the $N = 82$ r-process abundance peak do not last long enough to achieve β-flow equilibrium for this nucleus. This is consistent with the expectation that the r-process peaks at $N = 82$ and $N = 126$ are made under different conditions [4, 15]. Recent observations also indicate that the nuclides in the $N = 82$ and $N = 126$ abundance peaks are produced in different sites [16] (see also the contribution of John J. Cowan).

We have performed preliminary calculations for the half-lives of the $N = 50$ waiting-point nuclei. The computed half-lives are shorter than currently assumed in r-process simulations and confirm the results obtained in reference [12]. For ^{78}Ni all the previous estimates (including the HFB model) predict a half-life of ≈ 0.5 s while our computed half-life is ≈ 0.13 s. The difference is probably due to a limitation of the random phase approximation used in all

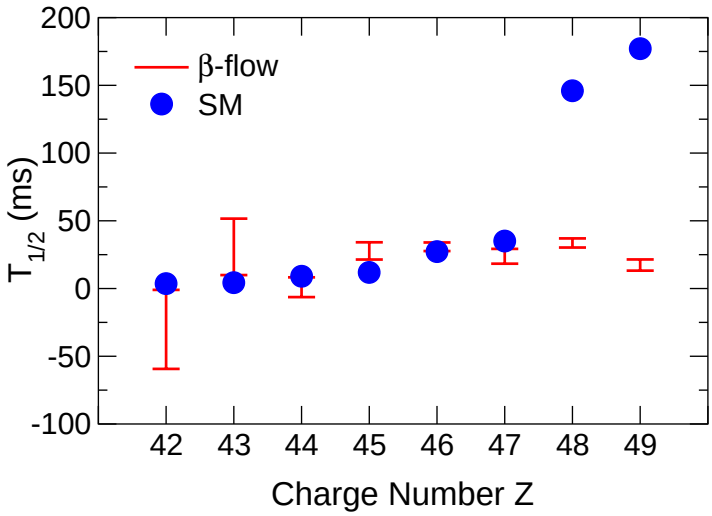

Figure 2: Test of β-flow equilibrium by comparing the shell-model half-lives for the $N = 82$ r-process waiting-point nuclei with the β-flow half-lives.

the other approaches.

References

[1] E.M. Burbidge, G.R. Burbidge, W.A. Fowler and F. Hoyle, Rev. Mod. Phys. **29**, 547 (1957)

[2] A.G.W. Cameron, Chalk River Report CRL-41 (1957)

[3] J.J. Cowan, F.-K. Thielemann and J.W. Truran, Phys. Rep. **208**, 267 (1991)

[4] K.L. Kratz, J.P. Bitouzet, F.-K. Thielemann, P. Möller and B. Pfeiffer, Astrophys. J. **403**, 216 (1993)

[5] S. E. Woosley, G. J. Mathews, J. R. Wilson, R. D. Hoffman, and B. S. Meyer, Astrophys. J. **433**, 229 (1994)

[6] E. Caurier, shell model code ANTOINE, IReS, Strasbourg (1989), unpublished

[7] G. Martínez-Pinedo and K. Langanke, Phys. Rev. Lett. **83**, 4502 (1999).

[8] K.-L. Kratz, H. Gabelmann, W. Hillebrandt, B. Pfeiffer, K. Schlösser, and F.-K. Thielemann, Z. Phys. A **325**, 489 (1986)

[9] K. L. Kratz *et al.*, in *Proccedings of the International Conference on Fission and Properties of Neutron-Rich Nuclei, Sanibel Island, 1997*, edited by J. H. Hamilton (World Scientific Press, 1998)

[10] P. Möller, J. R. Nix, and K.-L. Kratz, At. Data Nucl. Data Tables **66**, 131 (1997)

[11] I.N. Borzov, S. Goriely and J.M. Pearson, Nucl. Phys. A **621**, 307c (1997); http://astro.ulb.ac.be/Nucdata/Beta/tbeta_etfsi.sph

[12] J. Engel, M. Bender, J. Dobaczewski, W. Nazarewicz and R. Surman, Phys. Rev. C **60**, 014302 (1999).

[13] K.L. Kratz, F.K. Thielemann, W. Hillebrandt, P. Möller, V. Härms, A. Wöhr and J.W. Truran, J. Phys. G **24**, S331 (1988).

[14] H. Beer, F. Corvi, and P. Mutti, Astrophys. J. **474**, 843 (1997).

[15] G. J. Wasserburg, M. Busso, and R. Gallino, Astrophys. J. **466**, L109 (1996).

[16] C. Sneden, J. J. Cowan, I. I. Ivans, G. M. Fuller, S. Burles, T. C. Beers, J. E. Lawler, astro-ph/0002086.

Oscillations and convective motion in stars with URCA shells

G.S. Bisnovatyi-Kogan[1]

[1] *Space Research Institute, Moscow*

Abstract

It is shown that in presence of URCA shell pulsational energy losses due to neutrino emission and nonequilibrium beta heating are much less than energy losses by excitation of short-wavelength acoustic waves. Convective motion in presence of URCA shell is considered, and equations generalizing the mean free path model of convection are derived.

1.1 Introduction

It was suggested in [15] that in the convective region cooling of matter may be enhanced in presence URCA shells appearing when matter contains an isotope with a threshold Fermi energy for an electron capture, coresponding to a density less then the central one. Presence of such isotope leads to existence of a jump in the composition at a density, corresponding to a threshold energy. During convective motion the matter in eddies around this density crosses periodically the boundary. That implies continious beta capture and beta decay in the matter of these eddies.

Because of heating of a degenerate matter due to nonequilibrium beta processes [4], with account of convective URCA shell different conclusions had been done with respect to stabilizing or destabilizing the carbon burning in the convective degenerate core [6, 8, 16, 7, 13, 11, 12, 2, 14, 17]. Here we calculate damping of stellar oscillations in presence of URCA shell (see [1]), analyze physical processes in the convective URCA shells and formulate approximate quantitative approach to the solution of this problem.

1.2 Linear oscillations of a slab with a phase transition

Consider the plane-parallel layer in the constant gravitational field with an acceleration g, with a phase transition at the pressure P_*, and polytropic equation of state $P = K\rho^\gamma$, with $K = K_1$ at $P < P_*$ and $K = K_2$ at $P > P_*$, $K_1 > K_2$. In static equilibrium $P = gM\left(1 - \frac{m}{M}\right)$, $\rho = \left(\frac{gM}{K}\right)^{1/\gamma}\left(1 - \frac{m}{M}\right)^{1/\gamma}$. Here the pressure is continuous, but the density ρ has a jump at P_* due to the jump of the constant K, M is the mass of one cm^2 of the slab, m is the mass of one cm^2 of the slab under the layer with a Lagrangian coordinate x, which is related to the density as $\rho = \left(\frac{\gamma-1}{\gamma K}\right)^{\frac{1}{\gamma-1}}(C - gx)^{\frac{1}{\gamma-1}}$. In presence of a phase transition we have $\rho_0 = \left(\frac{gM}{K_2}\right)^{1/\gamma}$, $P_0 = gM$, $gx_* = C_2 - \frac{\gamma}{\gamma-1}\frac{P_*}{\rho_{2*}}$, $x_0 = \frac{C_1}{g}$, $C_2 = \frac{\gamma}{\gamma-1}(gM)^{\frac{\gamma-1}{\gamma}}K_2^{1/\gamma}$, $C_1 = C_2 + \frac{\gamma}{\gamma-1}\frac{P_*}{\rho_{2*}}(\lambda - 1)$. Here ρ_0 and P_0 are the density and the pressure at the bottom of the slab, x_0 and x_* are total thickness and thickness of the inner denser phase layer of the slab, $\lambda = \rho_{2*}/\rho_{1*}$. The phase transition in the slab happens only if its specific mass $M > P_*/g = M_*$.

Linear oscillations of the slab are reduced to Bessel equation for perturbations $\tilde{P}, \tilde{v} = \tilde{P}_a, \tilde{v}_a \exp(-i\omega t)$ with solutions

$$\tilde{P}_a = A\sqrt{z} J_{\frac{\gamma}{\gamma-1}}(\eta) + B\sqrt{z} Y_{\frac{\gamma}{\gamma-1}}(\eta), \tag{1}$$

$$\tilde{v}_a = \frac{i}{\sqrt{\gamma P_0 \rho_0}} z^{-\frac{1}{2\gamma}} \left[A J_{\frac{1}{\gamma-1}}(\eta) + B Y_{\frac{1}{\gamma-1}}(\eta) \right], \tag{2}$$

where for two phases $\eta_2 = \frac{2\gamma}{\gamma-1} \frac{M\omega}{\sqrt{\gamma\rho_0 P_0}} z^{\frac{\gamma-1}{2\gamma}}$, $\eta_1 = \eta_2\sqrt{\lambda}$, $z_* = 1 - \frac{m}{M}$. The frequency of oscillations ω and relations between constants A_1, B_1, A_2, B_2 are obtained from boundary conditions and from relations on the phase jump [9, 5, 10]. The dispersion equation are obtained analytically for a frozen

$$J_{\frac{\gamma}{\gamma-1}}\left(\Omega\sqrt{\lambda} z_*^{\frac{\gamma-1}{2\gamma}}\right) \left[J_{\frac{1}{\gamma-1}}(\Omega) Y_{\frac{1}{\gamma-1}}\left(\Omega z_*^{\frac{\gamma-1}{2\gamma}}\right) - J_{\frac{1}{\gamma-1}}\left(\Omega z_*^{\frac{\gamma-1}{2\gamma}}\right) Y_{\frac{1}{\gamma-1}}(\Omega) \right] \tag{3}$$
$$-\sqrt{\lambda} J_{\frac{1}{\gamma-1}}\left(\Omega\sqrt{\lambda} z_*^{\frac{\gamma-1}{2\gamma}}\right) \left[J_{\frac{1}{\gamma-1}}(\Omega) Y_{\frac{\gamma}{\gamma-1}}\left(\Omega z_*^{\frac{\gamma-1}{2\gamma}}\right) - J_{\frac{\gamma}{\gamma-1}}\left(\Omega z_*^{\frac{\gamma-1}{2\gamma}}\right) Y_{\frac{1}{\gamma-1}}(\Omega) \right] = 0$$

and equilibrium phase transition

$$J_{\frac{\gamma}{\gamma-1}}\left(\Omega\sqrt{\lambda} z_*^{\frac{\gamma-1}{2\gamma}}\right) \left[J_{\frac{1}{\gamma-1}}(\Omega) Y_{\frac{1}{\gamma-1}}\left(\Omega z_*^{\frac{\gamma-1}{2\gamma}}\right) - J_{\frac{1}{\gamma-1}}\left(\Omega z_*^{\frac{\gamma-1}{2\gamma}}\right) Y_{\frac{1}{\gamma-1}}(\Omega) \right]$$
$$-\left[\sqrt{\lambda}\, J_{\frac{1}{\gamma-1}}\left(\Omega\sqrt{\lambda} z_*^{\frac{\gamma-1}{2\gamma}}\right) - (\lambda-1)\frac{\gamma-1}{2} \Omega z_*^{\frac{\gamma-1}{2\gamma}} J_{\frac{\gamma}{\gamma-1}}\left(\Omega\sqrt{\lambda} z_*^{\frac{\gamma-1}{2\gamma}}\right) \right] \tag{4}$$
$$\times \left[J_{\frac{1}{\gamma-1}}(\Omega) Y_{\frac{\gamma}{\gamma-1}}\left(\Omega z_*^{\frac{\gamma-1}{2\gamma}}\right) - J_{\frac{\gamma}{\gamma-1}}\left(\Omega z_*^{\frac{\gamma-1}{2\gamma}}\right) Y_{\frac{1}{\gamma-1}}(\Omega) \right] = 0.$$

In the limiting case $m_* = 0$, when the boundary between phases is on the inner boundary of the layer, and $z_* = 1$ the dispersion equation is reduced to $J_{\frac{1}{\gamma-1}}(\Omega\sqrt{\lambda}) = 0$ for a frozen, and

$$\sqrt{\lambda}\, J_{\frac{1}{\gamma-1}}(\Omega\sqrt{\lambda}) - (\lambda-1)\frac{\gamma-1}{2} \Omega J_{\frac{\gamma}{\gamma-1}}(\Omega\sqrt{\lambda}) = 0 \tag{5}$$

for an equilibrium phase transitions. At $m_* \to M$, $z_* \to 0$ when the level between phases is moving to the outer boundary, we have the dispesion equation $J_{\frac{1}{\gamma-1}}(\Omega) = 0$ in both cases. Here

$$\Omega = \frac{2\gamma}{\gamma-1} \frac{M\omega}{\sqrt{\gamma\rho_0 P_0}}, \tag{6}$$

To investigate the dependence of oscillattion modes with an ideal phase transition on γ it is convenient to introduce $\tilde{\Omega} = \frac{\gamma-1}{2\sqrt{\gamma}}\Omega$, with the first root $\tilde{\Omega}^2 \to \frac{1}{\lambda-1}$ at $\gamma \to \infty$. All other roots tend to infinity at $\gamma \to \infty$. First three roots of equations (3), (4) are presented in Figs.1,2[1].

[1] Numerical solution of dispersion equations had been done by O.V.Shorokhov.

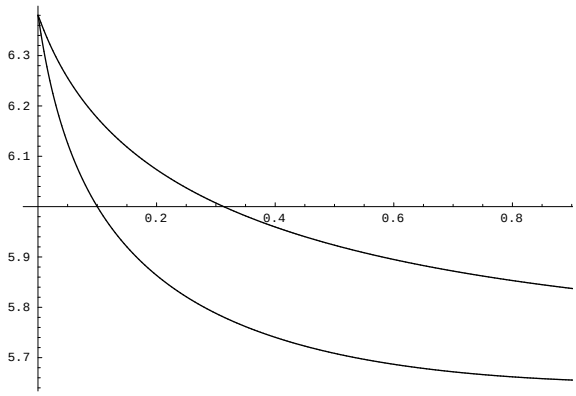

Figure 1:

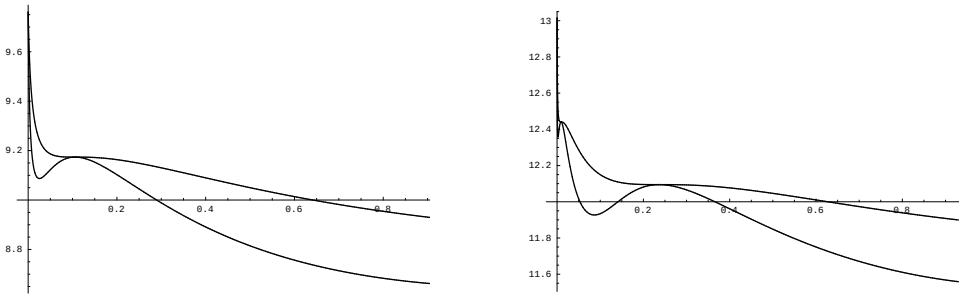

Figure 2: Frequencies Ω of the slab oscillations as functions of z_* of the basic mode (Fig.1), modes with one (left) and two (right) nodes. Upper and lower curves correspond to frozen and equilibrium cases, relatively. Frequencies of these two cases coincide, when one of the node coincides with the phase transition.

1.3 Damping of oscillations due to URCA shell in a highly degenerate matter

Consider ultrarelativistic degenerate electron gas a good approximation in most URCA shells. It corresponds to the polytrope with $\gamma = 4/3$, and constant $K = \frac{c\hbar}{12\pi^2}\left(\frac{3\pi^2}{\mu_Z m_p}\right)^{4/3}$, where $\mu_Z = \left(x_Z\frac{Z}{A} + x_{Z-1}\frac{Z-1}{A}\right)^{-1}$ is the average number of nucleons on one electron. Here a two component mixture is considered consisting of elements with an atomic weight A and atomic numbers Z and $Z-1$, with a beta transitions between them, x_Z and x_{Z-1} are mass concentrations of these elements, $x_Z + x_{Z-1} = 1$.

Let u_{fe} and δ be Fermi energy plus rest mass energy of the electrons, and threshold energy for a beta capture, in units of $m_e c^2$; g_z and g_{Z-1} be statistical weights of the elements (A, Z) and $(A, Z-1)$; $Ft_{1/2}$ be a nondimensional value measured in the beta-decay experiments, or estimated theoretically. For small difference $|\delta - u_{fe}| \ll 1$ we have simple expressions [3] for an entropy increase during beta decay and capture in a fully degenerate matter

$$\rho T\frac{\partial S}{\partial t}=\Phi(\delta-u_{fe})^4 n_{Z-1},\quad \rho T\frac{\partial S}{\partial t}==\Phi(u_{fe}-\delta)^4\frac{g_{Z-1}}{g_Z}n_Z,\quad \Phi=m_e c^2\ln 2\frac{(\delta^2-1)^{1/2}\delta}{12(Ft_{1/2})_{Z-1}}. \tag{7}$$

Here the rate of the entropy increase is equal to 1/3 of the energy loss rate by neutrino emission. During linear oscillations the beta reactions take place only in a thin layer of matter, crossing in its motion the boundary $x=x_*$, $m=m_*$, $P=P_*$. In this layer the pressure may be represented by an expansion

$$P=P_*-g(m-m_*)+\tilde{P},\qquad P^{1/4}=P_*^{1/4}+\frac{1}{4}P_*^{-3/4}[\tilde{P}-g(m-m_*)], \tag{8}$$

Equations describing change of concentrations during oscillations averaged over the layer $\Delta m=\tilde{P}_a/g$, are written as

$$\frac{d\bar{x}_Z}{dt}=-R\frac{P_*^{-9/4}}{256}\tilde{P}_a^3\cos^4\omega t\frac{g_{Z-1}}{g_Z},\qquad P_{eq}<P_*,\quad P>P_*; \tag{9}$$

$$\frac{d\bar{x}_{Z-1}}{dt}=-R\frac{P_*^{-9/4}}{256}\tilde{P}_a^3\cos^4\omega t,\qquad P_{eq}>P_*,\quad P<P_*.$$

Here $R=\ln 2\frac{(\delta^2-1)^{1/2}\delta}{3(Ft_{1/2})_{Z-1}}\left(\frac{12\pi^2\hbar^3}{m_e^4c^5}\right)^{3/4}$. To derive an equation describing decrease of the pulsational amplitude, we should take into account the change of pressure due to change of the electron concentration. Let $\tilde{p}$ be a perturbation of the pressure determined by the beta reactions $P=g(M-m)+\tilde{P}+\tilde{p}$, with $\tilde{p}=\frac{4}{3}P\frac{\tilde{x}_Z}{Z}$, $P_{eq}<P_*$, $P>P_*$; $\tilde{p}=-\frac{4}{3}P\frac{\tilde{x}_{Z-1}}{Z-1}$, $P_{eq}>P_*$, $P<P_*$.

In presence of damping we represent the velocity perturbation in a form $\tilde{v}=\tilde{v}_a(t)\sin\omega t$, and define $V(t)=\tilde{v}_{a,out}(m_*,t)$. so that $\tilde{v}=V\sin\omega t$. The amplitude of the perturbed outside pressure my be written as a function of V as $\tilde{P}_a=z_*^{\frac{7}{8}}\frac{\sqrt{\gamma P_0\rho_0}}{\sqrt{\lambda}}\frac{J_4(\eta_{1*})}{J_3(\eta_{1*})}V$, $\gamma=\frac{4}{3}$. The equation of motion gives the relation describing damping of oscillations in the layer $\Delta m(t)=\frac{\tilde{P}_a\cos\omega t}{g}$, after subtraction of the proper oscillations of the slab at the frozen composition and averaging over the motion of the whole slab

$$\sin\omega t\frac{dV}{dt}=-\frac{\Delta\tilde{p}}{\Delta m(t)}\frac{\Delta m}{M}\approx\frac{g\tilde{p}(m_*)}{\tilde{P}_a\cos\omega t}\frac{\Delta m}{M}, \tag{10}$$

where $\Delta m=\frac{\tilde{P}_a}{g}$. Taking into account, $M=gP_0$, we get

$$\sin\omega t\frac{dV}{dt}=\frac{g\tilde{p}(m_*)}{P_0\cos\omega t}. \tag{11}$$

Averaging over the oscillation period we obtain equation for decreasing of the amplitude of oscillations in the form

$$\frac{dV}{dt}=-D\,V^3,\qquad D=\frac{RgP_*^{-5/4}}{768\omega P_0 Z}\left(1+\frac{g_{Z-1}}{g_Z}\right)(\gamma\lambda P_0\rho_0)^{3/2}z_*^{\frac{21}{8}}\frac{J_4^3(\eta_{1*})}{J_3^3(\eta_{1*})}. \tag{12}$$

1.4 Energy balance and damping of oscillations

Averaging equations (7) over the time and space we get an expression for heating rate of the oscillating slab due to nonequilibrium beta processes in the layer around the URCA shell

$$\dot{Q}_\nu = R_1 \frac{P_*^{-3}}{g\, 32 \times 75\pi} \tilde{P}_a^5 \left(1 + \frac{g_{Z-1}}{g_Z}\right), \quad R_1 = \ln 2 \frac{(\delta^2-1)^{1/2}\delta}{12(Ft_{1/2})_{Z-1} A m_p} \frac{12\pi^2\hbar^3}{m_e^3 c^3}. \tag{13}$$

The rate of the neutrino energy losses L_ν (ergs/s/cm^2) is obtained by averaging over a time of losses in the whole oscillating layer. We get similar to (13)

$$L_\nu = 3R_1 \frac{P_*^{-3}}{g\, 32 \times 75\pi} \tilde{P}_a^5 \left(1 + \frac{g_{Z-1}}{g_Z}\right). \tag{14}$$

Similar dependence of neutrino energy losses during oscillations because of URCA shell had been obtained by Tsuruta and Cameron (1970), who also took (14) for the rate of loss of kinetic energy of oscillations. In the approximation of strong degeneracy the matter will be heated during oscillations with the rate (13), and neutrino luminosity is determined by (14). The source of both kind of energy fluxes is the pulsation energy of the slab, giving the rate of pulsation energy losses directly connected with beta reactions as

$$\dot{E}_{pul}^{(\beta)} = -(\dot{Q}_\nu + L_\nu) = -\frac{R_1 P_*^{-3}}{600\pi g} \tilde{P}_a^5 \left(1 + \frac{g_{Z-1}}{g_Z}\right). \tag{15}$$

Defining $E_{\rm pul} \approx \frac{1}{2} M V^2$, and using approximately $V = \frac{\tilde{P}_a}{\sqrt{\gamma P_0 \rho_0}}$, for URCA shell in the middle of the slab, we get from (12) the equation for decreasing of pulsational energy, connected with hydrodynamic processes, in the form

$$\dot{E}_{\rm pul}^{(\rm dyn)} = -\frac{R P_*^{-5/4}}{768\, Z\omega\sqrt{\gamma P_0 \rho_0}} \tilde{P}_a^4 (1 + \frac{g_{Z-1}}{g_Z}). \tag{16}$$

A ratio of damping rates of oscillation on i-th mode is $\frac{\dot{E}_{\rm pul}^{(\beta)}}{\dot{E}_{\rm pul}^{(\rm dyn)}} \approx \frac{\tilde{P}_a}{P_0}\frac{\omega_i}{\omega_1}$. It follows that the main source of damping of oscillations in presence of URCA shell is connected not with the neutrino emission / nonequilibrium heating, but with a dynamical action of the nonequilibrium layer of the slab, where beta reactions take place. This action leads to an exitation of short-wavelength acoustic waves with length $l \sim \frac{\Delta m}{\rho_0} \ll x_0$. When the wavelength of the excited eigen-mode approaches the thickness of the nonequilibrium layer Δx, formed by oscillations, both mechanisms of damping become comparable. For $l_i \sim \Delta x = \frac{\tilde{P}_a}{g\rho_*}$ with account of relations $\omega_1 \approx \frac{1}{x_0}\sqrt{\frac{P_0}{\rho_0}}$, $x_0 \sim \frac{P_0}{g\rho_0}$, $\omega_i \approx \frac{1}{l_i}\sqrt{\frac{P_0}{\rho_0}}$, and $\rho_* \sim \rho_0$, we get $\dot{E}_{\rm pul}^{(\beta)}/\dot{E}_{\rm pul}^{(\rm dyn)} \sim 1$. Importance of the dynamical damping of stellar oscillations in presence of URCA shell is connected with non-linearity of weak interaction rates, and deviations from eigen-oscillations under an action of weak interactions in this layer, leading to excitation of acoustic waves. The dissipation of pressure oscillations, connected with excitation of sound waves is inherent to any kind of dissipation, when the main term is nonlinear. The linear mechanism, connected with a conventional bulk viscosity, does not change the form of the eigenfunction of oscillations, and so no additional waves are excited.

1.5 URCA shell in a convective motion

It was concluded in [2] that nonequilibrium heating is balanced by the change in convective flow, leading to the net cooling due to convective URCA shell. Nine years later same authors [17] changed their mind, concluding that "convective URCA process can reduce the rate of heating by nuclear reactions but cannot result in a net decrease in entropy, and hence in temperature, for a constant or increasing density." This conclusion, as well as opposite one, made by using thermodynamic relations only, seems to be not convincing. Following this line, let us present two plausible scenarios, leading to two opposite conclusions.

A. Due to action of a nonlinear bulk viscosity, the convection is damping in the vicinity of the URCA shell, decreasing the convective heat flux from the central part of the star. In the general heat balance of the star it means that cooling become less effective, and nuclear reactions become thermally unstable and lead to a nuclear explosion earlier, than without a presence of the URCA shell. Nonequibrium heating give additional heating, supporting the earlier nuclear explosion.

B. Due to action of a nonlinear bulk viscosity, the convection is damping in the vicinity of the URCA shell, decreasing the convective heat flux from the central part of the star. Due to local decrease of the heat flux from the core the average temperature gradient increases, leading finally to increase of the convective flux soon after entering an URCA shell into a convective zone. If the increase of the convective flux prevails the nonequilibrium heating in the URCA shell, the general heat balance would be shifted to a larger temperature with more effective cooling, and the boundary of the thermal explosion would be postponed in time, if not eliminated.

I cannot choose between these two scenario without construction of the numerical model taking into account all processes mentioned above. In such a highly nonlinear system, as a star with nuclear reactions, neutrino losses, degeneracy, convection, and many feedback influences it seems to be impossible to make a conclusion about the direction of process under the action of addtional URCA shell, basing only on thermodynamical ground.

Convective modes belong to g-mode family, in which the local pressure perturbations are small, and could be neglected when the convective velocity is much less than the velocity of the sound. In this situation the sound wave dissipation of the convective modes imposed by URCA shell is negligible. The equations of stellar evolution in presence of URCA shell should take into account the following physical processes

1. loss of enegry due to neutrino emission in the URCA shell

2. heating of the matter in the convective region around URCA shell due to nonequilibrium beta processes.

3. Decrease of the convective velocity in the layer around the URCA shell due to energy dissipation connected with the nonequilibrium beta processes. Kinetic energy of the convection is the source of energy for neutrino losses and nonequilibrium heating of the matter. In the condition of static equilibrium only energy and heat transfer equations should be modified. In the energy equation

$$T\frac{dS}{dt} = \frac{dE}{dt} - \frac{P}{\rho^2}\frac{d\rho}{dt} = \epsilon_n - \epsilon_\nu + \epsilon_\nu^{CU} - \frac{1}{4\pi\rho r^2}\frac{dL_r}{dr}, \tag{17}$$

in addition to other neutrino cooling processes ϵ_ν, the new term ϵ_ν^{CU} is connected with heating due to nonequilibrium beta processes around the URCA shell. having in mind strong degeneracy of electrons in this region. Neutrino emission in nonequilibrium URCA processes

is accompanied by heating at high degeneracy, because the positive term $\sum \mu_i dn$ exceed the energy carried away by neutrino (Bisnovatyi-Kogan and Seidov, 1970). Convective motion, consisting of convective vortexes around an URCA shell is a source of additional neutrino energy losses, and of heating of the matter. This dissipation of convective energy may be described in the same way, as corresponding dissipation and heating during stellar pulsations. Therefore we use for description of these processes the formulae from the previous sections. If we accept that the pressure difference in the convective vortex is about one half of the local pressure, we use for the amplitude of pressure pulsations in (13) and (16) $\tilde{P}_a = \frac{\alpha_p}{4} P_*$. Taking also approximately $P_0 = P_*,\ \rho_0 = \rho_*,$ and $u_{fe} = \delta$ we get

$$\dot{Q}_\nu = \tilde{R} \frac{m_e c^2}{A m_p} \frac{\delta^8 \alpha_p^5}{g\, 2^{10} \times 75\pi}, \quad \tilde{R} = \ln 2 \frac{(\delta^2 - 1)^{1/2} \delta}{12 (F t_{1/2})_{Z-1}} \frac{m_e^4 c^5}{12\pi^2 \hbar^3} \left(1 + \frac{g_{Z-1}}{g_Z}\right). \tag{18}$$

Equation (18) is related to energy losses averaged over the whole slab. In the convective motion the losses are localized in the layer around the URCA shell radius r_*

$$r_* + l_{\rm conv} < r < r_* - l_{\rm conv}, \quad l_{\rm conv} = \alpha_p \frac{P}{\nabla P}, \tag{19}$$

here $l_{\rm conv}$ is taken from the mean free path model. The local rate is obtained from (18), if we take into account that the whole heating is concentrated inside the layer (19). We get than

$$\epsilon_\nu^{CU} = \frac{\dot{Q}_\nu}{2 \rho l_{\rm conv}}. \tag{20}$$

Convective velocity suffers from additional damping due to URCA shell, because kinetic energy of the convection is a source of both nonequilibrium heating and of additional neutrino losses. The only relation of the convetional mixing length model of the convetion (see e.g. [3]) should be modified, determining the convective velocity with an additional damping

$$\frac{1}{2} \rho v_{\rm conv}^2 = -\frac{1}{8} (\Delta \nabla T) l^2 \left(\frac{\partial \rho}{\partial T}\right)\Big|_P g - \frac{\dot{E}_{\rm conv}^{(\beta)}}{v_{\rm conv}}, \tag{21}$$

where $\dot{E}_{\rm conv}^{(\beta)} = 4\, \dot{Q}_\nu$ is found from (18). These relations may be applied for description of URCA shell convection only for sufficiently strong convective motion, when the first term in (21) exceeds considerably the second one. The equation (21) has roots only when

$$\dot{E}_{\rm conv}^{(\beta)} < \frac{1}{8\sqrt{\rho}} \left[-\frac{1}{3} (\Delta \nabla T) l^2 \left(\frac{\partial \rho}{\partial T}\right)\Big|_P g\right]^{3/2}. \tag{22}$$

Violation of this inequality may result in an abrupt termination of the convection in the layer (19) around the URCA shell. When analysing the URCA shell convection in star, it would be premature to predict the results of evolutionary calculations with account of convective URCA shell before such calculations are done. Two possibilities may be expected . One is connected with obtaining of a definite result which has a little sensitivity to the input parameters of the problem, such as α_p, $Ft_{1/2}$, accepted rates of nuclear reactions, neutrino losses etc. Another possibility could be a great sensitivity of the result to the same input parameters. If the second possibility would be realized we could still remain in situation of ambiguity, because the set of the input parameters for presupernovae model cannot be established with a sufficient precision.

Acknowledgements

Author is grateful to R.Canal, S.I.Blinnikov, J.Isern, R.Mochkovich for useful discussions; to W.Hillebrandt and E.Müller for the invitations and posssibility to participate in workshops "Nuclear Astrophysics', to O.V.Shorokhov for help. This work was partly supported by Russian Basic Research Foundation grant No. 99-02-18180 and grant of a Ministry of Science and Technology 1.2.6.5.

References

[1] J.M. Aparicio and J. Isern, A&A **272** (1993), 446.

[2] Z. Barkat and J.C. Wheeler, ApJ **355** (1990), 602.

[3] G.S. Bisnovatyi-Kogan, Physical Problems of the Theory of Stellar Evolution. (1989), Moscow, Nauka.

[4] G.S. Bisnovatyi-Kogan and Z.F. Seidov, Astron. Zh. **47** (1970), 139.

[5] G.S. Bisnovatyi-Kogan and Z.F. Seidov, Astrofizika **21** (1984), 563.

[6] S.W. Bruenn, ApJ **183** (1973), L125.

[7] R.G. Couch and W.D. Arnett, ApJ **196** (1975), 791.

[8] E. Ergma and B. Paczyński, Acta Astr. **24** (1974), 1.

[9] M.A. Grinfeld, Dokl. Akad. Mauk USSR **262** (1982), 1342.

[10] P. Haensel, J.L. Zdunik and R. Schaeffer, A&A **217** (1989), 137.

[11] I. Iben Jr., ApJ **219** (1978), 213.

[12] I. Iben Jr., ApJ **253** (1982), 248.

[13] B. Lazareff, A&A **45** (1975), 141.

[14] R. Mochkovitch, A&A **311** (1996), 152.

[15] B. Paczyński, Astr. Lett. **11** (1972), 47.

[16] B. Paczyński, Astr. Lett. **15** (1974), 147.

[17] J. Stein, Z. Barkat and J.C. Wheeler, ApJ **523** (1999), 381.

[18] S. Tsuruta and A.G.W. Cameron, Ap.Sp.Sci. **7** (1970), 374.

Helium Detonations on Neutron Stars

B. Fryxell[1,2], *M. Zingale*[2,3], *F.X. Timmes*[2,3], *D.Q. Lamb*[1,2,3], *K. Olson*[2,3,4], *A.C. Calder*[2,3], *L.J. Dursi*[2,3], *P. Ricker*[2,3], *R. Rosner*[1,2,3], *J.W. Truran*[1,2,3], *P. MacNeice*[4], *H. Tufo*[2,5]

[1] *Enrico Fermi Institute, The University of Chicago*
[2] *Center for Astrophysical Thermonuclear Flashes, The University of Chicago*
[3] *Dept. of Astronomy & Astrophysics, The University of Chicago*
[4] *NASA/Goddard Space Flight Center*
[5] *Dept. of Computer Science, The University of Chicago*

Compelling evidence exists that Type I X-ray bursts are due to thermonuclear flashes on the surfaces of accreting neutron stars. The standard model involves hydrogen thermonuclear runaways occurring in hydrogen/helium shells (see the reviews by [3], [4], [8], [5], and references therein). This model has been remarkably successful in reproducing the basic features of the X-ray burst phenomenon, including the short rise times, the recurrence time scales, the luminosities and energies of the bursts, the spectral softening during the decaying portion of the burst, and the ratio of the time-averaged burst luminosity to the persistent accretion luminosity.

Observations made by the Rossi X-Ray Timing Explorer (RXTE) satellite have revealed that many X-ray bursts exhibit large-amplitude brightness oscillations (see [7] for a review). These brightness oscillations provide evidence that nuclear burning may not be uniform over the surface of the neutron star, and that the oscillations may be due to rotation of the neutron star. An analysis of the brightness oscillations in X-ray bursts from 4U 1636-536 has found evidence that nuclear burning occurs at two nearly antipodal spots on the surface of the neutron star [6]. This result suggests that the dipole magnetic field of the neutron star may succeed in funneling and confining the accreting material onto the magnetic poles. The short time scale for the ignition of the second spot led [6] to suggest that the nuclear burning front propagates laterally around the neutron star as a detonation, rather than as a convective or conductive deflagration. This is consistent with a model in which the ignition of the thermonuclear flash occurs at a single point, and then propagates around the surface of the neutron star. In this context, X-ray bursts constitute a unique "astrophysical laboratory" for the study of thermonuclear flame propagation, a process that also plays a crucial role in Type Ia supernovae and classical novae.

Motivated by the possibility that, in X-ray bursts, the nuclear burning front may spread across the surface of the neutron star as a detonation wave, we have calculated the evolution of a helium detonation through the accreted envelope in two dimensions. These calculations were performed using the FLASH Code [1], an adaptive mesh, multidimensional hydrodynamics code for simulating astrophysical flashes. The calculations we describe here start from the initial model of [2], the only other multidimensional simulation of a helium detonation on an accreting neutron star. This is not the standard picture of an X-ray burst, but we expect many of the qualitative features exhibited in this calculation to be present in any thermonuclear flash on a neutron star.

The initial model consists of a neutron star accreting material from a binary companion at a rate of 2×10^{-11} $M_\odot$ yr^{-1}. As a result of the accretion, a shallow layer of pure helium accumulates on the surface of the neutron star. After the accreted material reaches a sufficient

depth (about 100 m) a thermonuclear runaway initiates at a single point in the layer under degenerate conditions, and a burning front (in this case a detonation) propagates across the surface of the neutron star, igniting the entire accreted layer.

The calculations were performed in two dimensions assuming cylindrical symmetry (r,z) on a grid 2 km wide by 1.5 km high. The smallest zones in the adaptive grid had a spatial resolution of 1 m in each direction. A fully refined grid would contain three million zones (2000 x 1500). The surface of the neutron star is assumed to be planar. Initiation of the runaway at a single point is accomplished by applying a small temperature perturbation to a few zones in the lower left corner of the grid.

The figure shows the density evolution of the neutron star at intervals of 30 μs after initiation of the runaway. The yellow line in the plots marks the transition from helium to nickel. The blue line indicates a density of 10 gm cm^{-3}, which gives a rough idea of the change in location of the surface of the neutron star. The first plot shows the initial model before the initiation of the runaway. At 30 μs, the propagation of the detonation front is clearly marked by the yellow line. The portion of the detonation propagating vertically along the axis has died out because of the lower density and temperature of the fuel. This portion of the burning front turns into a slowly propagating deflagration. At this time, the shock has broken through the surface and is expanding outward at a velocity much faster than the detonation speed.

The detonation front continues to propagate to the right at a velocity of 1.3×10^9 cm s^{-1}. At 60 μs, a Rayleigh-Taylor instability, which is just barely visible in the figure, develops along the deflagration front. The shock wave reaches a maximum height, and then begins to fall back due to the immense gravity of the neutron star. As a result, an oscillation develops with a period of approximately 50 μs. A second Rayleigh-Taylor instability develops along the contact discontinuity behind the shock.

At 90 μs, the photosphere, which is located at the contact discontinuity, is pushed upward off the grid and reaches an estimated height of 10 km. At this time, strong nonlinear waves can be seen propagating along the surface. The velocity of these waves is almost identical to that of the detonation front, which is consistent with shallow water wave theory. The breaking of the first wave ahead of the detonation is clear visible.

The final two plots, at 120 μs and 150 μs, show the continued propagation of the detonation and the surface waves, as well as the turbulent motions in the low density material above the surface. The detonation will continue to propagate through the accreted material, igniting the entire layer on a time scale of 3 ms.

Future calculations will look at different initial models, where the burning initiates at lower densities. In this case, the burning front will propagate as a deflagration wave rather than as a detonation. The calculations will also be extended to three spatial dimensions and the effects of magnetic fields and rotation of the neutron star will be included.

Acknowledgments

This work was supported by the Department of Energy under Grant No. B341495 to the Center for Astrophysical Thermonuclear Flashes at the University of Chicago. These calculations were performed on the Nirvana Cluster at Los Alamos National Laboratory and an SGI Origin 2000 at Argonne National Laboratory. Movies of the simulation can be found by following the gallery link off the Flash Center web page: http://www.flash.uchicago.edu.

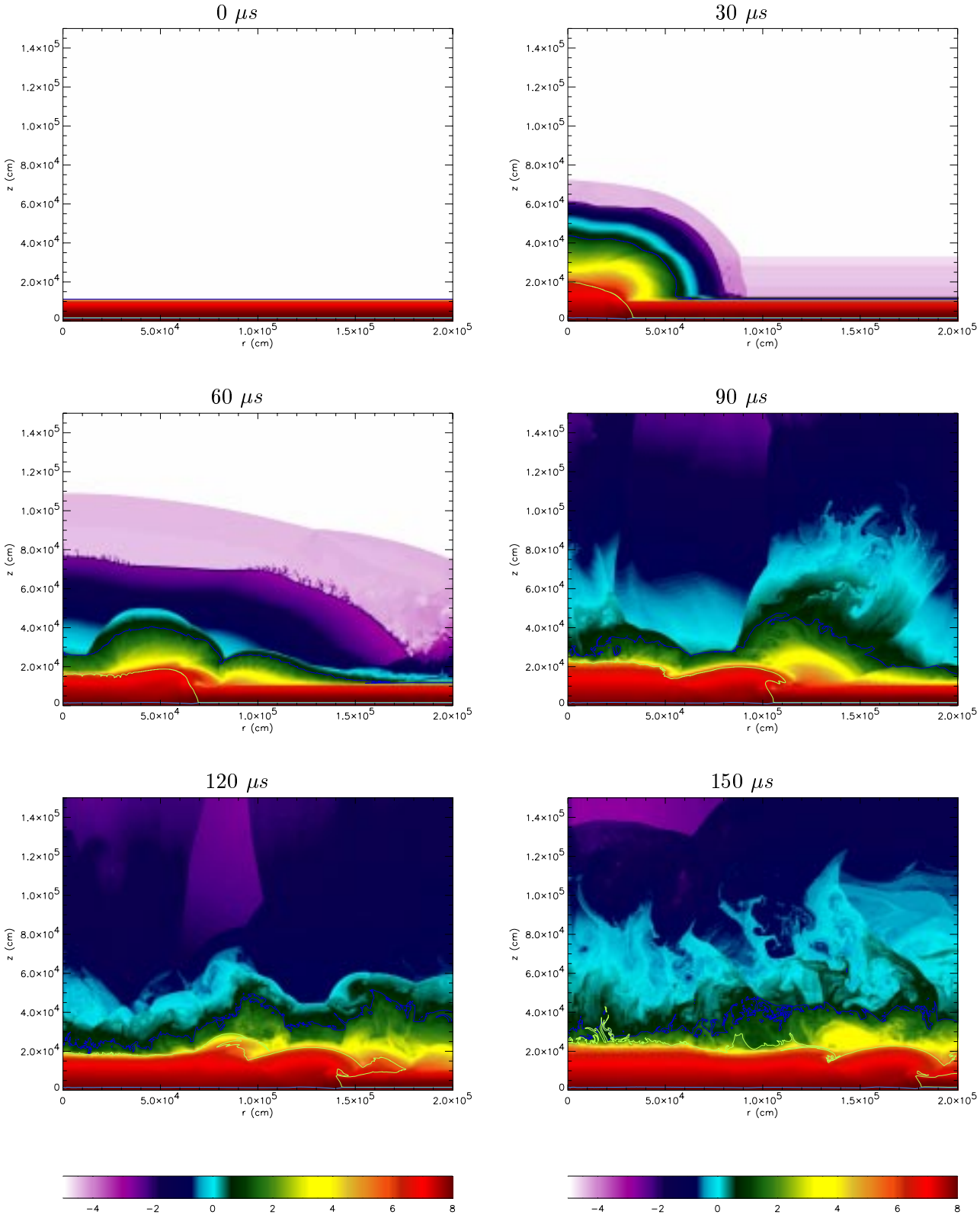

Density evolution of the helium detonation calculation shown every 30 μs.

References

[1] B. Fryxell, K. Olson, P. Ricker, F.X. Timmes, M. Zingale, D.Q. Lamb, P. MacNeice, R. Rosner, & H. Tufo, H., Ap. J. Supplement, in press (2000).

[2] B. Fryxell & S.E. Woosley, Ap. J., **258** (1982) 733.

[3] W.H.G. Lewin & P.C. Joss, SSRv, **28** (1983) 3.

[4] W.H.G. Lewin and P.C. Joss, in Accretion Driven Stellar X-Ray Sources, ed. W.H.G. Lewin and E.P.J. van den Heuvel (Cambridge: Cambridge U. Press) (1983) p. 41.

[5] W.H.G. Lewin, J. van Paradijs, & R.E. Taam, SSRv, **62** (1993) 223.

[6] M.C. Miller, Ap. J., **515** (1999) L77.

[7] T.E. Strohmayer, J.H. Swank, & W. Zhang, in Proceedings of the Symposium "The Active X-Ray Sky: Results from BeppoSAX and Rossi-XTE", Rome, Italy, 21-24 October, 1997, Nuclear Physics B Proceedings Supplements. Eds. L. Scarsi, H. Bradt, P. Giommi, and F. Fiore (astro-ph/9801219) (1998).

[8] R.E. Taam, Ann. Rev. Nuc. Part. Sci., **35** (1985) 1.

Type Ia supernova simulations: The quest for more energy

M. Reinecke[1], *W. Hillebrandt*[1]

[1] *Max-Planck-Institut für Astrophysik, Karl-Schwarzschild-Str. 1, D-85740 Garching, Germany*

1.1 Introduction and motivation

Since the late sixties, the simulation of type Ia supernova explosions has been a challenging task in numerical astrophysics, which has been approached by researchers in two principally different ways:

- While some of the empirical models — most notably the W7 model described in [1] — succeed in reproducing the observed spectra and light curves, they all share the disadvantage of free parameters whose choice cannot be motivated by theoretical considerations.
- Simulations that try to describe the explosion process purely based on first principles, on the other hand, failed to reproduce all the observables up to now, since they either predict a sufficient amount of released energy but the wrong chemical composition [2] or insufficient energy to unbind the progenitor star.

Nevertheless a proper understanding of the physical processes during a SN Ia is becoming more and more important in order to interpret the data obtained by the recent searches for high-redshift supernovae [3]. So far the empirical Phillips relation is used to calibrate the maximum absolute brightness of those distant events and then deduce constraints for H_0, q_0 and Ω_Λ, but a real understanding of this connection between absolute brightness and light curve shape would put those results on a firm theoretical foundation and greatly improve their acceptance.

1.2 Problem specification

In the following we will adopt the most widely accepted progenitor model for SNe Ia, consisting of an accreting C/O white dwarf which is disrupted by thermonuclear fusion reaction shortly before reaching the Chandrasekhar mass.

Probably the greatest difficulty of such simulations is the inherent multidimensionality and the extremely large range of involved length scales in these events. If we neglect the prompt detonation scenario (which produces results that are in clear contradiction with the observations), the explosion starts out as a thin subsonic reaction zone near the center of the white dwarf, where ^{12}C and ^{16}O are fused, in several steps, to ^{56}Ni. The width of this flame is well below 1mm, opposed to the star radius of $\approx$ 1000km. Moreover, this flame is subject to the hydrodynamical Rayleigh-Taylor and Kelvin-Helmholtz instabilities that lead to the formation of wrinkles on scales between $\approx$ 1cm and 100km and generate highly turbulent, inherently three-dimensional flow.

From those facts the following conclusions for a parameter-free simulation can be drawn:

- Any 1D calculation will not be able to describe the turbulence effects accurately enough and is therefore not suitable for our purpose. Even two-dimensional simulations cannot reproduce all effects of turbulent combustion properly and will most likely underestimate the energy generation rate. Only the simulation of all three spatial dimensions can be expected to give reliable results.
- Since it is not possible to resolve all relevant length scales on the computational grid, appropriate models must be incorporated to account for turbulent wrinkling of the thermonuclear flame on scales below the grid cell length.

1.3 Employed numerical models

For the solution of the Euler equations on the resolved scales, the PROMETHEUS code [5] was employed. The equation of state includes contributions of an arbitrarily relativistic and degenerate electron gas, the Boltzmann gas of the ionized nuclei, a photon gas and electron-positron pairs.

For the modeling of the turbulent flame propagation speed, the sub-grid model described in [6] was used. It must be noted here that this approach only gives reliable results as long as the burning takes place in the so-called *flamelet regime*, which is the case as long as $\rho > 10^7 \mathrm{g/cm}^3$ in a SN Ia. At lower densities burning was disabled for our preliminary calculations, so that our preliminary results for the total energy release must be interpreted as a lower limit.

To describe the geometry of the turbulent flame, we have made use of the so-called *level set method* which describes the $(n-1)$-dimensional front Γ as the zero level set of a n-dimensional function $G(\vec{r}, t)$:

$$\Gamma(t) := \{\vec{r} \mid G(\vec{r}, t) = 0\}$$

The temporal evolution of G is given by the PDE

$$\frac{\partial G}{\partial t} = (\vec{v}_F \vec{n} + s)|\vec{\nabla} G|,$$

where $\vec{n}$ is the front normal, $\vec{v}_F$ denotes the advection velocity and s is the burning speed obtained from the sub-grid model. This approach models the flame as a sharp discontinuity which is a more realistic approximation than the diffusive models used for SNe Ia so far. As a consequence, the formation of small structures in the front geometry is no longer suppressed by numerical diffusion, which becomes evident in Fig. 1.

A detailed description of the level set method and its integration into our hydrodynamical code is given in [7].

1.4 Early results

The first supernova simulations with the code described above were done on a 2-D cylindrical grid with 256^2 cells, assuming axial symmetry in the φ-direction (see Fig. 1). In the early phases the nonlinear growth of the RT-instability can be clearly observed, at later stages ($t \geq 1\mathrm{s}$) the formation of KH-instability becomes visible. It is apparent that the use of the level set model allows the formation of flame perturbations even on very small scales near the grid length, in contrast to the reaction-diffusion approach taken by, e.g., [4]. The

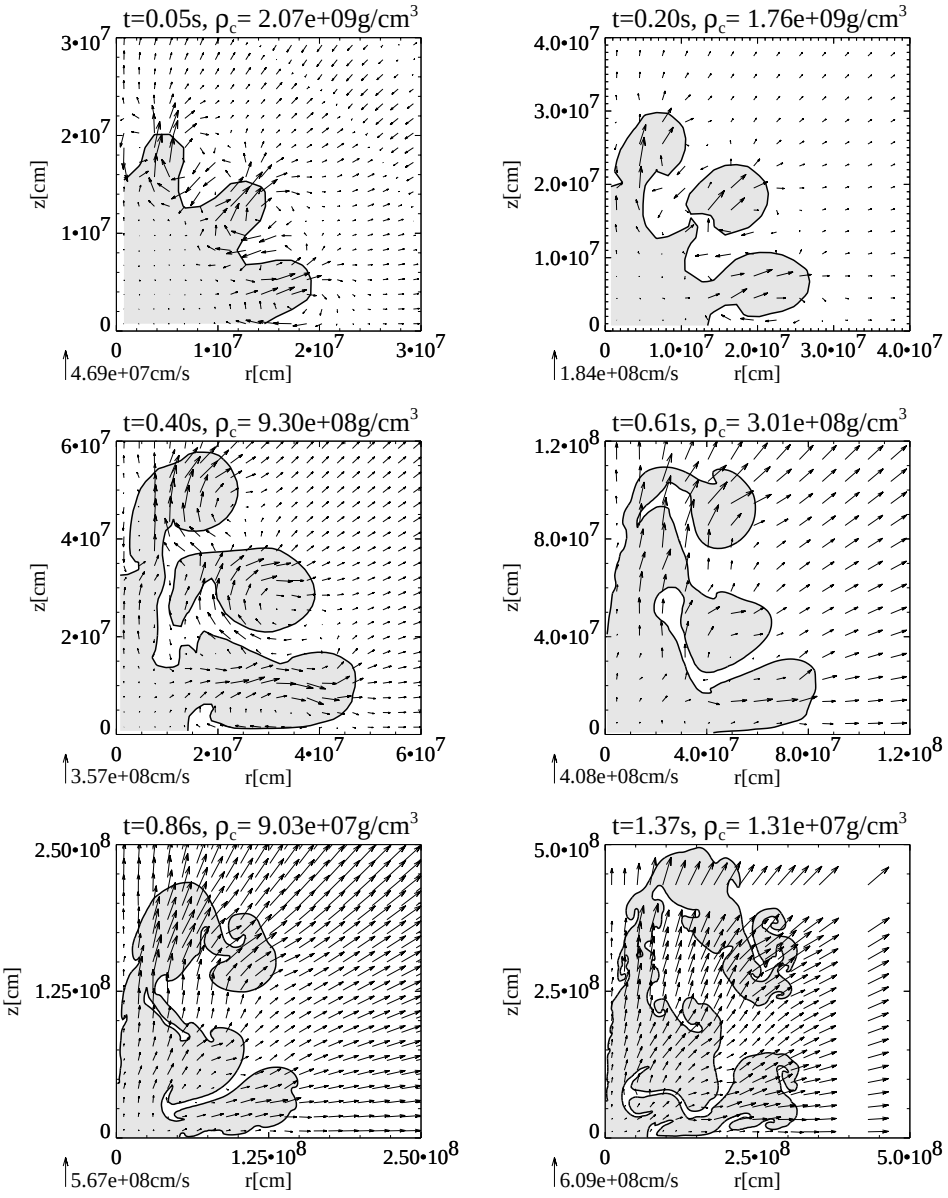

Figure 1: Temporal evolution of the front geometry of the two-dimensional model C3. Note that the scale changes with every snapshot.

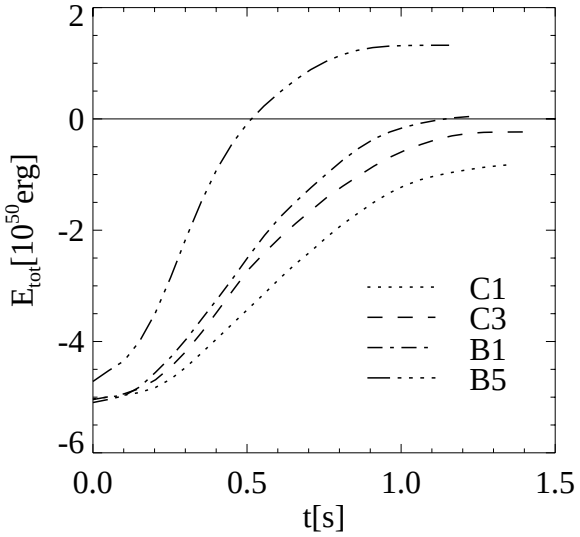

Figure 2: Evolution of the total energy for the various two-dimensional initial conditions

temporal evolution of the total energy for different initial flame geometries is shown in Fig. 2. As supposed in section 1.2, the energy produced during the 2D simulations is clearly not sufficient to power a typical SN Ia.

The setup and results of our 2D simulations are discussed in detail in [8].

The transition to three dimensions results in a considerably higher energy release. Fig. 3 shows a direct comparison of a 2D and 3D run with identical initial conditions; obviously, the removal of the axial symmetry constraint allowed for more structure in the flame, thus increasing the energy generation rate.

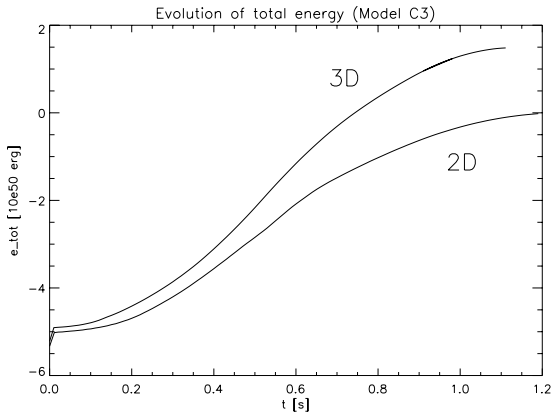

Figure 3: Comparison of the energy release for identical initial conditions in 2D and 3D

1.5 Conclusions

The results presented above indicate clearly that our current code still fails to reproduce the characteristics of a typical SN Ia because the total energy release is too low; all is not lost, however, since there is still room for improvements in the models for the turbulent flame propagation speed and the numerical description of the burning front. These changes are expected to result in a noticeably higher energy release. In any case the three-dimensional simulations release enough energy to unbind the star, which is a strong indication against the pulsational explosion models.

References

[1] K. Nomoto, F.K. Thielemann and K. Yokoi, ApJ **286** (1984) 644.

[2] W.D. Arnett, Astrophys. Space Sci. **5** (1969) 280.

[3] A.G. Riess, P.E. Nugent, A.V. Filippenko, R.P. Kirshner and S. Perlmutter, ApJ **594** (1998) 935.

[4] J.C. Niemeyer and W. Hillebrandt, ApJ **471** (1996) 903.

[5] B.A. Fryxell, E. Müller and W.D. Arnett, MPA Green Report **449** (1989).

[6] J.C. Niemeyer and W. Hillebrandt, ApJ **452** (1995) 769.

[7] M. Reinecke, W. Hillebrandt, J.C. Niemeyer, R. Klein and A. Gröbl, A&A **347** (1999) 724.

[8] M. Reinecke, W. Hillebrandt and J.C. Niemeyer, A&A **347** (1999) 739.

Some remarks on distributed burning in type Ia supernovae

W. Hillebrandt and A.M. Lisewski

Max-Planck-Institut für Astrophysik,
Karl-Schwarzschild-Str. 1, 85740 Garching, Germany

1.1 Abstract

We present results based a statistical description of a thermonuclear flame propagating in C+O white dwarf matter in the distributed burning regime. Based on a Monte Carlo description of turbulence we show that in this particular regime the flamelet model for the turbulent flame velocity loses its validity. In fact, at high turbulent intensities burning in the distributed regime can lead to a deceleration of the turbulent flame and thus induces a competing process to turbulent effects that cause a higher flame speed. We also show that the available turbulent energy in an exploding C+O white dwarf is probably too low in order to make a deflagration to detonation transition possible.

1.2 Introduction

The thermonuclear explosion of a C+O Chandrasekhar-mass white dwarf, which is believed to be the underlying process of a type Ia supernova (SN Ia), has been subject to numerous investigations. However, despite the fact that there are different plausible models explaining the history of the explosion ([15]; [18]; [12]; [11]; [6]; [1]; [13]; [3]; [Höflich 1995]; [17]; [4]), many important details still remain unclear. Thermonuclear reactions provide the source of energy which, very likely, unbinds the white dwarf. Thus, a SN Ia is characterized by the physics of thermonuclear flames that propagate through the star. The physical conditions of this flame vary drastically during the different temporal and spatial stages of this process. A better understanding of these conditions, their interaction with the flame and finally their consequences regarding the explosion itself are still important issues from the theoretical point of view.

Here, we focus on the interaction between thermonuclear burning and turbulence taking place during the burning process. Turbulence is caused by different kinds of instabilities (like shear instabilities or the Rayleigh-Taylor instability) that occur on certain length and time scales (for an overview, see [14]). Rough estimates give a turbulent Reynolds number $\mathrm{Re} \approx 10^{14}$ at an integral scale of $L \approx 10^6\,\mathrm{cm}$ ([2]). Consequently, the Kolmogorov scale l_k, i.e. the scale where microscopic dissipation becomes important, is about $10^{-4}\,\mathrm{cm}$. It is obvious, therefore, that turbulence is a characteristic feature during the explosion process and it must be considered in any realistic model of a SN Ia. The simultaneous coupling to energy generation due to nuclear reactions leads directly to the physics of turbulent combustion, where a few crucial problems, even for terrestrial conditions, still remain unsolved. These problems include the prescription of the effective turbulent flame speed or the existence of different modes in turbulent combustion along with their physical properties.

In this work we study the properties of turbulent flames in a certain state, the so-called *distributed flame regime*. The physical characterization of the latter is given by the situation

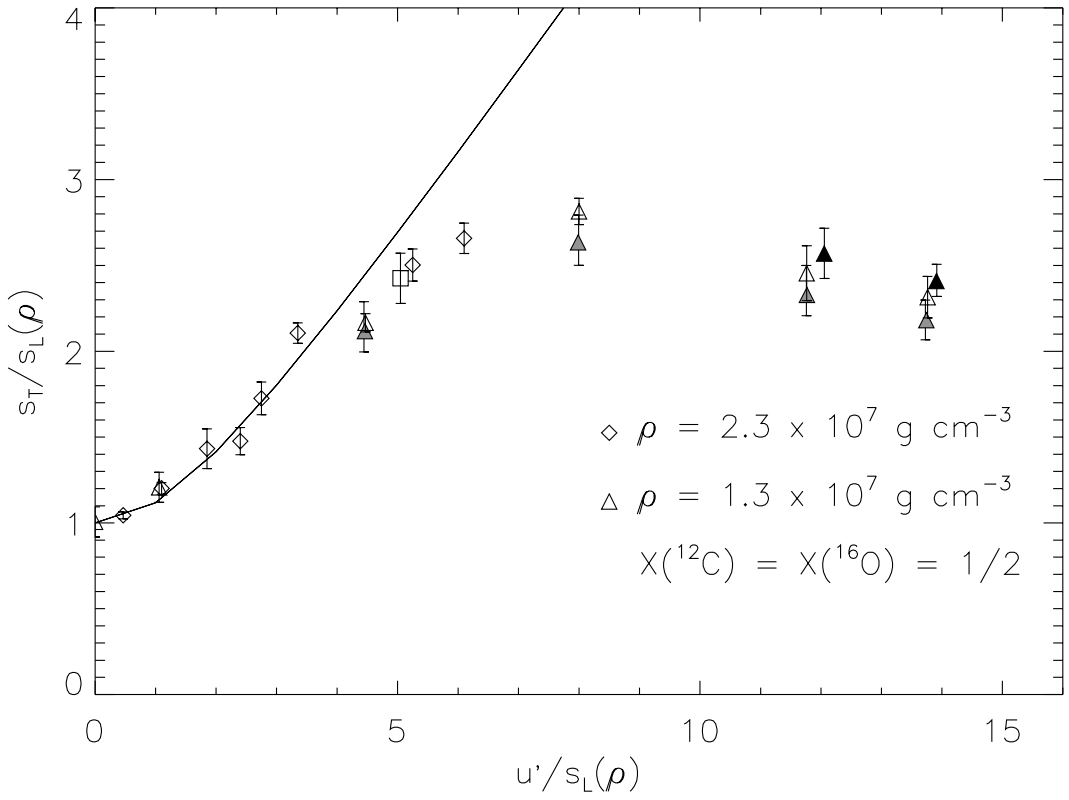

Figure 1: The dimensionless turbulent flame speed as a function of the dimensionless r.m.s. turbulent velocity fluctuations. At high strain rates there is a strong deviation from the flamelet model, which predicts $U_{\rm T} = (1 + \beta U^2)^{1/2}$ (solid curve with $\beta = 0.24$), (see for instance [16]). One numerical realization is depicted by a box The two black triangles give the results from other realizations having a four-times higher spatial resolution. The gray triangles represent speeds obtained by a different method, see [9] for more details.

where turbulent motions are fast enough to disturb the flame on microscopic scales. Therefore a distributed flame does locally not look like a laminar flame anymore which is a basic difference to turbulent flames in the flamelet regime. Turbulent burning fronts in an exploding white dwarf are flamelets at high and intermediate densities, but below $\sim 5 \times 10^7$g cm^{-3} one cannot expect that the flamelet picture is still valid ([14]).

1.3 One-Dimensional Turbulence

In order to attempt a representation of turbulent dynamics in the distributed flame regime, we use a model, formulated in one spatial dimension, which nevertheless provides essential features of three dimensional homogeneous turbulence. It consists of a statistical description of turbulent mixing and a deterministic evolution of the underlying microphysics. This method allows a systematical investigation of turbulence phenomena. When it is coupled to a nuclear reaction network, it gives first insights of how the flame structure is affected by turbulence on scales, which have not been resolved in direct numerical simulations. In particular, we investigate the flame properties in cases where the Gibson scale is comparable to the thickness of an undisturbed conductive flame. The Gibson scale $l_{\rm G}$ is defined as the length scale on

which the turbulent velocity fluctuations equal the laminar flame velocity. In the case of flames in degenerate white dwarf matter $l_{\rm G}$ becomes comparable to the thickness of the flame only for densities around 2×10^7 g cm^{-3} and below ([7]; [14]).

Since fundamental aspects of turbulence can be recovered from the knowledge of the statistical moments and correlations of the velocity flow, the statistical approach to turbulence is particularly appealing. Here we present a novel model of turbulence ([5]). It is a stochastic method, realized as a Monte Carlo simulation, which allows to compute statistical properties of the flow velocity and of passive scalars in stationary and decaying homogeneous turbulence. One-dimensional turbulence (ODT) represents many aspects of three-dimensional turbulence, but it is formulated in only one spatial dimension. It provides the temporal evolution of a characteristic transverse velocity profile $u(y,t)$ of the turbulent medium, where y is the spatial location on a finite domain $[0, Y]$ and t is the elapsed time. This is done in a two-fold way: $u(y,t)$ is subject to a molecular diffusion process and to a random sequence of profile rearrangements representing turbulent eddies. Reflecting the typical behavior of turbulence kinematics, the event rate of these profile rearrangements (so-called eddy mappings) is proportional to a locally averaged shear of the velocity profile u (see [5] and [9] for more details). An obvious advantage of this *ansatz* is the high spatial resolution of turbulence compared with multidimensional numerical models. In combination with the relatively moderate computational effort, ODT appears as a useful tool for performing parameter studies in turbulence theory. On the other hand, ODT does not consider any pressure fluctuations (dynamical or external) in the temporal evolution of the velocity profile u. However, for isobaric flows ODT appears to be an appropriate model of turbulence ([9]).

1.4 Turbulent Flames in Dense C+O Matter

The Gibson scale $l_{\rm G}$, defined earlier, can be used to measure the influence of turbulence on a flame. Here, we put our emphasis on the special situation where homogeneous, isotropic turbulence interacts with the microscopic structure of the laminar flame, i.e. where $l_{\rm G}$ becomes comparable to $\delta_{\rm l}$. The relation $l_{\rm G} \approx \delta_{\rm l}$ marks the transition into the distributed burning regime, where the smallest turbulent vortices can enter the interior of the laminar flame and can carry away reactive material before it is completely burned.

In our numerical simulations we choose the amplitude of velocity fluctuations of u to be $\sim 10^7$ cm s^{-1} at $\sim 10^6$ cm, and to obey Kolmogorov scaling. These values are motivated through the expected speed of buoyant unstable hot bubbles of size $L \approx 10^6$ cm, which become Rayleigh-Taylor unstable and eventually give the main contribution to turbulent energy on large scales. Having fixed this velocity at a certain length-scale, we can use Kolmogorov scaling to estimate $u'(l)$ on smaller scales l. Thus the amplitude of turbulent velocity fluctuations in our model is comparable to the expected small-scale velocity fluctuations within a SN Ia.

Our main results are shown in Figure 1. It clearly demonstrates that the turbulent flame speed at high turbulent strain rates, $U \gg 1$, does not follow a law valid in the flamelet regime. In the distributed burning regime there is a significant deviation from this law: stronger turbulent intensities do not necessarily lead to a faster burning rate. This effect is more pronounced in the low-density case, where higher turbulent velocities even cause a slight deceleration of the flame speed. This result confirms the intuitive picture that fast flames (flames at higher density) are more resistant to distortion through turbulence than the slower ones (flames at lower density), in agreement with laboratory experiments. However, we do not find complete flame quenching.

Thermonuclear flames in the distributed regime thus experience a two-fold effect through turbulence: One is the acceleration due to an enhancement of the heat transport produced by small-scale turbulence. The other is a slowing-down due to additional turbulent strain. However, we have to stress that we do not have revealed the actual physical mechanism responsible for the deceleration.

1.5 Some remarks on deflagration-to-detonation transitions (DDT)

Finally we briefly address the question whether burning in the distributed regime alone can lead to a DDT. Niemeyer & Woosley (1997) advocated this burning mode as a favorite model for DDT. Basically, they proposed that if turbulent burning is able to form a region of incompletely burned material with a certain temperature gradient, then a carbon detonation can occur when two presumptions are fulfilled. First, the aforementioned region must have at least a size of the critical radius necessary for a detonation (These critical radii could be calculated explicitly for different densities and nuclear compositions, see Niemeyer & Woosley 1997.). Second, the temperature gradient must be shallow enough in order to allow a sonic phase velocity of nuclear burning. For instance, consider a mixed region consisting of half carbon and oxygen at a density of 3×10^7g cm^{-3} and having a maximum temperature of $T_{\max} = 2 \times 10^9$ K. It then follows that this region must have a size of at least $L_c \sim 50$ m. Furthermore, temperature differences within it should not exceed $\sim 10^5$ K. Then a stable detonation wave can form. However, until now, it has not been demonstrated how turbulence can achieve or lead to such a high level of temperature homogeneity. In fact, our studies show ([10]) that a DDT in supernova matter is very unlikely, even in the distributed regime of nuclear burning.

1.6 Conclusions

The aim of this work was to investigate the physics of distributed burning in an exploding white dwarf of Chandrasekhar mass. With ODT as a new model for homogeneous, isotropic turbulence we are able to study the effective turbulent flame speeds resulting from this kind of burning in dense C+O matter. Our results show that in this regime the local properties of the thermonuclear flame are changed: the flame cannot be represented by the flamelet model anymore and moreover, higher turbulent intensities in general can lead to a lower local flame speed. This behavior has already been observed in laboratory experiments and is introduced the first time in the context of nuclear explosions in type Ia SNe. Using this method we also find that the conditions for a direct DDT are not met in these white dwarfs.

This work was supported by the Deutsche Forschungsgemeinschaft and the Deutscher Akademischer Austauschdienst.

References

[1] Arnett, W.D., and Livne, E. 1994, Astrophys. Journal, 427, 314

[2] Hillebrandt, W., and Niemeyer, J.C. 1997, in Thermonuclear Supernovae, ed. Ruiz-Lapuente et al., Dordrecht: Kluwer, 337

[Höflich 1995] Höflich, P. 1995, Astrophys. Journal, 443, 89

[3] Höflich, P., Khokhlov, A.M., and Wheeler, J.C. 1995, Astrophys. Journal, 444, 831

[4] Höflich, P., Khokhlov, A.M. 1996, Astrophys. Journal, 457, 500

[5] Kerstein, A.R. 1999, One–dimensional Turbulence, J. Fluid Mech., in press

[6] Khokhlov, A.M. 1991a, Astron. & Astrophys. , 245, 114

[7] Khokhlov, A.M., Oran, E.S., and Wheeler, J.C. 1997, Astrophys. Journal, 478, 678

[8] Lisewski, A.M. 1999, Astrophys. Journal, accepted for publication

[9] Lisewski, A.M., Hillebrandt, W., Woosley, S.E., Niemeyer, J.C., and Kerstein, A.R. 2000, Astrophys. Journal, in press

[10] Lisewski, A.M., Hillebrandt, W., Woosley, S.E. 2000, Astrophys. Journal, in press

[11] Livne, E. 1993, Astrophys. Journall, 406, L17

[12] Müller, E., and Arnett, W.D. 1986, Astrophys. Journal, 307, 619

[13] Niemeyer, J.C., and Hillebrandt, W. 1995, Astrophys. Journal, 452, 769

[14] Niemeyer, J.C., and Woosley, S.E. 1997, Astrophys. Journal, 475, 740

[15] Nomoto, K., Thielemann, F.-K., and Yokoi, K. 1994, Astrophys. Journal, 286, 644

[16] Pocheau, A. 1994, Phys. Rev. E, 49, 1109

[17] Wheeler, J.C., Harkness, R.P., Khokhlov, A.M., and Höflich, P. 1995, Phys. Rep., 256, 211

[18] Woosley, S.E., and Weaver, T.A. 1986, in Radiation Hydrodynamics in Stars and Compact Objects, eds. S.A. Bludman, R. Mochkovitch, J. Zinn-Justin, Amsterdam: Elsevier, 62

Simulation of the convective Urca process in white dwarfs

A. Kercek, M. Brüggen

Max-Planck-Institut für Astrophysik, Garching, Germany

1.1 Introduction

Type Ia supernovae are believed to be exploding carbon-oxygen white dwarfs close to the Chandrasekhar mass. Once the star reaches the Chandrasekhar mass by accretion of mass from a companion star the temperature and density in its center become high enough for explosive carbon burning to take place which leads to the complete disruption of the star.

For about three decades it has been speculated whether there could be a cooling mechanism close to the stellar center which is effective enough to provide a delay of the explosion of the star. As a consequence, the detonation itself could occur at higher central densities yielding a higher fraction of neutron rich nuclei in the ejecta.

The possible cooling mechanism proposed by [1] is the so called *convective Urca process* (CUP). The Urca process consists of two nuclear reactions, namely an electron capture and a subsequent β-decay reaction as, for instance, for the Na-Ne Urca pair:

$$\mathrm{e}^- + {}^{23}_{11}\mathrm{Na} \rightarrow {}^{23}_{10}\mathrm{Ne} + \nu_\mathrm{e} \quad (1)$$

$$ {}^{23}_{10}\mathrm{Ne} \rightarrow {}^{23}_{11}\mathrm{Na} + \mathrm{e}^- + \bar{\nu}_\mathrm{e} \quad (2)$$

where the electron has to be above a certain threshold energy ϵ_th in order to be captured by the sodium nucleus. Within the white dwarf the matter is electron degenerate and consequently electron capture can only occur where $\epsilon_\mathrm{f} > \epsilon_\mathrm{th}$, whereas β-decay can only take place in regions where $\epsilon_\mathrm{f} < \epsilon_\mathrm{th}$. A shell where $\epsilon_\mathrm{f} = \epsilon_\mathrm{th}$ marks the border between those two regions and is called the Urca shell.

In white dwarfs shortly before blow-off the Na-Ne Urca shell is located at a radius of about 400 km. At this stage central carbon burning drives a convective region which also contains the Urca shell. As a consequence, Na and Ne nuclei are continuously carried across the Urca shell undergoing electron capture and β-decay on the respective sides of the Urca shell. The neutrinos emitted in this process leave the star unhindered and carry away energy from the central regions of the white dwarf and thus may provide cooling and a delay of the detonation.

This simple picture of the CUP was contested by many authors up to date providing different answers to the problem and based either on the first or the second law of thermodynamics or on one-dimensional hydrodynamical simulations (See references in [2]). Some analyses are in favor of a cooling CUP, others conclude that it is heating. Ref. [2] provides a recent summary of the CUP.

The time scales in the convective core shortly before the thermonuclear carbon burning runs away are $\tau_\mathrm{d} \sim$ few 10 ms, $\tau_\mathrm{conv} \sim$ few 1000 s, $\tau_\mathrm{nuc} \sim 10^{12}$ s and $\tau_\mathrm{therm} \sim 10^{12}...10^{13}$ s, where τ_d is the dynamical time scale, τ_conv the convective time scale, τ_nuc the nuclear reaction time scale and τ_therm the thermal time scale. Thus, $\tau_\mathrm{d} \ll \tau_\mathrm{conv} \ll \tau_\mathrm{nuc} \leq \tau_\mathrm{therm}$.

On time scales, where the nuclear reactions are important or the thermal content of the star changes convection can be regarded as a stationary process.

According to Ref. [2] the entropy in the core cannot be reduced by the CUP. As stated previously ([3, 4, 5]) the CUP can only reduce the rate of heating but cannot lead to net cooling. Only the rate of heating can be reduced. The Urca neutrino losses and dissipation can damp convective motions and thus indirectly influence the carbon burning at the very center of the core.

1.2 The Problem

But how do the convective motion and the associated transport of nuclear species and energy influence the Urca energy generation rates? Does the Urca energy generation rate strongly depend on the strength of convection or can it flip from heating to cooling and vice versa as for instance in the careful analysis of Ref. [6].

To investigate this question we performed a set of two-dimensional simulations. We did not simulate the convection self-consistently but rather parameterized it in the way that we superimposed convective motions of different velocities in circular patterns. This shall be done for some overturn times in order to run into a quasi-static situation. Then the Urca energy production rates are calculated to verify if they lead to heating or cooling.

1.3 Calculation

As an initial model we used a one-dimensional model of a white dwarf from Dunina-Barkovskaya which has a convective core including a Na-Ne Urca shell. The carbon burning luminosity is $L \sim 1000 L_\odot$ and the central temperature and density $T = 3 \cdot 10^8$ K and $\rho = 3 \cdot 10^9$ g/cc, respectively. The model was mapped on a two-dimensional grid with 200 uneven radial and 180 angular (ϕ) grid points. The grid covered a radius of 500 km and a total opening angle of π.

We used PROMETHEUS, a hydro-solver for reactive flows based on the ppm scheme with a realistic equation of state for white dwarf matter. For the Urca reactions rates we used approximations given by Ref. [7].

We have chosen convective velocities from 10^4 to 10^6 cm/s. Rough estimates predict a convective velocity in the order of 10^4 to 10^5 cm/s for the model.

1.4 Results

The Figure shows a snapshot of the convective flows in a run that started out with convective rolls with a convective velocity of 10^5 cm/s after 0.1 turnover times. The arrows mark the velocity field while the underlying contour plot represents the Urca energy generation rate. Bright colors represent regions with Urca heating whereas dark regions represent Urca cooling.

A broad heating shell with a generation rate of 10^5 erg/g/s is clearly visible at a radius of about 300 km. On top of it there is a comparably thin cooling shell at about 380 km apart from the center and energy generation rate of about $0.6 \cdot 10^5$ erg/g/s. The corresponding Na-Ne Urca shell is located in between. The integration of the rates over the volume gives a total energy generation rate from the Urca processes of about $7 \cdot 10^{36}$ erg/g which means that in this model the CUP leads to heating.

We did not get into a steady state convection phase for any of the runs yet. In order to lower the mixing time scale we used initial convective velocities as high as 10^6 cm/s. Even

in this case we only computed one turnover time of the convective eddies. This phase can be considered as a transition phase hopefully into a steady state condition. But, in none of the cases we met a dramatic change of the overall energy production by the CUP. The CUP remains heating. Surely, the simulation has to be extended towards longer times, to give a firm estimation of the behavior of the Urca energy generation terms.

1.5 Figures

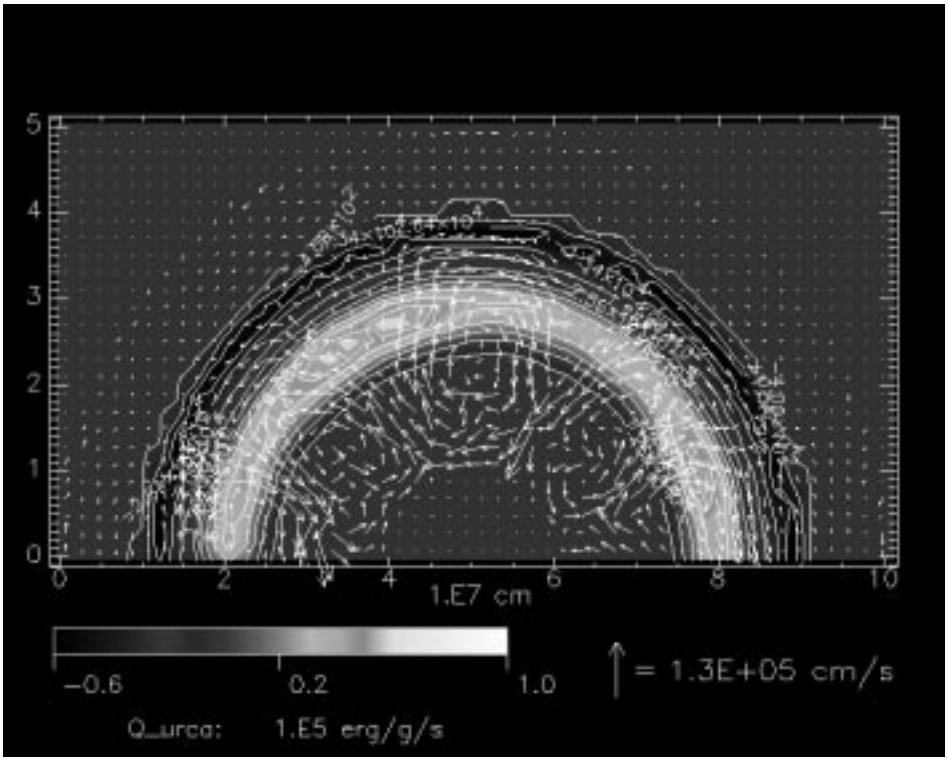

Figure 1: Velocity field and Urca energy generation terms (contours).

Acknowledgements

We thank Natalia Dunina-Barkovskaya for providing us with the initial white dwarf model. We are grateful for many helpful discussions with Wolfgang Hillebrandt, Sergei Blinnikov and Gennadi Bisnovaty-Kogan. All calculations were performed on a Cray T3E 600 at the Rechenzentrum Garching.

References

[1] B.E. Paczyński, ApLett **11** (1972) 53.

[2] J. Stein, Z. Barkat and J.C. Wheeler, ApJ **523** (1999) 381.

[3] G.S. Bisnovaty-Kogan and Z.F. Seidov, Astron. Zh. **47** (1970) 139.

[4] B. Lazareff, A&A **45** (1975) 141.

[5] R. Mochkovitch, A&A **311** (1996) 152.

[6] I. Iben ApJ **253** (1982) 248.

[7] N.V. Dunina-Barkovskaya, Astron. Lett. **22** (1996) 499.

The role of NCO reaction chain on the He ignition in degenerate stellar structures

L. Piersanti [1,2], *S. Cassisi* [2] & *A. Tornambé* [2,3]

[1] *Dipartimento di Fisica dell'Università degli Studi di Napoli "Federico II", Mostra d'Oltremare, pad. 20, 80125, Napoli, Italy, luciano@astrte.te.astro.it*
[2] *Osservatorio Astronomico di Collurania, Via M. Maggini, 64100, Teramo, Italy, cassisi@astrte.te.astro.it*
[3] *Dipartimento di Fisica dell'Università degli Studi de L'Aquila, via Vetoio, 67100, L'Aquila, Italy, tornambe@astrte.te.astro.it*

Some 25 years ago [5] it has been suggested that the $^{14}N(e^-,\gamma)^{14}C(\alpha,\gamma)^{18}O$ reaction (NCO reaction chain) plays a pivotal role in the onset of the Helium flash in the core of a low mass Red Giant Branch (RGB) star (see [3] and [4]). In fact in the He core the Fermi energy is large enough to approach the energy for the e-capture on ^{14}N well before the 3α reactions produce energy at a significant level so that a not negligible amount of ^{14}C is produced in the most internal regions. In the physical conditions typical of a star approaching the tip of the RGB α captures on ^{14}C dominate over 3α reactions. In 1980 [6] argued that the NCO reaction does not affect the He ignition in a star at the tip of RGB because the physical conditions in the inner region, particularly the density, do not allow the NCO reaction to be dominant over the 3α reaction. Successively, in 1986, Hashimoto, Nomoto, Arai & Kaminisi [1] recomputed the NCO cross sections and found that this reaction "... dominates over 3α reaction to heat up the central region" of a low mass star approaching the tip of the RGB [2].

Woosley & Weaver [8] accounted for this reactions chain to compute the pre-supernova models of cooled down CO WDs accreting He rich matter. They find that the inclusion of NCO reaction does not prevent the occurrence of an He detonation. Recently, Piersanti, Cassisi, Iben & Tornambé ([7]) have included the NCO chain in the evolution of a low mass CO WD accreting H and He rich matter at a rate suitable to obtain an He detonation. Their investigation shows that the differences determined by the inclusion of the NCO chain are negligible, the final outcome remaining an explosion. They point out that their result is due to the fact that they use an evolutionary model, obtained by evolving an intermediate mass star with moderate mass loss from the Main Sequence phase till the cooling sequence. In such a model the ^{14}N abundance at the base of the He shell, where the He flash takes place, is zero.

In any case it is important to evaluate if the $^{14}N(e^-,\gamma)^{14}C(\alpha,\gamma)^{18}O$ reaction plays some role in stellar evolution. In fact if this chain does trigger the onset of the central He flash in low mass star then it stops the growth in mass of the He core, modifying the luminosity level of the RGB tip and of the Horizontal Branch. In addition, if the NCO chain plays a role in heating up the He shell in low mass CO WDs accreting hydrogen or helium rich matter, then He burning could occur steadily allowing the CO core to grow in mass until the Chandrasekhar mass limit.

In order to better understand if this reaction has some role in the evolution of RG stars we have analyzed three sets of models at different metallicity (namely Z=0.0001, 0.001 and 0.02): for each sets we consider three different masses (namely M=0.6, 0.7 and 0.8 $M_\odot$). We

Z	Y	M_{tot} $(M_\odot)$	$M_{He-core}$ $(M_\odot)$
0.0001	0.244	0.520	0.498
0.001	0.238	0.515	0.510
0.02	0.980	0.800	-

Table 1: The main characteristics of the models we have computed from the central He burning phase until the cooling sequence. Note that the last model refers to a pure He star.

follow the evolution of these models from the Pre-Main Sequence phase until the onset of the He flash at the tip of the RGB. Being the e-capture strongly dependent on the density and being the maximum density located at the center, the physical conditions suitable for the NCO reaction are attained first at the center of the He core.

We find that for the higher metallicity cases (Z=0.02 and 0.001) the 3α reaction occurs well before the central density exceeds the critical value at which the NCO reaction becomes active ($\overline{\rho} = 10^6$ g cm^{-3}). Therefore in this case they do not play any role at all. For models with Z=0.0001 the central density becomes greater than $\overline{\rho}$ before the 3α ignites, therefore all the central ^{14}N is converted into ^{14}C and the ^{14}C is converted into ^{18}O, delivering a small amount of energy that heats up the center. Despite this, the successive evolution is similar to models which do not include the NCO reaction, in the sense that the 3α reaction is ignited in the same physical conditions and the final He core mass is the same.

As a whole, we conclude that the NCO chain does not affect at all the evolution of a low mass star climbing the RGB. In fact for high metallicity the central density is too low to allow the onset of the electron capture on ^{14}N; on the contrary, for lower metallicity, the central density exceeds the critical value for the onset of the NCO reaction but in this case the ^{14}N abundance is very low and the produced energy can not heat up efficiently the structure.

Our result is in good agreement with [6] but it is quite different with respect to those obtained by [2]. This occurrence is due to the fact that Hashimoto and co-workers simulate the behavior of the He core of a low mass star accreting He rich matter on a cooled down He WD. In this way they ignore the presence of the overlying H-shell that keeps hot the He core. As a consequence, for a fixed metallicity, their models attain a too high central density with respect to realistic models.

For what concerns mass accreting CO WDs, it is interesting to note preliminary that an evolutionary model presents a CO core surrounded by a He shell and eventually by an H shell. We have computed three different models from the central He-burning phase until the cooling sequence, as indicated in Table 1. In the cooled models the ^{14}N abundance at the physical base of the He shell overlying the CO core is very small ($< 10^{-10}$ by mass). This is due to the fact that during the He-shell burning ^{14}N is converted into ^{18}O via direct α-capture (NO reaction).

The accretion of H or He rich matter causes the growth in mass of the He layer surrounding the CO core; the He-layers, accreted directly or by H-burning by-products, are rich of ^{14}N so that one can expect that in this case the NCO reaction could play some role at the ignition of the He burning. To verify this scenario we focus the attention on the model of a low mass CO WD accreting He rich matter at a low rate, suitable for a violent dynamical He ignition (see [7]). As it can be seen in Figure 1 (panel a)) as soon as the physical conditions suitable for NCO burning are attained, ^{14}N is completely converted into ^{14}C. The latter element

undergoes α-captures to produce ^{18}O, heating up locally the structure (see panel *b)*). While the time elapses, the He layer continues to grow in mass and the $^{14}N(e^-,\gamma)^{14}C(\alpha,\gamma)^{18}O$ occur in more and more external zones. Therefore, it is possible to identify the existence of a ^{14}C shell which moves outwards. This situation goes on until the 3α reactions ignite in high degenerate physical condition causing the disruption of the accreting structure as Type Ia supernova. We stress once again that the final outcome remains an explosion triggered by 3α reactions, the only difference with respect to the model without NCO chain being a very small reduction in mass of the He layers at the runaway.

We conclude that the $^{14}N(e^-,\gamma)^{14}C(\alpha,\gamma)^{18}O$ chain does not play any role at all in the ignition of the He flash in degenerate and semi-degenerate physical conditions due to the fact that the ignition density for the e-capture on ^{14}N is very high. If the threshold density for the e-capture were lower than current value, then the NCO reaction would become of some importance. We believe that an up-date of the cross section for the e-capture on ^{14}N is strongly required.

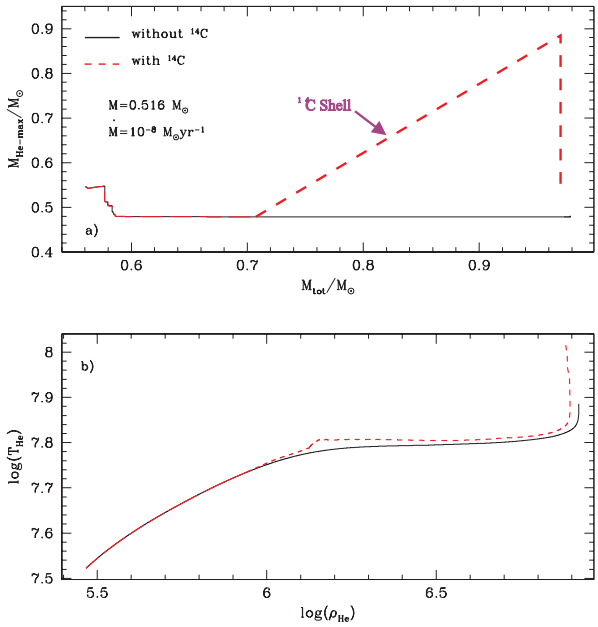

Figure 1: Selected evolutionary properties of a CO WD of 0.516 $M_\odot$ accreting He-rich matter at $\dot{M} = 10^{-8}$ $M_\odot$ yr^{-1} with and without NCO reactions. *Panel a)*: the temporal evolution of the mass coordinate where the energy production via He-burning is a maximum. *Panel b)*: the evolution in the $\rho - T$ plane of the base of the He-shell.

References

[1] M.A. Hashimoto, K.I. Nomoto, K. Arai & K. Kaminisi, Phys. Rep. Kumamoto Univ. **6** (1984) 75

[2] M.A. Hashimoto, K.I. Nomoto, K. Arai & K. Kaminisi, ApJ **307** (1986) 687

[3] K. Kaminisi & K. Arai, Phys. Rep. Kumamoto Univ. **2** (1975) 19

[4] K. Kaminisi, K. Arai & K. Yoshinaga, Phys. Rep. Kumamoto Univ. **53** (1975) 1855

[5] R. Mitalas, ApJ **187** (1974) 155

[6] R.G. Spulak Jr., ApJ **235** (1980) 565

[7] L. Piersanti, S. Cassisi, I. Iben Jr & A. Tornambé, ApJ Lett **521** (1999) L59

[8] S.E. Woosley & T.A. Weaver, ApJ **423** (1994) 371

The First Hours of a Core Collapse Supernova

K. Kifonidis[1], *T. Plewa*[2,1], *H.-Th. Janka*[1], *E. Müller*[1]

[1] *Max-Planck-Institut für Astrophysik, Karl-Schwarzschild-Strasse 1, D-85740 Garching, Germany*
[2] *Nicolaus Copernicus Astronomical Center, Bartycka 18, 00716 Warsaw, Poland*

Abstract

New two-dimensional, high-resolution calculations of a core collapse supernova in a $15\,M_\odot$ blue supergiant are presented, which cover the entire evolution from shock revival until the first few hours of the explosion. Explosive nucleosynthesis, its dependence upon convective mixing during the first second of the evolution and the growth of Rayleigh-Taylor instabilities at the composition interfaces of the progenitor star are all modeled consistently and allow for a comparison with observational data. We confirm our earlier findings, that the perturbations induced by neutrino driven convection are sufficiently strong to seed large-scale Rayleigh-Taylor mixing and to destroy the onion-shell structure of the stellar He-core. As in our earlier calculations, the strong deceleration of the nickel clumps in the layers adjacent to the He/H interface suggests that the high velocities of iron-group elements observed in SN 1987 A cannot be explained on the basis of currently favored progenitor models. Possible solutions to this dilemma and the implications of the mixing for type Ib explosions are briefly discussed.

1.1 Introduction

Recent observations of the Cas A remnant by NASA's Chandra X-ray observatory [3] appear to directly disclose for the first time the nature of the violent processes which are responsible for the synthesis of heavy and intermediate mass elements in core collapse supernovae. The spatial separation of silicon and iron emission observed by Hughes et al. [3] has been interpreted as the result of a large-scale overturn during the earliest phases of the explosion of the Cas A progenitor. Together with the numerous indications of strong mixing in e.g. SN 1987 A [1] and SN 1993 J [7] these new observations begin to assemble into a picture in which hydrodynamic instabilities in supernova explosions are inevitable and must be regarded as a key to an understanding of these events. Thus multidimensional hydrodynamic simulations are urgently required which must cover the entire evolution from shock formation until shock breakout through the stellar photosphere.

In [5] we have reported on first preliminary results of such calculations and found that neutrino driven convection is able to seed strong Rayleigh-Taylor mixing at the Si/O and (C+O)/He interfaces of the SN 1987 A progenitor model of [8] within only about a minute after core bounce. The stellar metal core was found to have been completely shredded only five minutes after bounce and high-velocity clumps of newly synthesized elements were observed to be ejected up to the outer edge of the helium core. However, these were substantially decelerated in a dense shell that formed at the He/H interface after the supernova shock entered the hydrogen envelope of the star. In this contribution we present more refined calculations for the same presupernova star, which cover a longer period of the evolution and which are used to test the numerical sensitivity of our earlier results.

1.2 Models

In our new calculations we have accomplished to overcome the numerical problems due to "odd-even decoupling" that were observed in [5], to increase the spatial resolution and to include gravity into the adaptive mesh refinement (AMR) calculations of the Rayleigh-Taylor growth phase, which now cover the time span from 820 ms up to more than 20 000 s after bounce. Different from [5] we have also used a new, somewhat more energetic explosion model ($E_{\rm expl} = 1.8 \times 10^{51}$ ergs as compared to $E_{\rm expl} = 1.5 \times 10^{51}$ ergs). Note, however, that since gravity was neglected in our old AMR calculations, the old model resulted in a kinetic energy at infinity of $E_{\rm expl} \approx 1.8 \times 10^{51}$ ergs which is by about 20% *larger* than in the new simulations. This, of course, resulted in a slower overall expansion in our new calculations, giving the Rayleigh-Taylor instability somewhat more time to grow before the clumps reached the outer edge of the He core.

Not being affected by noise due to odd-even decoupling, our new simulations show qualitative differences in the growth of the Rayleigh-Taylor instability. Seeded by neutrino driven convection in the deeper layers of complete silicon burning, the instability starts to grow about 50 s after bounce at the Si/O interface on much smaller angular scales (of the order of $\leq 1^\circ$) than found in [5]. Superposed upon the resulting mushrooms, which grow out of the highest frequency perturbations that can still be resolved on our grid, are long-wavelength perturbations of the entire interface which are caused by the convective blobs beneath it. From these perturbations evolve initially cusps and subsequently fully-grown fingers, which start to perturb also the unstable O/He interface. Fig. 1 shows the situation 1170 s after core bounce when the instabilities at both interfaces are already fully developed. Depicted are the spatial distribution of the mass density as well as the partial densities of oxygen, silicon and nickel. Fine-grained filaments of dense material which includes silicon as well as newly synthesized ^{56}Ni (and other nuclides) are visible, which are embedded in broader oxygen fingers that penetrate through the He-core. However, no overturn of the ^{28}Si and ^{56}Ni rich layers as suggested by [3] is found in which the ^{56}Ni is mixed much farther out than the silicon. Both elements are rather evenly distributed throughout the He-core.

We find maximum ^{56}Ni velocities around 3000 km/s before the clumps penetrate into the dense shell at the He/H interface (see [5]) 1600 s after bounce, and their velocities decrease to about 1000 km/s at the end of our calculations. Both of the quoted values are substantially lower than in our earlier simulations. The dense shell is caused by the compression of the post-shock matter behind the decelerating shock, which encounters a flatter slope of the density profile once it crosses the He/H interface and enters the hydrogen envelope. The strong flattening of the density gradient is a generic feature in all presupernova models proposed for SN 1987 A and makes dense shell formation inevitable during the explosion. Thus our new calculations underline that on the basis of presently favored progenitor and current multidimensional explosion models, it is not possible to explain the high nickel velocities in two-dimensional calculations.

1.3 Conclusions

Though in detail differences as compared to [5] are found, the main results and conclusions of our earlier work remain unchanged. We confirm that neutrino driven convection succeeds in seeding large-scale mixing processes in the exploding star which destroy its onion-shell structure on a time-scale of *minutes*. Although our calculations do not yield the kind of

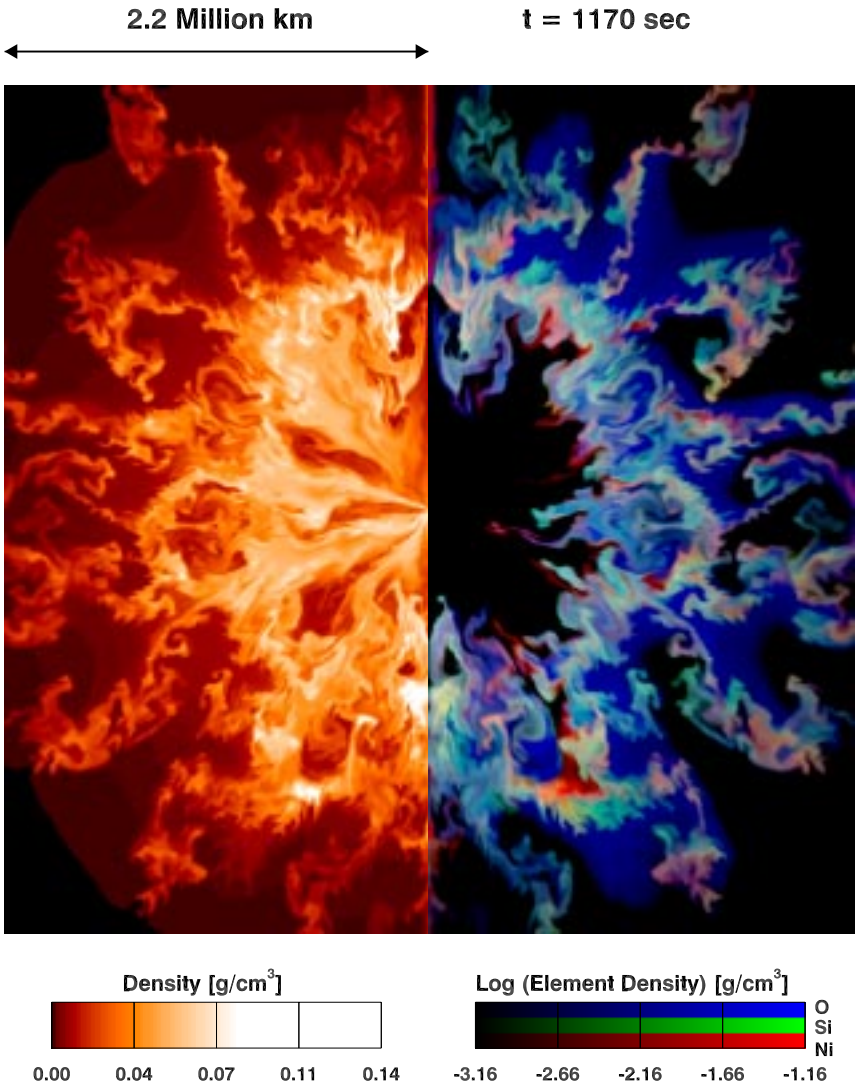

Figure 1: Spatial distribution of the density (left) and the partial densities (right) of ^{16}O (blue), ^{28}Si (green, turquoise, white), and ^{56}Ni (red, pink) in the inner He-core of the exploding star 1700 seconds after bounce. At this time, the supernova shock is already propagating through the hydrogen envelope. The onion shell structure of the core has been completely shredded by Rayleigh-Taylor instabilities at the Si/O and (C+O)/He interfaces. ^{28}Si, ^{56}Ni and all other products of explosive oxygen and silicon burning are localized in dense, rapidly expanding clumps which are propelled through the He core.

overturn of iron and silicon-rich layers claimed to be present in Cas A by [3], they appear to yield a natural explanation for the mixing occuring in type Ib supernovae (see also [9]).

The situation is much more unclear in case of SN 1987 A. Definitely, a reliable modeling of the deceleration of the nickel clumps in the dense shell at the He/H interface has to take into account the different drag that genuinely three-dimensional "mushrooms" experience as compared to two-dimensional tori [4]. Thus three-dimensional calculations are required before one will be able to draw definite conclusions. However, the present calculations indicate that standard stellar evolution models for the progenitor of this supernova might have to be abandoned in favor of merger models, which appear to be the most likely explanation for such large differences of the hydrogen-envelope structure as our hydrodynamic simulations require.

An alternative explanation might, however, be sought in "missing physics" in the modeling of the explosion itself. Large-scale asymmetries, e.g. produced by jets [2], [6], may accelerate the products of complete silicon burning to velocities that might be sufficient to propel these elements up to the stellar hydrogen envelope.

Acknowledgements

It is a pleasure to thank S. E. Woosley for providing us with his progenitor models and for pointing out the importance of the mixing for the spectra of Type Ib explosions.

References

[1] W.D. Arnett, J.N. Bahcall, R.P. Kirshner, S.E. Woosley, Ann. Rev. Astron. Astrophys. **27** (1989) 341.

[2] C.L. Fryer and A. Heger, ApJ submitted (astro-ph/9907433)

[3] J.P. Hughes, C.E. Rakowski, D.N. Burrows and P.O. Slane, ApJ **528** (2000) L109.

[4] J. Kane, D. Arnett, B.A. Remington, S.G. Glendinning, G. Bazán, E. Müller, B.A. Fryxell, and R. Teyssier, ApJ **528** (2000) 989.

[5] K. Kifonidis, T. Plewa, H.-Th. Janka and E. Müller, ApJ **531** (2000) L123.

[6] S. Nagataki, T.M. Shimizu and K. Sato, ApJ **495** (1998) 413.

[7] J. Spyromilio, MNRAS **266** (1994) L61.

[8] S.E. Woosley, P.A. Pinto and L. Ensman, ApJ **324** (1988) 466.

[9] S. E. Woosley and R. Eastman. In *Thermonuclear Supernovae. Eds. P. Ruiz-LaPuente, R. Canal and J. Isern, Dordrecht: Kluwer*, (1997) 821.

On the Site of the Weak r-Process Component

James W. Truran [1] *John J. Cowan* [2]

[1] *Department of Astronomy and Astrophysics, Enrico Fermi Institute, University of Chicago, Chicago, IL, 60637*
[2] *Department of Physics and Astronomy, University of Oklahoma, Norman, OK, 73019*

1.1 Abstract

There is increasingly strong observational evidence that the r-process isotopes identified in solar system matter are in fact the products of two distinct classes of r-process events. The r-process abundance pattern in the mass range A $\gtrsim$ 130-140, the signature of which is unambiguously imprinted upon the abundance patterns of the most metal deficient halo field stars, are generally assumed to have been synthesized in an environment tied to massive stars (M $\gtrsim$ 10 $M_\odot$) and associated Type II supernovae. Observations both of the oldest stars and of the abundances of short lived radioactivities in primordial solar system matter indicate, however, that a second r-process nucleosynthesis site is necessary to explain the abundances of the r-process nuclei in the range A $\lesssim$ 130-140. We present preliminary calculations which suggest that this site may be associated with the shock processing of the helium and/or carbon shells of Type II supernovae.

1.2 Introduction

While the general nature of the r-process and its contributions to the abundances of heavy elements in the mass range through uranium and thorium are generally understood, the details remain to be worked out. There are considerable uncertainties associated both with the basic nuclear physics of the r-process - which involves the neutron-capture, beta-decay, and fission properties of unstable nuclear species far from the region of β-stability - and with the characteristics of the stellar or supernova environments in which r-process synthesis occurs. Until recently, it was at least reassuring that, in contrast to s-process, it appeared a single r-process site was involved. Observations reviewed in the next section now suggest that this is not true - rather, there must be distinct classes of r-process events operating in the mass regimes above and below masses A $\approx$ 130-140. These abundance clues will be briefly discussed in the next section.

We report here exploratory calculations of the consequences of r-process synthesis in helium shells of Type II supernovae. We begin with the assumption that the site of operation of the main r-process component is not in these helium shells but rather occurs elsewhere (e.g. outside the neutronized core, in magnetic jets from the collapsing core, or in neutron-star mergers, ...). We then ask what the helium and carbon shells might be able to contribute to r-process nucleosynthesis. We feel confident that the temperature/density conditions to which the helium and carbon rich regions of massive stars (M $\gtrsim$ 10 $M_\odot$) will be subjected in the wake of the outgoing shock will yield some r-process nuclei. Can this environment be responsible for the entire weak r-process component, does it contribute significantly to the some of the r-process anomalies identified in presolar grains, is its level of activity in the oldest stars consistent with the observed abundances of the light n-capture elements in low metallicity stars? We first review current theoretical models for the production of the main

r-process component (A $\gtrsim$ 130-140) and then present calculations relevant to the synthesis of the lighter r-process elements.

1.3 Abundance Clues to r-Process Synthesis Sites

r-Process abundances in low metal stars provide several important clues to the nature of the r-process site:

- r-Process synthesis of A $\gtrsim$ 130-140 isotopes happens early in Galactic history [1], prior to input from AGB stars to the abundances of heavy s-process isotopes.
- The r-process mechanism for the synthesis of the A $\gtrsim$ 130-140 isotopes (which we will refer to as the 'main' component) is extremely robust. This is reflected in the fact that the abundance patterns in the most metal deficient (oldest) stars, which may have received contributions from only one or a few r-process events, are nevertheless entirely consistent with the r-process abundance pattern which characterizes solar system matter. (The abundance patterns for the two stars CS 22892-052 [2, 3] and HD 115444 [4, 5] shown in Figure 2 of the Cowan, Truran, & Sneden [6] paper in these proceedings reveal this remarkable agreement for two stars of low metallicity but high [r-Process/Fe].)
- Of relevance to our discussion in this paper, the abundance pattern in the mass regime below A $\approx$ 130 does not exhibit this consistency [6]. It is the source of these lighter r-nuclei (the 'weak' component) that we seek to identify in this paper.

It is also interesting to note that there exists evidence for a second, weak r-process component from another source. Wasserburg, Busso, & Gallino [7] have pointed out that the abundance levels of the short-lived isotopes ^{107}Pd and ^{129}I in primordial solar system matter are inconsistent with their having been formed in uniform production together with the heavy r-process radioactivities (specifically, ^{182}Hf, ^{235}U, ^{238}U and ^{232}Th). They suggest that these two different mass ranges of nuclei require different timescales for production and therefore suggest two distinct r-process sites. This seems entirely compatible with the weak (A $\leq$ 130-140) and main (A $\geq$ 130-140) r-process components as we have identified them above.

1.4 r-Process in Helium/Carbon Shells in Type II Supernovae

The appearance of r-process nuclei in the oldest known stars in our Galaxy strongly suggests the identification of the site of the main r-process component (A $\gtrsim$ 130-140) with massive stars and associated Type II supernova environments. We note that the three mechanisms currently considered for the r-process are all associated in some way with this environment. This includes nucleosynthesis associated with: (i) neutrino-driven winds from forming neutron stars [8, 9]; (ii) neutron star mergers [10, 11]; and (iii) magnetic jets from collapsing stellar cores [12].

An alternative possible site for r-process synthesis is that associated with the helium and carbon shells of massive stars undergoing supernovae [13, 14, 15]. Shock processing of these regions can give rise to significant neutron production via such reactions as $^{13}C(\alpha,n)^{16}O$, $^{18}O(\alpha,n)^{21}Ne$, and $^{22}Ne(\alpha,n)^{25}Mg$, involving residues of hydrostatic burning phases. The early studies cited above were motivated by the desire to produce the entire range of r-process nuclei through uranium and thorium. It was found, however, that this could be accomplished only with the use of excessive and quite unrealistic concentrations of e.g. ^{13}C [16].

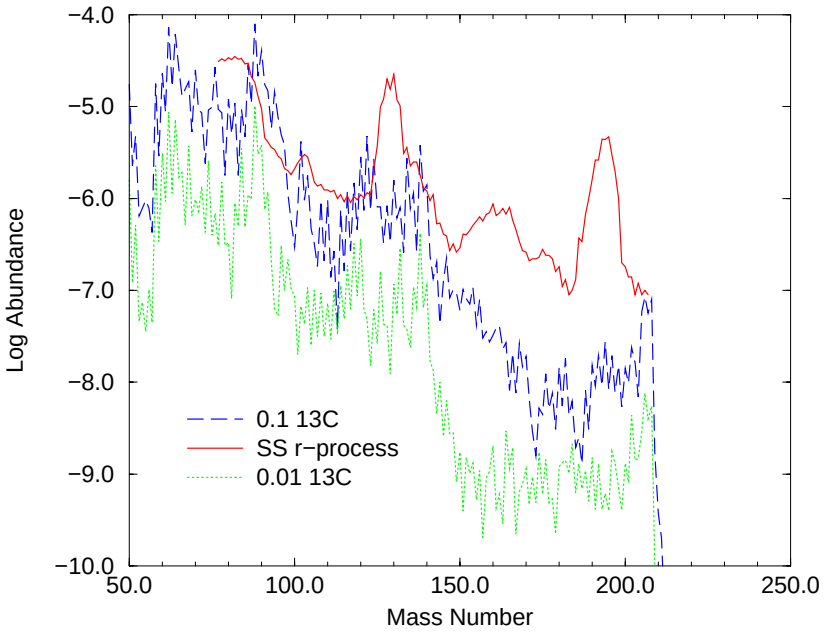

Figure 1: The r-process abundance patterns resulting from two representative ^{13}C(α,n)^{16}O neutron exposures in the helium shell of a massive star are compared with the solar system r-process abundance distribution (solid line).

The observational and theoretical considerations discussed previously serve to ease these demands: we need now only to be able to produce the r-process nuclei in the mass range through A $\approx$ 130-140. Guided by stellar models for massive stars at the end of their hydrostatic evolution [17], we have calculated the r-process history of matter processed through the shock heated helium shell for two choices of the initial abundance of ^{13}C: X_{13}=0.1 and 0.01. The initial (post shock) temperature and density were taken to be 7x10^8 ^{o}K and 10^4 g/cc, respectively. Here we have assumed an active ^{13}C(α,n)^{16}O neutron source acting on a preexisting solar abundance pattern as seed nuclei, and calculated nucleosynthesis occurring on an expansion time scale. (We note that we might also expect important contributions from the $^{18}O(\alpha,n)^{21}Ne$ and $^{22}Ne(\alpha,n)^{25}Mg$ reactions.) The results are displayed in Figure 1, where the calculated abundance patterns for the two choices of X_{13} are compared with the solar system r-process pattern. We note that for the more realistic case of X_{13}=0.01, the element abundance enrichments fall sharply in the range A $\gtrsim$ 130. The r-process products are thus confined to the light mass region that seems not to receive significant contributions from the main r-process component.

1.5 Conclusions

Our results confirm that the helium and carbon layers of massive stars, when subjected to outgoing shocks characteristic of Type II supernovae, can represent an important nucleosynthesis site - specifically for the light r-process nuclei. The great sensitivity to conditions of temperature, density, and initial composition that we have found in our exploratory survey strongly suggest that this r-process mechanism will prove less robust in its ability to reproduce the observed r-process pattern in the mass range A $\lesssim$ 130-140.

References

[1] Truran, J.W. (1981) A&A **97**, 391-393.

[2] Sneden, C., McWilliam, A., Preston, G.W., Cowan, J.J., Burris, D.L., Armosky, B.J. (1996) ApJ **467**, 819-832.

[3] Sneden, C., Cowan, J.J., Ivans, I. I., Fuller, G. M., Burles, S., Beers, T. C., Lawler, J. E. (2000) ApJ **533**, L139.

[4] Westin, J., Sneden, C., Gustafsson, B., Cowan, J.J. (2000) ApJ **530**, 783.

[5] Sneden, C., Cowan, J.J., Burris, D.L., Truran, J.W. (1998) ApJ **496**, 235-245.

[6] Cowan, J.J., Truran, J.W., Sneden, C. (2000), these proceedings.

[7] Wasserburg, G.J., Busso, M., Gallino, R. (1996) ApJ **466**, L109-L113.

[8] Woosley, S.A., Wilson, J.R., Mathews, G.J., Hoffman, R.D., Meyer, B.S. (1994) ApJ **433**, 229.

[9] Takahashi, K., Witti, J., Janka, H.-T. (1994) A&A **286**, 857.

[10] Lattimer, J.M., Mackie, F., Ravenhall, D.G., Schramm, D.N. (1977) ApJ **213**, 225.

[11] Freiburghaus, C., Rosswog, S., Thielemann, F.-K. (1999) ApJ **525**, L121-L124.

[12] LeBlanc, J.M., Wilson, J.R. (1970) ApJ **161**, 541.

[13] Truran, J.W., Cowan, J.J., Cameron, A.G.W. (1978) ApJ **222**, L63-L67.

[14] Thielemann, F.-K., Arnould, M., Hillebrandt, W. (1979) A&A **74**, 175.

[15] Blake, J.B., Woosley, S.E., Weaver, T.A., Schramm, D.N. (1981) ApJ **248**, 315.

[16] Cowan, J.J., Cameron, A.G.W., Truran, J.W. (1985) ApJ **294**, 656.

[17] Woosley, S.A., Weaver, T.A. (1995) ApJS **101**, 181.

Abundances and Ages in Halo Stars

John J. Cowan, [1], *James W. Truran* [2] *and Christopher Sneden* [3]

[1] *Department of Physics and Astronomy, University of Oklahoma, Norman, OK, 73019, cowan@mail.nhn.ou.edu*
[2] *Department of Astronomy and Astrophysics, Enrico Fermi Institute, University of Chicago, Chicago, IL, 60637, truran@nova.uchicago.edu*
[3] *Department of Astronomy and Macdonald Observatory, University of Texas, Austin, TX, 78712, chris@verdi.as.utexas.edu*

1.1 Abstract

Ground-based and space-based observations have detected a large number of neutron-capture elements in metal-poor Galactic halo stars. The heavier n-capture elements (Z $\geq$ 56) in all of the most metal-poor stars observed to date have an abundance pattern consistent with the scaled solar system r-process abundance distribution. For the first time many lighter n-capture elements (from Z = 41–48) have been detected in the ultra-metal-poor star CS 22892–052. The abundances of these elements are not consistent with the solar system distribution and lend support to suggestions of more than one r-process site. Observations of r- and s-process elements indicate the early occurrence of the r-process at very low metallicities (i.e., early Galactic epochs) followed by the onset of the s-process at higher metallicities and later Galactic times. These observations also demonstrate a large star-to-star scatter in the n-capture/Fe abundance ratios at low metallicities. Utilizing the radioactive (r-process) element thorium, age determinations have been made for several of the metal-poor halo stars placing constraints on both Galactic and cosmological age estimates.

1.2 Introduction

The neutron-capture elements are formed as a result of either the rapid(r)- or the slow(s)-process. The abundances of these elements in metal-poor (i.e., low iron abundance) Galactic halo stars can be used to determine the nature of the progenitors and the nucleosynthesis history in the early Galaxy. In addition, abundance trends over changes in metallicities (and times) can provide clues about the nature of Galactic chemical evolution and the sites for n-capture synthesis. Finally, the abundances of long-lived radioactive elements (a.k.a. chronometers), such as thorium and uranium, in the metal-poor stars provides a direct stellar age determination.

1.3 Observations of Metal-Poor Halo Stars

Recent ground-based [1, 2, 3, 4] and space-based [5, 6] studies have been made to determine the abundances of the n-capture elements in metal-poor halo stars. Particular attention has been made of the ultra-metal poor, but n-capture rich, star CS 22892–052 [7, 1, 4]. Many elements detected in this star had not previously been seen in other such stars. Figure 1 illustrates a comparison of the n-capture abundances in CS 22892–052 with the scaled solar system r-process pattern. It is apparent from this figure that the heavier n-capture abundances (Z $\geq$ 56) are consistent with the solar system distribution.

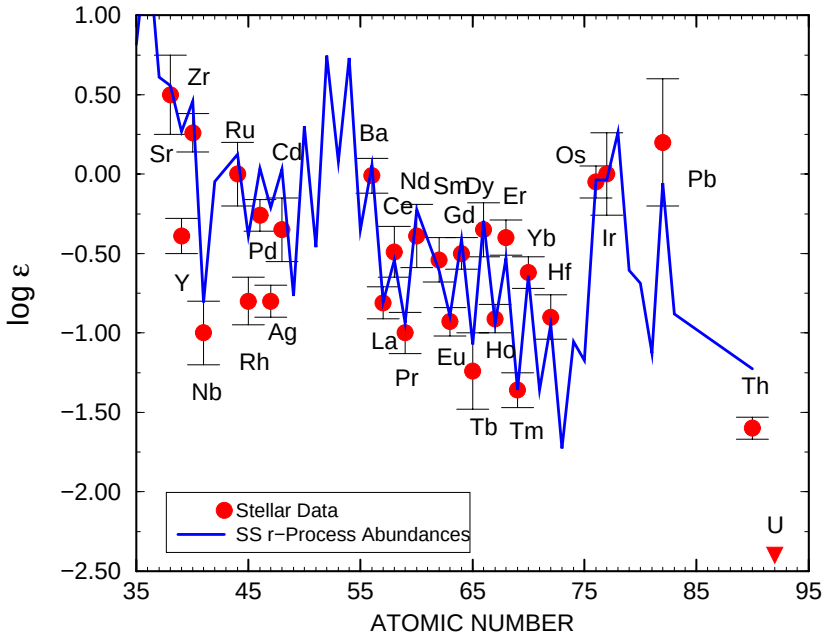

Figure 1: The heavy element abundance patterns for CS 22892-052 compared with the scaled solar system r-process abundance distribution (solid line) [4]

While the abundance pattern for this star has been noted previously [7, 1, 8, 9, 10], there is new evidence that other stars show the same agreement with the solar r-process pattern. Recent work by Westin *et al.* (2000) obtained detailed abundance determinations for the metal-poor halo star HD 115444. Figure 2 illustrates a comparison of the abundance pattern of this star with CS 22892-052. (HD 115444 has been displaced vertically downward to make comparisons easier.) It is apparent that both stars have abundance patterns that mimic the solar system r-process distribution strongly suggesting that this behavior may be common in other halo stars. Additional support for this contention is found in the very recent work of Sneden et al. (2000b) who report that the abundances of the heavier ($Z \geq 56$) elements for three stars in the globular cluster M15 are well matched by a scaled solar-system r-process abundance distribution.

Recently Sneden *et al.* (2000a) obtained detections of six new elements in the relatively unexplored elemental regime from Z = 41–48 in CS 22892–052. As is clear from Figure 1, the agreement between the heavier n-capture elements and the simple scaled solar system r-process pattern does not extend to the lighter elements below Ba. These observations lend support to suggestions [13] for a second r-process component for the mass region below A $\approx$ 140.

1.4 Galactic Abundance Trends

Since CS 22892 and HD 115444 are old (see below) and among the earliest generations of Galactic stars, the presence of the r-process elements in these stars demonstrates that the r-process operated early in the Galaxy, and points to rapidly evolving progenitors such as massive stars or perhaps neutron-star binaries [14]. Earlier suggestions [15], that even elements such as Ba, which are predominantly produced in the s-process, must have initially

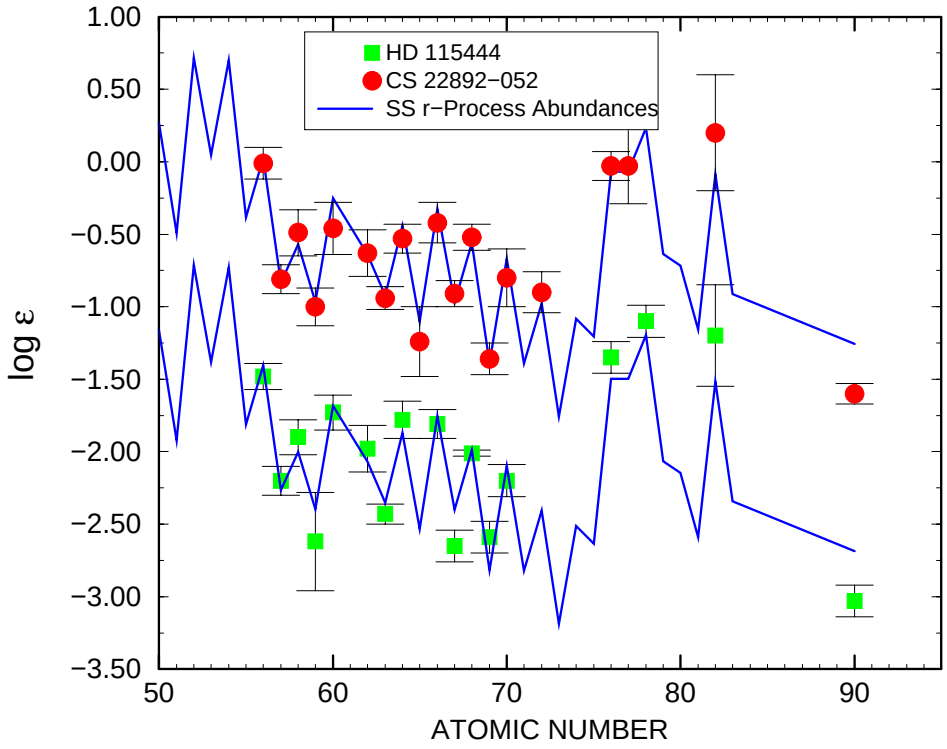

Figure 2: The heavy element abundance patterns for the two stars CS 22892-052 and HD 115444 are compared with the scaled solar system r-process abundance distribution (solid lines) [1, 11, 4]

been synthesized in the r-process, are dramatically confirmed by the "pure" r-process pattern observed in stars such as CS 22892–052 and HD 115444. Additional insight into the nature and evolution of the n-capture elements is provided by stellar abundance studies for a range of metallicities. Burris et al. (2000) has recently detailed the changing nature of elemental synthesis with increasing metallicity. They also note the purely r-process nature of the abundances at lowest metallicities, with the onset of the s-process occurring near metallicities [Fe/H]=–2.7. Their study also confirms earlier work [16] demonstrating a pronounced scatter in the n-capture/iron abundance ratios in stars at lowest metallicities. This scatter, which is most likely due to an inhomogeneous, chemically unmixed Galaxy at early times, disappears at higher metallicities. Additional theoretical work to examine the nature of early Galactic nucleosynthesis is ongoing [17].

1.5 Chronometric Ages

As illustrated in Figure 2, thorium has been detected in both CS 22892–052 and HD 115444. Upper limits on the uranium abundance in both stars have also been obtained. [11, 4]. Comparison of the observed stellar thorium abundance with the initial zero-age abundance produced in an r-process site leads directly to chronometric ages. Several studies [1, 9, 10, 11, 4] have determined ages for CS 22892–052 and HD 115444 on the order of 15 ± 4 Gyr. Sneden *et al.* (2000b) report on thorium detections in several stars in the globular cluster M15. They

obtain ages that are consistent with those found for the halo stars. This technique offers promise as an independent dating technique which can provide (lower) limits on the age of the Galaxy, and hence, the universe.

1.6 Conclusions

Our ground-based and space-based observations, complemented by our theoretical studies, have (1) detected a number of neutron-capture elements, many for the first time, in halo (and globular stars). We have detected almost half (!) of the periodic chart in CS 22892–052. (2) The presence of neutron-capture elements from Ge through Th in these very old, metal-poor stars confirms the operation of an r-process in the early Galaxy. This further suggests rapidly evolving progenitors, either supernovae, or perhaps neutron-star binaries. (3) In the most metal-poor halo stars, and now in at least one globular cluster, where detailed observations are available, the heavy ($Z \geq 56$) n-capture elements have relative proportions consistent with the solar r-process abundances. In contrast, the lighter n-capture elements detected in CS 22892-052 do not follow the solar system pattern. This lends support to suggestions of more than one astrophysical r-process site. (4) The abundances of the n-capture elements, with respect to iron, demonstrate a large star-to-star scatter at the lowest metallicities. These Galactic abundance studies further show the onset of the s-process at a higher metallicity and presumably a later time. (5) Finally, the presence of Th in the metal-poor halo stars, as demonstrated in CS 22892–052 and HD 115444, and now at least some globular cluster stars, can be used to determine chronometric stellar ages and thus to put constraints on both Galactic and cosmological age estimates.

We are grateful to Al Cameron and Jerry Wasserburg for their continuing helpful comments and to all of our collaborators for their invaluable contributions to this work. This research was funded in part by NSF grants AST-9618332 (JJC) and AST-9618364 (CS) and by the ASCI/Alliances Center for Astrophysical Thermonuclear Flashes at the University of Chicago under DOE contract B341495 (JWT). Additional support was provided through grant GO-06748 from the Space Science Telescope Institute, which is operated by the Association of Universities for Research in Astronomy, Inc., under NASA contract NAS5-26555.

References

[1] Sneden, C., McWilliam, A., Preston, G.W., Cowan, J.J., Burris, D.L., Armosky, B.J. (1996) ApJ **467**, 819

[2] McWilliam, A. (1998) AJ, **115**, 1640

[3] Burris, D.L., Pilachowski, C.A., Armandroff, T., Sneden, C., Cowan, J.J., Roe, H. (2000) ApJ, in press

[4] Sneden, C., Cowan, J.J., Ivans, I. I., Fuller, G. M., Burles, S., Beers, T. C., Lawler, J. E. (2000a) ApJ **533**, L139

[5] Cowan, J.J., Sneden, C., Truran, J. W., & Burris, D. L. (1996) ApJ, **460**, L115

[6] Sneden, C., Cowan, J.J., Burris, D.L., Truran, J.W. (1998) ApJ **496**, 235

[7] Cowan, J. J., Burris, D. L., Sneden, C., Preston, G. W., McWilliam, A. (1995) ApJ, **439**, L51

[8] Pfeiffer, B., Kratz, K.-L., Thielemann, F.-K. (1997) Z. Phys. A, **357**, 235

[9] Cowan, J. J., McWilliam, A., Sneden, C., Burris, D. L. (1997) ApJ, **480**, 246

[10] Cowan, J. J., Pfeiffer, B., Kratz, K.-L., Thielemann, F.-K., Sneden, C., Burles, S., Tytler, D., Beers, T. C. (1999) ApJ, **521**, 194

[11] Westin, J., Sneden, C., Gustafsson, B., Cowan, J.J. (2000) ApJ, **530**, 783

[12] Sneden, C., Smith, G. H., Johnson, J., Kraft, R. P., Cowan, J. J. Bolte, M. S. (2000b) ApJ, submitted

[13] Wasserburg, G.J., Busso, M., Gallino, R. (1996) ApJ **466**, L109

[14] Mathews, G.J., Bazan, G., Cowan, J.J. (1992) ApJ **391**, 719

[15] Truran, J.W. (1981) A&A **97**, 391

[16] Gilroy, K. K., Sneden, C., Pilachowski, C. A., Cowan, J. J. (1988) ApJ, **327**, 298

[17] Truran, J.W., Fields, B.D., Cowan, J.J. (1999) preprint.

Beta-delayed fission and formation of transuranium elements.

I.V. Panov[1,2], C. Freiburghaus[2], F.-K. Thielemann[2]

[1] *State scientific center-Institute for Theoretical and Experimental Physics, B.Cheremushkinskaya 25, Moscow, 117259, Russia.*
[2] *University of Basel, Klingelbergstr. 82, CH-4056 Basel, Switzerland*

Introduction

While the study of beta-delayed fission in the r-process has a long history (see e.g. [1], [2], [3]), its main focus was related to cosmochronometers ([4], [5], [6]). In this respect it was also noticed that its effect was of small influence on the majority of r-process abundances, if utilized with realistic fission barriers ([2], [7]). For that reason, many recent investigations of the r-process employed beta-delayed fission of trans-uranium nuclei in a very simplified manner:

1. $P_{\beta df} \equiv P_{sf} = 1$ for all A > 240 [8].
2. $P_{\beta df} \equiv P_{sf} = 1$ for all A > 256 [5].

One exception to this finding was shown in Rauscher et al. [21], when fission cycling is important for the abundance distribution of nuclei with A<130. On the other hand, the last observations of metal-poor stars emphasize just this mass region. One notices that these nuclei are underabundant and the solar system r-process must have at least two components, one which dominates for A<130 and a second one which dominates for A>130 ([9]). The observation of the second component in low metallicity stars and the observed abundances for A<130 can possibly give strong clues to fission properties, as there seems to be only one explanation possible source of explaining these abundance feature: the expansion of low entropy neutron star matter with a high neutron supply which leads to fission cycling.

Previous calculations made use of the results of Thielemann et al. ([1]) for beta-delayed fission rates in the trans-lead and trans-uranium regions. For our calculations we implemented the QRPA-results by Staudt et al. [10]. To our knowledge this is the first application of these β-delayed fission rates. We considered their influence upon r-element formation, beyond A $\approx$ 196 (Z > 80) and before A ≈ 130 (Z < 50) either.

We tryed to understand either - whether the isotopes of these chemical elements could be produced after beta-delayed fission of transuranium elements during r-process nucleosynthesis in neutron star merges. And, from the other hand, could be the observational data the check-point for fission rates and modes of fission?

1.1 Model and nuclear data

For the numerical r-process calculations we used the kinetic model (nuclear reaction network) [11], [12], [13], solves the full set of differential equations for all species, including neutrons (opposite to simplified approximations which assume a slowly varying neutron abundance [2], [8]).

This method was tested for different conditions and compared with other codes [14]. The full number of equations in the present application was approximately equal to 3100. The

boundaries of the network were chosen in such a way: $Z_{min} = 20$ (calcium), $Z_{max} = 99$, A_{min} and A_{max} for every Z were defined by stable and α-decay nuclei from one side and neutron drip line from another side according to different mass formulae [15], [16], [17] used.

The neutron capture rates were taken from Cowan et al. [2], beta-decay rates from [18] and beta-delayed fission data - from [10].

At first the impact of the new fission rates was tested based on the simple dynamical r-process model (i.e. network calculation under constant neutron densities and temperature, the FRDM masses were used for these runs).

Then we considered the conditions founded in neutron stars mergers [19] which were previously used for r-process calculations [20] with a very simplefyed inclusion of beta-delayed fission (100% instantaneous fission for all nucleons with A >240 [5], for these calculations ETFSI-masses were used).

1.2 Physical basics

In the calculations by Thielemann et al. [1] the values of beta-delayed fission probabilities for large number of short-lived neutron-rich nuclei stand up to 100% at the r-process path. In such a parametric study r-process stops in the region of nuclei with A $\approx$ 250-260. That is why the approximation of 100% instantaneous fission in the vicinity of A$\sim$260 (for simplicity A=260) was a rather good approximation [5], [7], [21]. Moreover, when using a full network without the assumption of the waiting point approximation ($(n,\gamma)-(\gamma,n)$approximation) in dynamical calculations, it is very attractive to include the detailed beta-delayed fission data especially when the abundance features of the fission products for $A < 130$ is of interest.

In the papers of [5], [21] beta-delayed fission was considered 100% symmetric (what is natural for A=260). In the most general case the ratio of different modes of fission (symmetric and asymmetric) of transuranium nuclei:

$$R_{\beta f}^{fis} = \frac{\sum_{A_i,Z_j} P_{\beta f}^{symm} Y_{A_j,Z_j} \lambda_{\beta}^{ij}}{\sum_{A_i,Z_j} P_{\beta f}^{asym} Y_{A_j,Z_j} \lambda_{\beta}^{ij}}$$

may define the contribution of symmetric fission.

The branching ratio $R_{\beta f}^{fis}$ depends strongly on A and Z of the fissioning nucleus. Based on the available data [22], [23], we used for simplicity in the present calculations a simple model, considering that 100% symmetric fission occurs only for $A > 255$, otherwise asymmetric fission started and becomes the main fission branch.

In a dynamical calculation the r-process path becomes arbitrarily wide (when falling out of $(n,\gamma)-(\gamma,n)$ equilibrium) with decreasing density and temperature and rather large number of fissioning nuclei take part in recycling. Therefor, contributions from both modes of fission - symmetric and asymmetric, have to be included. Though for the new fission rates [10] the fission is fully symmetric for thorium and transthorium elements ($Z \geq 90$). The asymmetric contribution into mass fragments distribution we got only after fission of translead nuclei ($Z \leq 90$).

1.3 Results and discussion

The preliminary comparative analysis of the influence of fission modes upon the results of nucleosynthesis was made in a simple approximation of the dynamical r-process model: T_9=1,

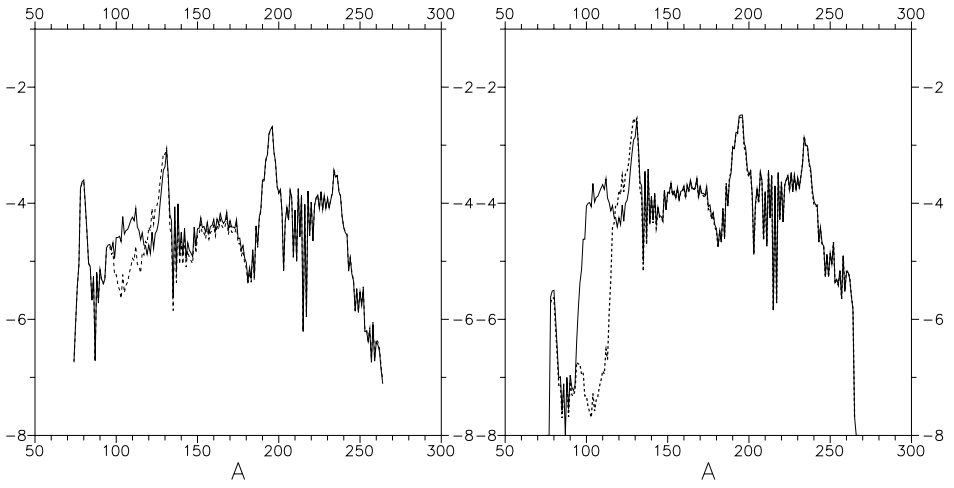

Figure 1: The comparison of influence of asymmetric (or symmetric) mass fragment distribution after beta-delayed fission in r-process nucleosynthesis on final calculated abundances: left - n/p initial ratio ≈3.3. T_9^0=1, $\rho = 10^5$; right: n/p=8.3; dashed curve - only symmetric fission is included; solid line - a combined model of different modes of mass-fragments distribution is used;

$\rho = 10^5 cm^{-3}$ and a duration time of the r-process τ=10s $>> \tau_{cycle}$. Here τ_{cycle} denotes the fission cycle time. The results are shown in Fig. 1.

For the initial conditions we considered simple model of hot Boltzman gas, consisted from neutrons, protons and small amount of seeds. (In our case ^{56}Fe). n/p-ratio was chosen in one run =3.3, in the other - 8.3. The nuclei from A=70 to A=250 formed before neutrons were exhausted. The final curve was obtained after taking into account the beta-decays into stable nuclei (Fig.1).

It is easily seen (see Fig. 1), that when asymmetric fission was apploed, nuclei with A=100-120 were formed.

Due to the significant difference between symmetric and combined fission upon r-process, we apploed fission to the calculations of r-process in highly neutronized matter, occuring also after neutron star mergers [20].

All further calculations were made for the conditions obtained in neutron stars mergers [19]. This site was chosen because of the strong evidences that r-nuclei with $Z > 50$ (maybe $>$ 45) were formed under small entropy and Y_e (see, for example [5], [8] and references therein). The entropy is rather small (~ 1) and the electron density varies within the limits of $0.05 < Y_e < 0.18$. The Y_e is not fully determined, but these limits are in reasonable range (see [20] and references therein). The time dependence of temperature and density for r-process calculations were chosen as in [20]. The Y(A) for $120 < A < 240$ practically coincide with the calculations with simplified fission assumption (A_{fiss}=240, [5]), but differs strongly for mass numbers $100 < A < 120$ and $A > 240$ (see Fig. 2).

An excellent agreement between calculations and observations can be seen for Y_e=0.08-0.12, at least, for a number of elements (Fig. 3), i.e. for $56 < Z < 76$ and Y_e=0.05. But for Z $\approx 46 - 48$ and $Z \approx$ 76-78 (i.e. in the peaks) the calculations with Y_e= 0.10-012 show the better agreement.

We do not present a superposition of solutions in order to show an excellent fit to solar

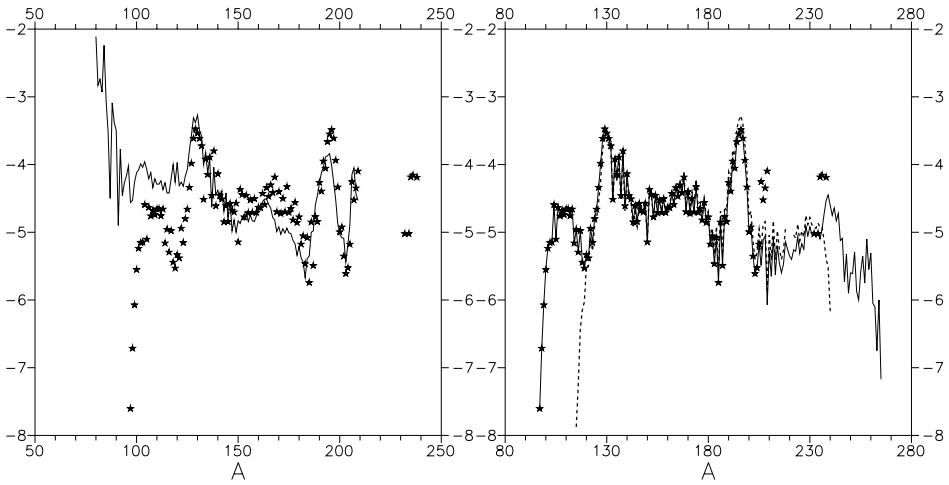

Figure 2: The comparison with solar pattern - left, where is line reflects "observed" data and rigth - influence of extended beta-delayed fission data - (see the details in the text); line - present calculation, stars show the final distribution after α-decays into stable or very long-lived nuclei Pb, Bi, Th and U; dashed line - previous [20] calculations.

abundances. Our aim: to understand the tendencies from variations in Y_e and taking into account beta-delayed fission rates for the entire region of heavy nuclei.

On the basis of the results we can conclude:
1. For the initial elements pattern appearing after neutron star mergers, when a high neutron exposure time is compatible with the r-process duration time, the yields of transuranium elements formed in the r-process has the tendency to be overestimated and all of the abundances, except, may be $Y(Z)$ for $56 < A < 60$ are sensitive to the value of Y_e. From the other hand, the yields of chemical elements with Z=46-48, at least in part, could be formed in such site. And the latter could be the evidence of asymmetric mode presence in beta-delayed fission.
2. The other important question is a question of fission rates. There is a number of observational evidences [9] in favor of an existance of the conditions when only chemical elements heavier A=130 could be formed.

In this case, comparison with the observations could be used either for testing the fission data: which set of fission rates could provide a better yields agreement of nuclei with Z=46-48 (and $Z > 80$)?

We suppose the future work could get answer for some of these questions.

References

[1] F.-K. Thielemann, J. Metzinger, H.V. Klapdor-Kleingrothaus, Zt.Phys., **A309** (1983) 301.

[2] J.J. Cowan, F.-K. Thielemann, J.W. Truran, Phys. Reports, **208** (1991) 267.

[3] I.V. Panov, Yu.S. Lyutostansky, V.I. Ljashuk, Bull. Acad. Sci. Ussr, Phys. ser. (USA) **54** (1990) 2137.

[4] J.J. Cowan, F.-K. Thielemann, J.W. Truran, ApJ **323** (1987) 543.

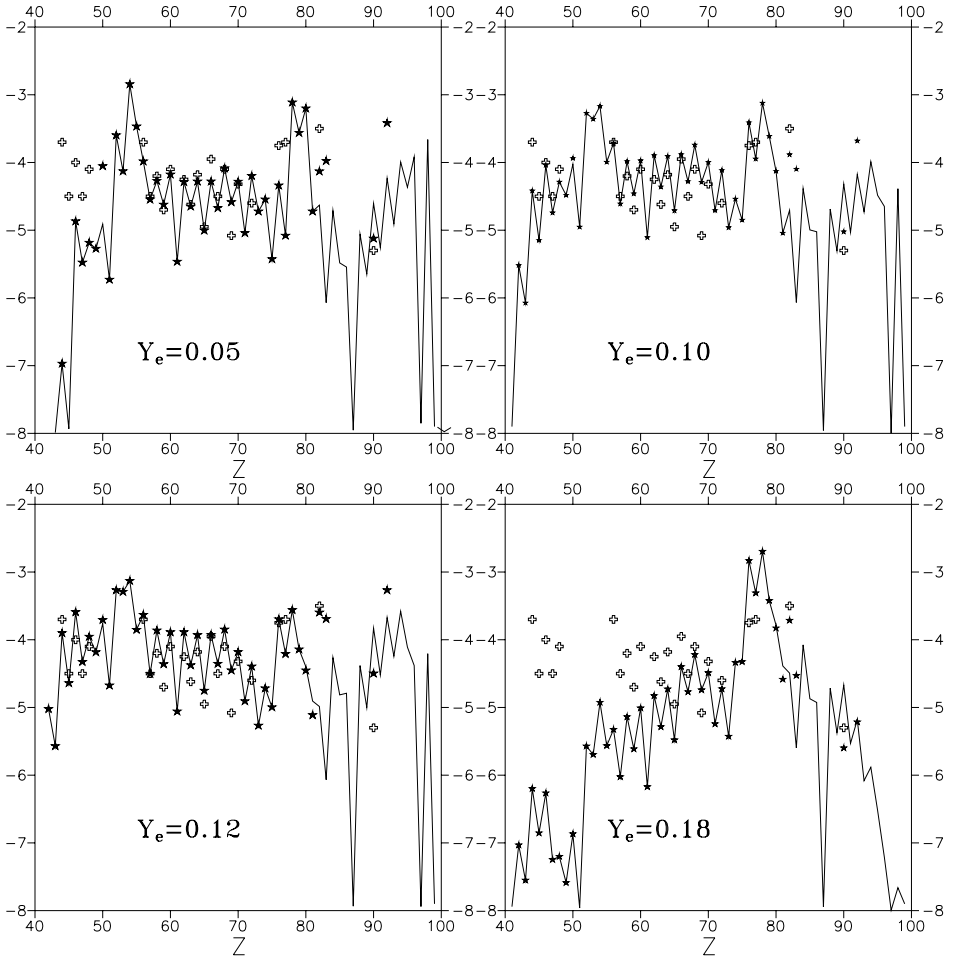

Figure 3: The calculated abundances Y(Z) for different Y_e and comparison with observations of poor-metal stars [9].

[5] J.J. Cowan et al., ApJ, **521** (1999) 194.

[6] V.M. Chechetkin, Yu.S. Lyutostansky, S.V. Malevanny, I.V. Panov, Sov.J. Nucl.Phys. (USA), **47** (1988) 780.

[7] F.-K. Thielemann, A.G.W. Cameron, J.J. Cowan, 1989, Int. Conf. 50 years with Nuclear Fission, ed. J. Behrens, A.D. Carlson, p. 592.

[8] C. Freiburghaus et al., ApJ, **516** (1999) 381.

[9] C. Sneden, J.J. Cowan, I.I. Ivans et al. astro-ph/0003086, 7.03.2000.

[10] A. Staudt, H.V. Klapdor-Kleingrothaus, NP, **A549** (1992) 254.

[11] S.I. Blinnikov, I.V. Panov, Astronomy Letters, **22** (1996) 39

[12] D.K. Nadyozhin, I.V. Panov, S.I. Blinnikov, A&A, **335** (1998) 207

[13] I.V. Panov, D.K. Nadyozhin, Astronomy Letters. **33** (1999) 333

[14] I.V. Panov, S.I. Blinnikov and F.-K. Thielemann, in preparation.

[15] E.R. Hilf, H.V. Groote, K. Takahashi. Proc. 3 Int. Conf. on Nucl. far from Stability, 1976, CERN-76-13, 142.

[16] H.V. von Groote, E.R. Hilf, K. Takahashi, ADNDT **17** (1976) 431

[17] J.M. Pearson. R.C. Nayak, S. Goriely, Phys. Lett. **B387** (1996) 455.

[18] K.-L. Kratz et al., ApJ **403** (1993) 216.

[19] S. Rosswog, F.-K. Thielemann, M.B. Davis et al. Astron. Astrophys. **341** (1999) 499.

[20] C. Freiburghaus, S. Rosswog, F.-K. Thielemann. ApJ **525** (1999) L121.

[21] T. Rauscher, J.H. Applegate, J.J. Cowan, F.-K. Thielemann, M. Wiescher, ApJ **429** (1994) 499.

[22] D.C. Hoffman Nucl.Phys. **A502** (1989) 21c.

[23] 4 Int. Conf. on Dynamical Aspects of Nuclear Fission. Slovakia, 19-23 October 1998.

Problems of Abundance Determinations from M dwarf atmospheres

R. Wehrse[1,2]

[1] *Institut f. Theoretische Astrophysik, Tiergartenstrasse 15, D-69121 Heidelberg*
[2] *Interdisziplinäres Zentrum f. Wissenschaftliches Rechnen, Im Neuenheimer Feld 368, D 69121 Heidelberg*

1.1 Introduction

M dwarfs are of interest from several points of view: they are by far the most frequent stars in the solar neighborhood and –in spite of their small individual mass– they dominate the mass balance, they form the transition from classical stars to brown dwarfs, and due to their slow evolution potentially contain a lot of information about early stages of the evolution of the Galaxy. The latter is mainly contained in the patterns of the element abundances which has to be determined by spectral analysis.

Unfortunately, the atmospheres of these stars are still poorly understood. The main reason is the myriad of molecular lines which contribute to the extinction coefficient and which often have only badly known parameters. At least equally important is the fact that the convection zone extends to optically very thin layers so that there is a strong interaction between blanketing and convection which –due to the lack of a proper theory of convection– can be modelled to now only with great uncertainties.

Since the strengths of lines depend strongly on the temperature for this spectral class it is obvious that element abundances derived from spectra are reliable only when the temperature distribution is accurate.

1.2 Observations and model calculations

In order to gain some empirical insight in the temperature distributions we have obatined ISO PHOT S and high resolution ground based spectra of the M dwarfs Gl 1 (spectral type M1.5), Gl 832 (M1.5), Gl 887 (M0.5), and Gl 866 (M5.5e). The first three objects are considered single and non-active, whereas the last one is known to be multiple and active.

First reductions of the ISO data (see [1]) seemed to indicate that the early M dwarfs have a cool chromosphere ($T \approx 4000 - 5000$ K) with a surprisingly high optical depth but in subsequent reductions the indications became much weaker. On the other hand, in the ground based observations (Figs. 1 and 2) the visibility of CaII emission and the visibility of Hα as well as of 2 neigboring TiI lines and a narrow CaI line clearly shows the presence of outer matter with temperatures higher than the effective temperature. Additional very high solution (30 mÅ pixel widths) revealed that the profiles of the latter transitions are very deep (less than 10% residual intensity in some cases) and narrow (less than 2 km/s close to the cores).

Many attempts to fit the line spectra with a single vertical temperature distribution (e.g. of the type of the 'Next Generation Models' of Hauschildt et al.,[2] , with or without an additonal chromosphere) and with the assumption of LTE failed. Instead, we only could reproduce the atomic lines well (Fig. 3) if we assumed that they are formed in scattering

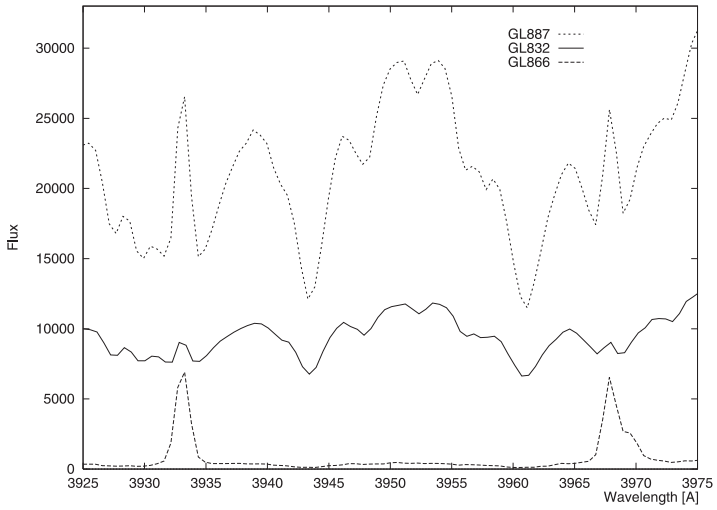

Figure 1: Spectra of Gl 887, Gl 832 and Gl 866 (from top to bottom) in the region of Ca II K and H. Note that the inactive stars Gl 887 and Gl 832 have much smaller but still clearly visible Ca II emissions compared to the multiple object Gl 866. The strong absorption features at 3943 and 3961 Å are due to AlI resonance lines.

mode mainly in an outer 'warm' chromosphere as originally suggested by the ISO observations. However, the molcular features come out far too weak from such a stratification: they must be formed in a more or less classical distribution!

1.3 Discussion

We infer from this behavior that the cores of the deep atomic lines must be formed in shallow layers of low density where LTE no longer prevails and that the early M dwarfs have horizontally inhomogeneous atmospheres. We suspect that the inhomogeneities are caused by the convection since the rising and descending elements with their quite different temperatures should very well visible since an upper radiative layer as in the Sun is essentially missing in the early M dwarfs. We estimate that the resulting uncertainties in the element abundances can reach 1 dex or even more (cf. Fig. 3). 3D radiation hydrodynamic models as those of the Copenhagen and Potsdam groups for the Sun (see e.g. [3], [4]) are therefore urgently needed.

A complete presentation of the data, the modelling and the consequences will be given in a separate paper.

Acknowledgements

I am indebted to M.S. Bessell for obtaining and reducing the ground based data. Without Ph. Rosenau, P. Araham, and Chr. Leinert the ISO observations could not been performed and analysed. Many very helpful discussions J. Liebert are gratefully acknowledged.

References

[1] R. Wehrse, Ph. Rosenau, A. Suvernev and Chr. Leinert, Astrophys. Sp. Sc. **255** (1998), 127

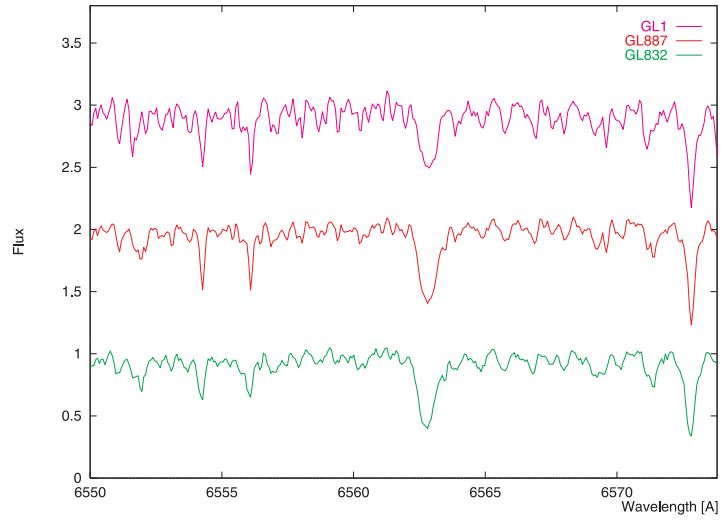

Figure 2: Spectra of Gl 1, Gl 887, and Gl 832 (from top to bottom) of the region around Hα which is in absorption in all objects. Of high importance are the appearance of the TiI lines at 6554 and 6556 Å, since they have lower levels with excitation potentials of 1.44 and 1.46 eV, resp.. Note also the forbidden Ca I line at 6573 Å which originates from the ground state. The ubiquitous weak features are essentially all due to TiO transitions.

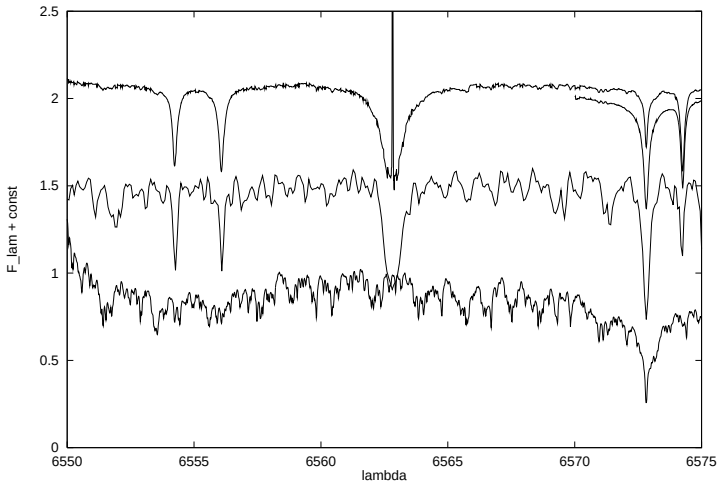

Figure 3: Comparison of high resolution observations of Gl 866 (center), and synthetic spectra calculated with a classical vertical temperature distribution (bottom) and with an additional cool chromosphere (top). The first one represents the TiO features satisfactorily but it completely fails to reproduce the atomic features. On the other hand, with the second stratification the molecular features do not show up correctly, the strengths and profiles of Hα, the CaI as well as of the Ti I lines are well reproduced. Since we were unable to reproduce both types of features by one vertical temperature distribution, we infer that the atmospheres of early M dwarfs are horizontally inhomogeneous. The composition in the model with the classical stratification is assumed to be solar except for Ca which is reduced by 1 dex. For the stratification with a chromosphere both [M/H]=-1 (upper curve) and [M/H]=0 are shown.

[2] P.H. Hauschildt, F. Allard, E. Baron, Ap.J. **512** (1998) 377

[3] R.F. Stein and Å Nordlund, Ap.J. **499** (1998), 914

[4] M. Steffen, in: Pacific Rim Conf. on Stellar Atmospheres, Kluwer (2000), in press

Pop III: the ancestors of the present generation of galactic stars

O. Straniero[1], *I. Dominguez*[2], *M. Limongi*[3], *A. Chieffi*[4]

[1] *Osservatorio Astronomico di Collurania, straniero@astrte.te.astro.it*
[2] *Dpto. de Fisica Teorica y del Cosmos, Univ. de Granada, inma@ugr.es*
[3] *Osservatorio Astronomico di Roma, marco@nemo.mporzio.astro.it*
[4] *Istituto di Astrofisica Spaziale (CNR), achieffi@ias.rm.cnr.it*

Following the standard homogeneous Big Bang nucleosynthesis scenario, the primordial Universe was mainly composed by ^{1}H, ^{4}He and a small quantity of other light elements (lighter than Carbon). Thus, the first generation of stars, the so called population III, was built with a gas essentially deprived of metals. Stellar evolution, since star formation, was significantly affected by the lack of heavy elements. Under this condition, molecular Hydrogen, rather than dust or heavy molecules, provided the cooling of a collapsing clouds of primordial gas, which was needed to reduce the Jeans mass down to the stellar values ([1]). Then the formation of the first stellar population proceeded trough a series of fragmentations of the original unstable clouds. This process stopped when the gas became opaque due to the H_2 line absorbtion. Yoshii and Saio [2] found that the peak of the resulting initial mass function (IMF) for Pop III stars ranges between 4 and 8 $M_\odot$. Uheara et al. [3] have derived that the minimum stellar mass should be of the order of the Chandrasekhar mass (i.e. $\sim$1.4 $M_\odot$). Recently Nakamura & Umemura [4] have obtained that the typical mass of the pop III stars should be around 3M$_\odot$; this value may further increase by accretion of the environmental gas up to 16 M$_\odot$. In this framework, intermediate mass stars (namely $3 \leq M/M_\odot \leq 8$, thereinafter IMS), rather than low mass stars, were the dominant constituents of the first stellar population. Of course even few massive objects ($11 \leq M/M_\odot \leq 16$), exploding as type II supernovae, were capable to rapidly increase the iron (and other heavy elements) content of the pre galactic gas (up to [Fe/H]$\sim$-4). However the evolutionary lifetime of an intermediate mass star is not to much greater than that of a massive star. Thus it is possible that the pre galactic gas was also polluted with the matter processed inside Pop III IMS,

So a detailed description of the advanced evolutionary phases of zero metal intermediate and massive stars is needed to reconstruct the post big bang chemical evolution. For this reason we decided to systematically explore the evolutionary properties and the related nucleosynthesis of these ancestors of the present stellar populations. We have used the latest version of our evolutionary code (FRANEC; [5]) to compute stellar models with masses ranging between 4 and 25 $M_\odot$, from the pre main sequence up to the AGB phase or up to the Iron core collapse. The explosive yields of massive stellar models with Z=0 may be found in [6] or in our database on the web (http://www.mporzio.astro.it/ mandrake/orfeo.html).

Concerning intermediate mass stars, the most important contribution to the chemical evolution comes from the Asymptotic Giant Branch phase (AGB). Due to the concomitant action of the deep external mixing and the huge mass loss, the interstellar gas is enriched with the ashes of the internal nucleosynthesis occurring in these stars

Despite their promising importance for the chemical evolution, only one paper reports evolutionary calculation of a pop III IMS throughout the AGB phase ([7]). Their main finding (also confirmed by the general theory of the thermal instability in very low metal

stars, [8]) was that AGB zero metal IMS skips the thermally pulsing AGB phase.

In the following we summarize the main evolutionary properties of our models of intermediate mass zero metal stars.

1) The pre main sequence of these stars is rather different from the one of a more metal rich intermediate mass stars. Owing to the lack of CNO nuclei they approach the H burning phase as low mass stars do.

2) During the first part of the main sequence the pp chain controls the H burning. A convective core initially develops whose size recedes (in mass), as H is converted into He, and rapidly disappears. The H burning extends far from the center (about 80 % in mass of the star is involved). The central region does not stop to contract and the temperature increases up to 80-90 MK. Then the 3αa reactions start. When the central carbon mass fraction is $\sim 10^{-10}$, the H burning switches from the pp chain to the more efficient CNO cycle. Then a new convective core appears and the final part of the main sequence proceeds as in more metal rich stars.

3) At the H exhaustion the central temperature is so large that the He burning immediately follows. As usual, this evolutionary phase is characterized by a growing (in mass) convective core.

4) Only after the He exhaustion the star becomes a red giant. Thus the envelope composition at the beginning of the AGB is, practically, the original one, namely Z=0.

5) A convective envelope firstly develops during the early AGB. Immediately the surface composition changes: primary He appears at the surface well before that the inner border of the convective envelope approaches the H/He discontinuity. At the end of the early AGB the He mass fraction in the envelope is about 0.35 (the initial one was 0.23). For M$\geq$5 $M_{\odot}$ the convective envelope actually penetrates the region where H is exhausted. In this region the 3α reaction were active since the central H burning. As a consequence the Carbon (and Nitrogen) abundance in the envelope increases. Thus, at variance with the classical second dredge up, the total amount of surface CNO increases. At the end of the early AGB we found a mass fraction of CNO in between 10^{-10} and 10^{-6} (for masses between 4 and 7 $M_{\odot}$). As a consequence weak but evident thermal pulses (TPs) develop in stellar models with M$\geq$5 $M_{\odot}$.

6)After few TPs, the convective shell, which usually developes during the He flash, extends up to the the H/He discontinuity. Then the Carbon produced during the thermal pulse is diluted over the whole intershell region. The resulting C mass fraction in the most external layers of the intershell is about 0.2. After about 14-15 TPs the convective envelope penetrates the H/He discontinuity during the quiescent He burning. Similarly to the classical third dredge-up (actually this is the second) the envelope composition is enriched with primary Carbon. But the temperature at the base of the convective envelope is so large that this Carbon is rapidly converted into Nitrogen.

7) In the 4 $M_{\odot}$ model the amount of CNO at the end of the E-AGB is too low for the TPs. Thus a rather hot H burning shell, in which the 3α are partially active, and a quiescent He burning shell are simultaneously at work. However, after some time the intershell region becomes unstable against convection. Thus a significant amount of Carbon is brought close to the H burning shell. Subsequently, a convective shell appears at the base of the envelope whose inner border penetrates into the C rich zone. An H flash follows. The mass fraction of CNO in the envelope is now as large as 10^{-6}. From this moment in advance "normal" TPs occur.

From our calculations we obtaine that Pop III IMS stars can provide important amount of He, C and N. Some Oxygen is also produced. Interesting enough is that these AGB models

are Li rich. The He yields is $0.5 - 1 M_{\odot}$ (depending on the stellar mass). For comparison a 15 $M_{\odot}$ of Z=0 produces 5 $M_{\odot}$ of He. The C and N yields depend on the duration of the TP AGB phase which is mainly determined by the mass loss rate. Typically we found that after each dredge up episode about $3x10^{-4}$ $M_{\odot}$ of Carbon are dredged up in the envelope. This Carbon is mostly converted into Nitrogen at the base of the convective envelope, where the CN cycle takes place. Then for each pulse the amount of N and C in the envelope increase of about $1.8x10^{-4}$ $M_{\odot}$ and $1.2x10^{-4}$ $M_{\odot}$ respectively. Thus, after just 50-60 TPs (which roughly correspond to an average AGB mass loss rate of $4x10^{-5} M_{\odot}/yr$), the Nitrogen yields will be of the order of 0.01 $M_{\odot}$. This value corresponds to the amount of Nitrogen realized by a 15 $M_{\odot}$ of Z=0 exploding as type II supernova. Similarly we found that the Carbon production of an IMS is about 10 times lower than that of the same massive star. However, by using the IMF of Yoshii & Saio [2] we find that for each massive star (M$\geq$11 $M_{\odot}$) about 5-10 intermediate mass stars were produced from the primordial gas. Thus we conclude that Pop III IMSs have significantly contributed to the Nitrogen and Carbon synthesis of the early galaxy.

References

[1] Palla, F., Salpeter, E.E., Stahler, S.W,, 1983, ApJ, 221, 632

[2] Yoshii, Y., Saio, H., 1986, ApJ, 301, 587

[3] Uheara, H., Susa, H., Nishi, R., Yamada, M., 1996 ApJ, 473, L95

[4] Nakamura, F., Umemura, M., 1999, ApJ, 515, 239

[5] Chieffi, A., Limongi, M., Straniero, O., 1998, ApJ, 737, 762

[6] Limongi, M., Straniero, O., Chieffi, A., 2000, ApJ in publication

[7] Chieffi, A., Tornambè, A., 1984, ApJ, 287, 745

[8] Fujimoto, M.Y., Iben, I.J., Chieffi, A., Tornambè, A., 1984, ApJ, 287, 749

On a physical mechanism of extra-mixing in red giants

P.A. Denissenkov[1], *C.A. Tout*[2]

[1] *Astronomical Institute, St. Petersburg University, Russia*
[2] *Institute of Astronomy, Cambridge University, UK*

Abstract

For the first time we propose a real physical mechanism of extra-mixing in red giants which can *quantitatively* interpret all the known star-to-star abundance variations in globular clusters. For more physical and technical details see [5].

1.1 Introduction

We denote by "extra-mixing" (EM) any mixing process in a star which is different from ordinary convection, semiconvection and convective overshooting. In observations the presence of EM has been most convincingly demonstrated in massive MS stars ([8], and references therein) and in low-mass red giants (RGs) on their first ascent along the red giant branch (RGB) [6]. In particular, a common feature of RGs in many globular clusters is the so-called "global anticorrelation" of [O/Fe] versus [Na/Fe] ([7]; Fig. 1, symbols). One of the plausible explanations of its origin is the following. A RGB star consists of an electron-degenerated helium core with a hydrogen burning shell (HBS) atop of it surrounded by an extended convective envelope. The HBS and the base of the convective envelope (BCE) are separated by a thin radiative zone. Denissenkov & Denissenkova [2] have shown that at the top of the HBS the temperature is high enough for the reaction ^{22}Ne(p,γ)^{23}Na to proceed (due to a resonance!) even faster than O is depleted in the CNO-cycle. If in globular cluster RGs EM (which is undoubtedly present between the HBS and the BCE in *all* low-mass RGs both in the field and in clusters [1, 3, 6]) can reach layers where O begins to decrease then it will bring material enriched in Na and impoverished in O to the stellar surface.

Usually, EM in RGs has been modeled by diffusion without specifying its physical mechanism [1, 3]. Such models have free parameters to be adjusted to fit the observations. In particular, the diffusion model of Denissenkov & Weiss [3] has two parameters, the relative depth $\delta m_{\rm mix}$ ($\delta m = 0$ at the bottom of the HBS and 1 at the BCE) and the rate $D_{\rm mix}$ of EM. The global anticorrelation of [O/Fe] vs. [Na/Fe] has been quite satisfactorily reproduced theoretically by this diffusion model with the mixing parameters $\delta m_{\rm mix} = 0.06 - 0.07$, $D_{\rm mix} = 1 - 5 \cdot 10^9$ cm^2·s^{-1} (Fig. 1, dot-dashed line).

1.2 The proposed mechanism of extra-mixing

Analysis of results obtained with the diffusion model led us to the following important conclusions. The spread of the global anticorrelation in [Na/Fe] depends primarily on the mixing depth, whereas the variation in [O/Fe] tells us mostly about the rate of mixing. In this respect globular cluster RGs can be used as a unique "laboratory" and the global anticorrelation itself as an efficient "tool" for testing various mechanisms of EM. In particular, the morphology of

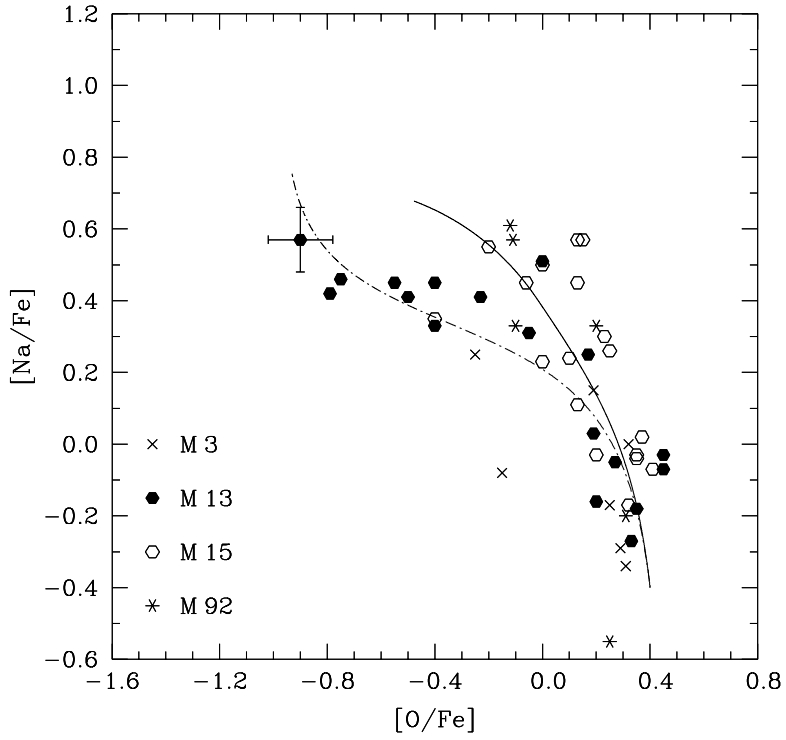

Figure 1: The global anticorrelation of [O/Fe] vs. [Na/Fe] and its theoretical reproductions by the diffusion (dot-dashed line, mixing depth $\delta m_{\rm mix} = 0.06$ and rate $D_{\rm mix} = 2.5 \cdot 10^9$ cm^2·s^{-1}) and Zahn's (solid line) model.

the global anticorrelation implies that the depth of EM in globular cluster RGs seems to be approximately the same in all the clusters but its rate is different, giants in M 13 experiencing the fastest mixing (Fig. 1, symbols).

Quite recently a first real physical mechanism of EM in RGs has been proposed by Denissenkov & Tout [5]. This is Zahn's mechanism [10, 12]. It considers EM in a radiative zone of a star as a result of joint operation of rotation-driven meridional circulation and turbulent diffusion. A brief description of this mechanism is given below.

In a rotating star the surfaces of constant entropy do not coincide with the equipotential surfaces. Consequently, the spherically symmetric radiative flux cannot support a state of thermal equilibrium and, as a result, meridional circulation begins. This advects angular momentum so that an initial state of uniform rotation tends towards differential rotation. It is assumed that turbulence induced by hydrodynamic instabilities, associated with the differential rotation, is highly anisotropic with horizontal components of the turbulent viscosity strongly dominating over the vertical. This basic assumption ensures that the star settles into a state of shell-like rotation with the angular velocity depending only on the distance from the centre, and the problem can then be treated as one-dimensional. Among various hydrodynamic instabilities the shear (Kelvin-Helmholtz) instability has one of the short-

est (dynamical) growth timescales. A radial thermal stratification acts against the growth of perturbations and an appropriate stability criterion should be applied. If the perturbations can grow then the vertical shear turbulence (the "turbulent diffusion") competes with the meridional circulation in redistributing angular momentum. On the other hand, on the equipotential surfaces nothing can prevent the perturbations from becoming large enough to initiate horizontal turbulence even in the presence of very weak shear flows. This justifies the basic anisotropy assumption.

Linearization of the heat, Poisson's and hydrostatic equilibrium equations, with the ratio of the centrifugal acceleration to the gravity $\varepsilon = r\Omega^2/g$ as a small parameter, leads to a dependence of the meridional circulation velocity on the angular velocity Ω, the mean molecular weight μ and their derivatives with respect to radius in the form

$$U = U_1(\Omega, \frac{\partial\Omega}{\partial r}, \frac{\partial^2\Omega}{\partial r^2}, \frac{\partial^3\Omega}{\partial r^3}) + U_2(\mu, \frac{\partial\mu}{\partial r}, \frac{\partial^2\mu}{\partial r^2}, \frac{\partial^3\mu}{\partial r^3}).$$

Denissenkov & Tout [5] have developed an efficient algorithm and computer code which solves (by the relaxation method) a strongly nonlinear equation

$$\frac{\partial}{\partial t}(\rho r^4\Omega) = \frac{1}{5}\frac{\partial}{\partial t}[\rho r^4\Omega(U - 5\dot{r})] + \frac{\partial}{\partial r}(\rho r^4 D_{\rm v}\frac{\partial\Omega}{\partial r})$$

describing the angular momentum transport by meridional circulation (U) and turbulent diffusion ($D_{\rm v}$). This equation has such a structure that under stationary conditions meridional circulation and turbulent diffusion cancel each other after a short (thermal) time. This happens, for example, in the radiative envelope of a massive MS star. As a result, rotation-driven EM in the MS OB-stars is expected to be very slow, in spite of their fast rotation, which explains the delay in the He enrichment of their atmospheres [4, 8].

The latter equation has been solved together with the nuclear kinetics network

$$\frac{\partial y_i}{\partial t} = \left(\frac{\partial y_i}{\partial t}\right)_{\rm nucl} + \frac{\partial}{\partial M_r}\left[(4\pi r^2\rho)^2 D_{\rm mix}\frac{\partial y_i}{\partial M_r}\right].$$

The second term on the right hand side of this equation is used to model EM by diffusion with the coefficient

$$D_{\rm mix} = D_{\rm v} + D_{\rm eff}, \text{ where } D_{\rm eff} = \frac{|rU|^2}{30D_{\rm h}}.$$

The coefficient of the horizontal turbulent diffusion is approximated by $D_{\rm h} \propto r\sqrt{U^2 + V^2}$, where V is the amplitude of the horizontal component of the meridional circulation velocity. For the first time the above equations were derived in [10, 12].

As an appropriate criterion for the shear instability Denissenkov & Tout [5] have used

$$\frac{1}{5}\left(r\frac{d\Omega}{dr}\right)^2 > \frac{g}{H_P}\nabla_\mu$$

from [9]. For the physical conditions prevailing in the radiative zone of a RG [9] also gives the following estimate for the coefficient of (vertical) turbulent diffusion

$$D_{\rm v} \approx 2K\frac{\frac{1}{5}\left(r\frac{d\Omega}{dr}\right)^2 - \frac{g}{H_P}\nabla_\mu}{\frac{g}{H_P}(\nabla_{\rm ad} - \nabla_{\rm rad})}.$$

Here H_P and K are the pressure scale height and the thermal diffusivity, respectively, $\nabla_{\rm ad}$ and $\nabla_{\rm rad}$ the adiabatic and radiative logarithmic temperature gradients (with respect to pressure), and $\nabla_\mu = (\partial \ln\mu/\partial \ln P)$.

1.3 Basic results

The main result obtained in [5] was pointing out that in the radiative zone between the HBS and the BCE in a RG there is a stationary flow (described by the term $\dot{r}$ in the above angular momentum transport equation) of hydrogen rich material directed inwards (it feeds the HBS) and that rotation-driven EM has practically no influence on this flow. The angular momentum conservation law then requires a rather steep profile of the angular velocity ($\Omega \propto r^{-2}$). Hence, this radiative zone may be in a state of strongly differential rotation and, as a consequence, Zahn's mechanism can work here very efficiently.

Another new exciting result was an independent determination of the correct value of the mixing depth $\delta m_{\rm mix} = 0.06 - 0.07$ (compare this with the above semi-empirical value estimated with the diffusion model of Denissenkov & Weiss [3]) obtained with Zahn's mechanism in which $\delta m_{\rm mix}$ is no longer a free parameter. The only free parameter left, the rate of EM, can be *in principle* constrained by observations because $D_{\rm mix}$ is found to be proportional to the squared rotational velocity at the BCE. However, for this we have to know a relation between $\Omega_{\rm BCE}$ and the surface rotation velocity.

The solid curve in Fig. 1 was calculated by Denissenkov & Tout [5] with Zahn's mechanism. The rate of EM (dependent on the parameter $\Omega_{\rm BCE}$) was chosen to reproduce the global anticorrelation for the most globular clusters except the unique cluster M 13. Note that when transformed into the surface rotational velocity (under the assumption of the constant specific angular momentum distribution in the convective envelope), the chosen mixing rate turns out to be consistent with the observed rotational velocities in these clusters. The hypothesis of a rotation-driven EM in globular cluster RGs is supported by observations of Peterson et al. [11] who found that horizontal branch stars in M 13 rotated about twice as fast as stars in M 3, M 15 and M 92.

Acknowledgements

PAD expresses his gratitude to Wolfgang Hillebrandt and Ewald Müller who continue the good tradition of organizing the workshop on nuclear astrophysics in the Ringberg Castle.

References

[1] C. Charbonnel, ApJ **453** (1995) L41

[2] P.A. Denissenkov and S.N. Denissenkova, SvA Lett. **16** (1990) 275

[3] P.A. Denissenkov and A. Weiss, A&A **308** (1996) 773

[4] P.A. Denissenkov, N.S. Ivanova and A. Weiss, A&A **341** (1999) 181

[5] P.A. Denissenkov and C.A. Tout, MNRAS (2000), accepted

[6] R.G. Gratton, C. Sneden, E. Carretta, A. Bragaglia, A&A **354** (1999) 169

[7] R.P. Kraft, PASP **106** (1994) 553

[8] L.S. Lyubimkov, Ap&SS **243** (1996) 329

[9] A. Maeder and G. Meynet, A&A **313** (1996) 140

[10] A. Maeder, J.-P. Zahn, A&A **334** (1998) 1000

[11] R.C. Peterson, R.T. Rood and D.A. Crocker, ApJ **453** (1995) 214

[12] J.-P. Zahn, A&A **265** (1992) 115

Lithium Synthesis by Extra-Mixing in Red Giants

P.D. Denissenkov[1,2], *A. Weiss*[1]

[1] *Max-Planck-Institut für Astrophysik, Garching, Germany*
[2] *Astronomical Institute of the St. Petersburg University, Russia*

1.1 Introduction

Lithium (here we consider the ^{7}Li isotope) is one of the few elements created during the Big Bang Nucleosynthesis in measurable amounts. In stars, it is destroyed by the $^7\mathrm{Li}(p,\alpha)^4\mathrm{He}$ reaction (part of the pp-chains), whenever $T > 2.5\cdot10^6$ K, which is true for most of the stellar interior. If some mixing between the photosphere and the deep interior exists, low ^{7}Li surface abundances will be observed. On the other hand, there are processes for ^{7}Li-production, e.g. spallation of heavier nuclei by cosmis ray particles, and – important for this work – the Cameron-Fowler-mechanism: Here, the pp-chain is interrupted at the reaction $^3\mathrm{He}(\alpha,\gamma)^7\mathrm{Be}$ by transporting ^{7}Be faster to cooler regions than the subsequent p-capture can take place. It is then converted by e^--capture to ^{7}Li, which can survive. This process is known to take place in AGB-stars, and we will show how it can work in stars on the first giant branch as well.

Canonical stellar evolution theory predicts (for low-mass stars of $M < 2.5M_\odot$) only very minor changes of the surface abundances due to the first dredge-up on the red giant branch (RGB). Fig. 1 shows observed surface values (taken from [1]) for *field* stars compared to theory. The dotted lines correspond to the abundances before, the dashed ones to those after the dredge-up, when nuclei of the CNO-cycles are mixed with the pristine convective envelope mixture. While the agreement at low luminosity is very good, the observed data indicate a further mixing beyond $\log L/L_\odot \approx 2$, where the hydrogen shell reaches homogeneous layers left behind during the dredge-up. At this point, C and N abundances change significantly, indicating that the mixing goes deeper than before. Also, ^{7}Li is reduced. All changes can be modeled by invoking *an additional diffusive mixing* between the outer hydrogen shell and the convective envelope. In several papers, we have shown that this mechanism is able to reproduce the observations quite well [2]. Extra-mixing can also explain O-underabundances which anticorrelate with Na-overabundances in some globular clusters (most prominently in M13); for this effect, which is not observed in field stars, one has to invoke faster and deeper mixing, however.

Quite in contrast to the ^{7}Li depletion discussed by now, there exist about 40 *Li-rich K-giants* in the field [3] and a few *Li-rich cluster giants* (e.g. in M3; [4]) with overabundances of 1 dex as compared to the primordial value! Sackmann & Boothroyd [5] tried to explain this by the Cameron-Fowler mechanism invoked by deep mixing. However, to do so, one has to invoke *very fast and shallow* mixing with parameters in strong conflict with those needed for the O-Na-anticorrelation. Since the ^{7}Li-rich M3-giant shows O and Na anomalies, too, this points to an independent, additional process in this star, which otherwise is very similar in its abundances to three ^{7}Li-normal giants investigated in [4] for comparison. Also, this simple approach causes the problem that ^{7}Li-abundances stay high (cf. line 2 in Fig. 2), which is contrast to the results of [3], who found strong arguments that the ^{7}Li-rich phase is limitied in time (of order 10^5 yrs). Any scenario to explain the ^{7}Li-rich giants must therefore also include rapid *destruction* of ^{7}Li after the creation phase!

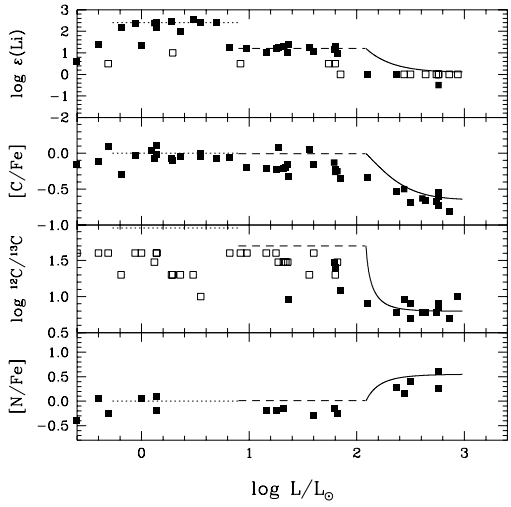

Figure 1: Abundance changes during main-sequence and red-giant evolution for low-mass field stars (data from [1] compared to theoretical predictions (see text). About 90% of all field stars show the abundance changes at high luminosity, which can be explained consistently by additional diffusive mixing.

1.2 ^{7}Li-rich giants due to planet capture

Siess & Livio [6] suggested that the ^{7}Li-richness of giants could be the result of having captured a massive planet or brown dwarf, which would add its own primordial ^{7}Li to the giant's envelope. This scenario would explain the circumstellar shells observed as an IR-excess in the K-giants (see [3]) and the timescales. However, it predicts – at most – primordial ^{7}Li abundances (for Pop. II stars $\log \mathrm{Li} \approx 2.1$ on the scale where $\log \mathrm{H} = 12.0$), while observed values are up to $\log \mathrm{Li} = 3$. In the following we describe our scenario which combines planet capture and deep mixing:

Let us assume that the giant – due to its increasing radius – engulfs a companion, which will spiral in, and according to [6] dissolves at the bottom of the convective envelope for a mass of about $10\,M_\mathrm{J}$. Since the companion had near-Keplerian speed, it will deposit its angular momentum implying near-breakup rotation at the dissolving point. Denissenkov & Tout [7] have elaborated on a theory linking depth and diffusion constant of the extra-mixing to rotation. Within this theory one can demonstrate that the latter is of order $10^{11}\,\mathrm{cm^2 s^{-1}}$ for near-breakup rotation.

If the region of very fast rotation remains restricted, i.e. no angular momentum transport to deeper regions sets in, no abundance changes at the surface will be visible at first, because the layers immediately below the convective envelope are unaffected by nuclear reactions. However, in the course of nuclear evolution, the hydrogen shell advances outwards and the convective envlope receeds. Matter with high specific angular momentum will therefore exhibit a relative movement towards the shell (to lower δm). The timescale for this "Ω-wave" to sweep from $\delta m \approx 1$ (corresponding to the bottom of the convective envelope) to 0 (the bottom of the hydrogen shell) is of order $8 \cdot 10^5$ yrs, which is about an order of magnitude

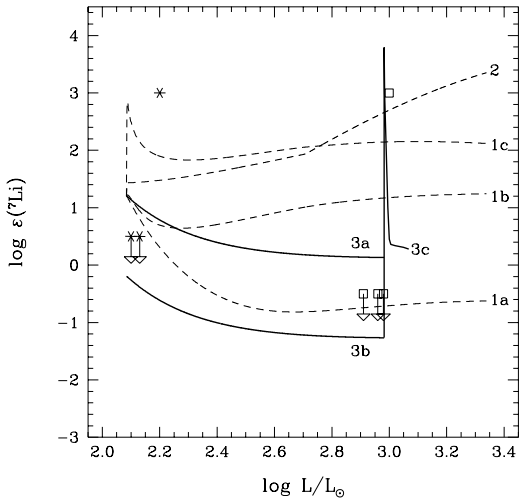

Figure 2: ^{7}Li evolution as function of luminosity on the RGB for several choices of the parameters for extra-deep mixing. See text for explanation of symbols and lines.

longer than timescales for the ^{7}Li abundance to rise and fall as infered from the field K-giants ([3]) and their circumstellar envelopes. The wave will, of course, also encounter layers where ^{7}Li-production via the Cameron-Fowler mechanism is favored, but, later on, then reach layers of higher temperature and ^{7}Li-depletion will result. It is the time needed to pass through this region which has to be compared with observations.

The results of our calculations are summarized in Fig. 2, where ^{7}Li-abundance as function of luminosity is plotted. The symbols are stars with observed ^{7}Li-abundances in M3 (open squares) and the open cluster Berkeley 21 (asterisks). They demonstrate that ^{7}Li-enrichment can happen at any time during the RGB evolution. Curves labeled 1 have the mixing depth most favorable for ^{7}Li-production ($\delta m = 0.14$); cases a–c correspond to $D_{\rm mix} = 10^9, 5 \cdot 10^9, 10^{11}$. Increasing mixing speed leads to higher ^{7}Li. However, in all three curves the necessary ^{7}Li-destruction does not take place.

The line labeled 2 corresponds to mixing depth $\delta m = 0.17$ and $D_{\rm mix} = 10^{11}$ (similar to the models by [5]). Again, ^{7}Li-enrichment is a permanent feature. Since at least the ^{7}Li-rich star in M3 also exhibits the O-Na-anomaly, one had to explain how two very different mixing depths and velocities can be present in the star permanently.

Finally, the solid lines (3) correspond to parameters explaining the standard ^{7}Li-depletion on the upper RGB (see Fig. 1) and the O-Na-anticorrelation. Parameters are $\delta m = 0.06$ and $D_{\rm mix} = 5 \cdot 10^8$ for two different initial ^{7}Li abundances (curves a and b). In case 3c we then have added additional mixing with $D_{\rm mix} = 10^{12}$, but limited to a very restricted mass range, which sweeps through the shell-convective envelope-interlayer at an evolutionary speed of 0.01 per 8000 years (from $\delta m = 0.16$ to 0.06). This case leads to a short-time event of high ^{7}Li lasting 80,000 years, in agreement with observations.

1.3 Conclusions

While ^{7}Li-poor giant stars can be explained self-consistently with CNO-cycle isotope abundances by invoking moderate diffusive mixing between the hydrogen shell and the convective envelope, for ^{7}Li-rich giants, which are observed both in the field and in some globular clusters, a special scenario has to be invoked. This is for two reasons: (i) The object in M3 displays O-Na-anomalies as many other stars in this cluster and differs only in its ^{7}Li-abundance. (ii) While the O-Na-anticorrelation can be modeled with deeper extra-mixing, the ^{7}Li-overabundance requires very shallow, but very fast mixing and a subsequent depletion process. The rise and fall of the ^{7}Li-abundance seems to be an event of limited duration, and thus a single, external event seems to be a promising route to be followed.

We presented our scenario which combines the "external event" of planet or brown dwarf engulfment with the "internal mechanism" of fast mixing and the Cameron-Fowler process for ^{7}Li production. The mixing speed would be a natural consequence of the angular momentum carried by the companion. The mixing depth would follow from the nuclear evolution of the red giant (shell movement). The timescales agree with estimates from field stars; peak ^{7}Li abundances are as observed. At present, there is no inconsistency in our model with the observations. In spite of this, our picture faces some problems: First of all, the physics of the companion capture and its dissolution is unknown; second, [3] have argued that no time-delay between capture, circumstellar shell ejection and ^{7}Li rise exists. It requires additional assumptions to make our scenario agree with this; finally, no circumstellar material (IR-excess) has been observed for the cluster ^{7}Li-rich giants. Therefore, the initial motivation to explain this pattern by capture of a companion does not exist for cluster stars.

Nevertheless, our proposed scenario appears to be a promising starting point to explain ^{7}Li-rich giants.

References

[1] Gratton R.G., Sneden C., Carretta E., Bragaglia A. (1999), A&A 354, 169.

[2] Denissenkov P.A., Weiss, A. (1996), A&A 308, 773.

[3] De la Reza R., Drake N.A., Da Silva L., Torres C.A.O., Martin E.L. (1997), ApJ 448, L1.

[4] Kraft R., R.P., Peterson R.C., Guhathakurta P., Sneden C., Fulbright J.P., Langer G.E. (1999), ApJ 518, L53.

[5] Sackmann I.-J., Boothroyd A.I. (1999), ApJ 510, 217.

[6] Siess L., Livio M. (1999), MNRAS 308, 1133.

[7] Denissenkov P.A., Tout C.A. (2000), MNRAS, accepted.

New results on electron screening and the effect on the Garching Solar Model

M. Flaskamp[1], *A. Weiss*[1], *V.N. Tsytovich*[2,3]

[1] *Max-Planck-Institut für Astrophysik, Garching, Germany*
[2] *Dep. of Theoretical Physics, General Physics Institute, Russian Academy of Sciences, Moscow, Russia*
[3] *Max-Planck-Institut für extraterrestrische Physik, Garching, Germany*

1.1 Introduction

There has been, again and again, the suggestion that the solar neutrino problem might find its solution – or at least a modification – in a correct treatment of the Coulomb screening of the nuclear reactions. Although approaches aimed at improving the standard Salpeter formula ([1]) for weak screening have been refuted (see, e.g. [2] and references therein), it cannot be excluded that indeed Salpeter's static screening formula can be improved. One of the latest approaches to do so is by [3], to which we refer the reader for the details (see also [4]). The results of this approach are rather surprising in that the screening actually leads to a *reduction* of the nuclear rates, which can be quite significant. This is contrary to expectations based on the static approach. Table. 1 reproduces data from [4].

Reaction	Λ_{ij}	Λ_{ij}^S	F_{ij}	$F_{ij}-1$
$p+p$	-0.051	+0.05	1.106	10.6%
^{3}He $+^3$ He	-0.186	+0.20	1.223	22.3%
^{3}He $+^4$ He	-0.190	+0.2	1.223	22.3%
^{7}Li $+p$	-0.268	+0.15	1.571	57.1%
^{7}Be $+p$	-0.458	+0.2	2.087	108.7%
^{7}Be $+e^-$	-0.567	+0.2	2.166	116.6%

Table 1: Result on screening from [4]. For 6 key reactions of the pp-chains, the screening factor $1+\Lambda_{ij}$, as obtained from the theory of [3] is compared to that of [1] (Λ_{ij}^S). $F_{ij} = \frac{1+\Lambda_{ij}^S}{1+\Lambda_{ij}}$ is the factor going from Salpeter's to the new formula, $F_{ij}-1$ the fractional change.

Although the discussion about the validy of the new results has just started, it is interesting to compute standard solar models with the new screening to see its influence and the reaction of the solar model.

1.2 Standard solar models

We have computed a solar model with standard solar model physics (see [5] for details about the standard model and the physics involved) with the exception that for reasons of CPU-economy only H/He-diffusion, but no metal-diffusion was included. Also, the number of grid points and timesteps is smaller than in our best model. The latter, as is shown in Fig. 1, agrees with the two best models available in the literature (Bahcall BP98, Christensen-Dalsgaard

CD-S) very well. All models lie, with the exception of a small region below the convective envelope (at $r/R \approx 0.70$) within the error-range of the derived solar sound speed profile. In Fig. 2 we show how the new screening ("Tsytovich"-screening, as opposed to "Salpeter"-screening) influences the sound speed.

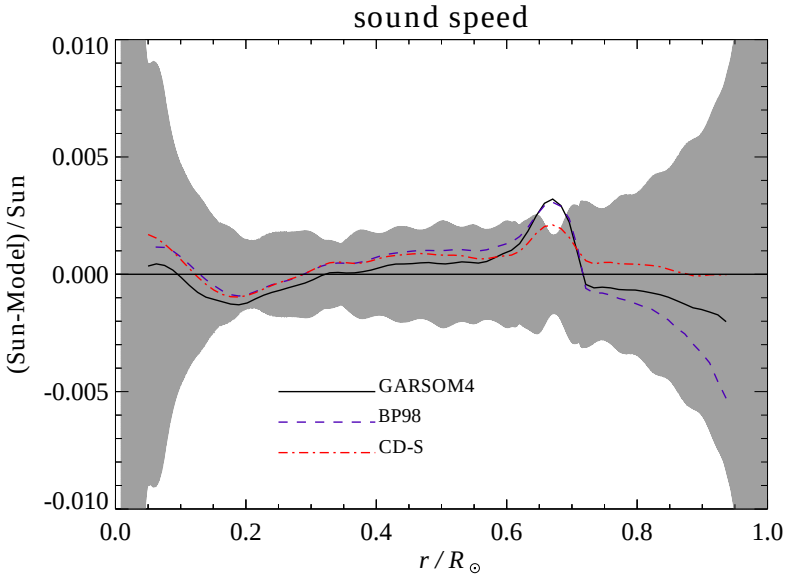

Figure 1: Relative error of standard solar models' sound speed as compared to that derived from solar p-mode oscillations. Our model (GSM) is shown by the solid line. The very conservative error range is taken from [6].

In the center, the sound speed is increased by 0.9% for $r/R < 0.10$, which is (see Fig. 1) outside the error range allowed by the seismic model. Below the convective envelope, the sound speed is increased by 0.4%. Although this change is smaller, the error range in that region is much smaller than at the center, and therefore again the modified model with Tsytovich-screening is inconsistent with the seismic model.

	Salpeter	Tsytovich	GSM
$Y_{\rm i}$	0.2689	0.2660	0.2747
$\alpha_{\rm i}$	1.754	1.714	0.975
$(\frac{Z}{X})_{\rm i}$	0.0253	0.0250	0.0282
T_c	$1.55 \cdot 10^7$	$1.58 \cdot 10^7$	$1.56 \cdot 10^7$
$Y_{\rm s}$	0.239	0.237	0.245
$R_{\rm b.c.z.}$	0.711	0.716	0.713

Table 2: Initial and final parameters of the two models calculated and our best standard solar model GSM. In the latter, a different convection theory has been used; the values for $\alpha_{\rm i}$ can therefore not be compared directly.

Finally, Tables 2 and 3 list the model properties and the predicted neutrino fluxes for both models along with that of our best model (GSM) to indicate that changes due to the new screening. It is important to note the increase of the boundary of the convective envelope

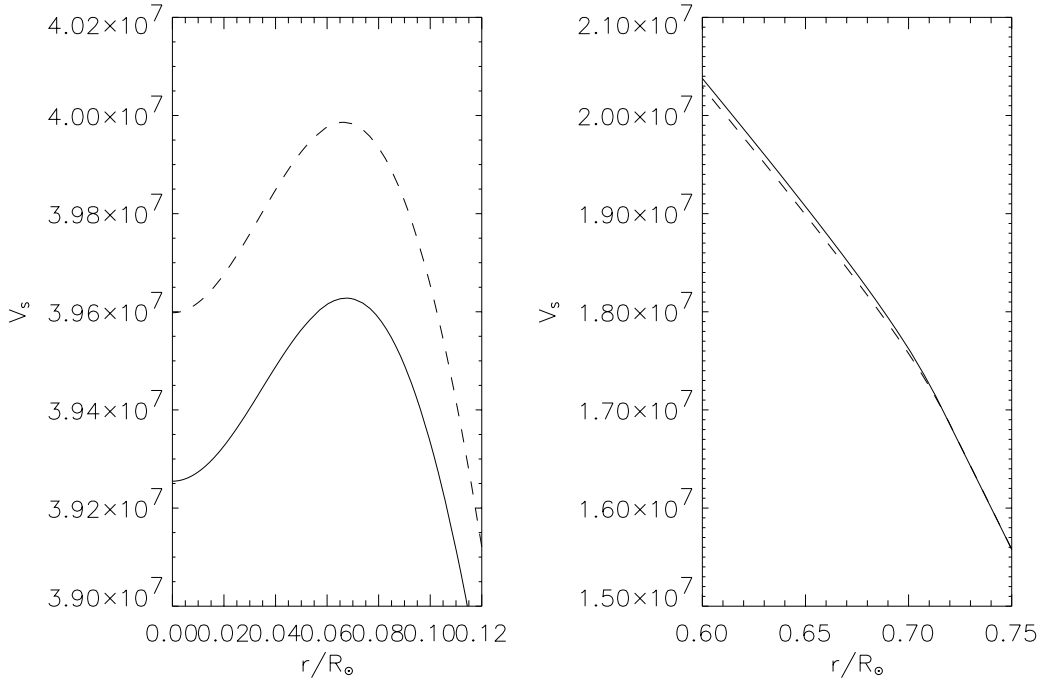

Figure 2: Solar model sound speed from a model with Salpeter-screening (solid) and one with Tsytovich screening (dashed). Left: at the center; right: at the border of the convective zone.

($R_{\mathrm{b.c.z.}}$), which is at the border of the observationally allowed value ($R_{\mathrm{b.c.z.}} = 0.713 \pm 0.002$), and the drastically reduced ν-flux of the reactions involved in the ppII and ppIII chains and the CNO-cycle. In particular the change in the ^{8}B-flux is so severe that a prediction *below* the measurement of Superkamiokande is possible. This would imply an *inverse* neutrino problem. However, one has also to keep in mind that the fluxes of the two models calculated for this investigation also differ from that of the best model. We can therefore only assume that the relative changes would be similar when computing model GSM with Tsytovich-screening.

ν	Salpeter	Tsytovich	GSM
pp	$5.92 \cdot 10^{10}$	$5.94 \cdot 10^{10}$	$5.93 \cdot 10^{10}$
pep	$1.39 \cdot 10^{8}$	$1.46 \cdot 10^{8}$	$1.39 \cdot 10^{8}$
hep	$2.13 \cdot 10^{3}$	$2.82 \cdot 10^{3}$	$2.07 \cdot 10^{3}$
7Be	$4.49 \cdot 10^{9}$	$4.08 \cdot 10^{9}$	$4.81 \cdot 10^{9}$
8B	$4.24 \cdot 10^{6}$	$1.49 \cdot 10^{6}$	$5.06 \cdot 10^{6}$
13N	$4.43 \cdot 10^{8}$	$6.06 \cdot 10^{8}$	$5.85 \cdot 10^{8}$
15O	$3.78 \cdot 10^{8}$	$5.41 \cdot 10^{8}$	$5.07 \cdot 10^{8}$
17F	$4.58 \cdot 10^{6}$	$6.71 \cdot 10^{6}$	$6.25 \cdot 10^{6}$
$\sum[\frac{1}{s \cdot cm^2}]$	$6.47 \cdot 10^{10}$	$6.48 \cdot 10^{10}$	$6.54 \cdot 10^{10}$

Table 3: Neutrino fluxes of the same models as in Table 2.

1.3 Conclusions

We have calculated standard solar models with conventional Salpeter- and the new Tsytovich-screening. We find that the reduced nuclear reaction rates, in particular the strongly reduced ^{7}Be reaction rates, lead to a solar model which appears to be inconsistent with present-day seismic sound speed results, provided the error range given for the seismic inversion is correct. Since the standard model with Salpeter-screening agrees very well with the seismic model over the largest part of the Sun, this is a severe result indicating the need for a more precise calculation of the new screening values.

However, one has to keep in mind that the new approach, which has been adopted from plasma physics perturbation theory, with which the screening is calculated, also predicts changes in the equation of state and in the opacities. Both effects have not been included in our models. They are therefore, to some extent, inconsistent.

Second, in [3] it has already been noted that a further improvement of the screening rates is possible, if not necessary. It was estimated that the screening rates, when calculated in the next order of the expansion approach, will possible be corrected by as much as 25% in the *opposite* direction. Therefore the effects on sound speed and neutrino fluxes could be less strong as found in our calculations.

We conclude therefore with stating that within our test calculation the new screening faces severe challanges from helioseismic results and that further improvements and investigations will be necessary to decide on its correctness.

Acknowledgements

We thank H. Schlattl for assisting us in the calculation of the models and in discussing the results. This work has been supported in part by the Sonderforschungsbereich SFB-375 (Astro-Teilchen-Physik) of the DFG.

References

[1] Salpeter E.E., Australian J. Phys., 7, 353 (1954)

[2] Brueggen M., Gough D.O., Astrophys. J., 488, 867 (1997)

[3] Tsytovich V.N., Bornatici M., Plasma Physics Reports, accepted (2000)

[4] Tsytovich V.N. , A&A Letters, submitted (2000)

[5] Schlattl H., PhD thesis, Tech. Univ. Munich (1999)

[6] Degl'Innocenti S., Dziembowski W.A., Fiorentini G., Ricci B., Astropart. Phys., 7, 77 (1997)

A two-code method for studying some episodes of stellar nucleosynthesis

D.K. Nadyozhin[1,2], *I.V. Panov*[1], *A.Yu. Deputovich*[1]

[1] Institute for Theoretical and Experimental Physics (ITEP), Moscow, Russia

[2] Max-Planck-Institut für Astrophysik, Garching, Germany

Abstract

First, we present some results of our study aimed at facilitating the collaboration between the people studying the nucleosynthesis of the light and intermediate elements and those interested in the creation of the heavier elements. The two corresponding nuclear networks are connected through the exchange of neutrons and, if the temperature $T_9 \gtrsim 1.5$, that of protons as well. We propose a method that allows to obtain a selfconsistent solution by iterating the neutron and proton fluxes between the two codes. Second, we describe simple analytical formulae constructed to approximate the temporal behavior of the temperature, density, and radius of a stellar layer immediately after the arrival of the supernova shock wave. The formulae are expected to be useful for people doing nucleosynthesis in supernovae but having no possibility at the moment to control the propagation of the shock waves in supernovae.

Introduction

The two-code approach was already used in literature. For instance, in [1] there were organized iterative calculations of the nucleosynthesis by running simultaneously two networks. The yields of the elements lighter than Kr, calculated with one code, were iteratively coupled through neutron channel to those of heavier elements obtained with the aid of another code. In the case of the neutrino-induced nucleosynthesis in stellar helium shell, the two-code method was employed in [2] to calculate selfconsistently the density of neutrons that is strongly dependent on the rate of the neutron absorption by heavy nuclei in the r-process network. The advantage of the two-code method as compared to the usage of one huge nuclear network, including all the nuclides in one calculating scheme, consists in bringing together the specialists in different areas of stellar nucleosynthesis. Such an approach is indispensable for critical understanding of the results and mutual control of the calculations.

Another example of ideologically the same approach is the "off-line" calculation of nucleosynthesis in stellar matter heated by the supernova shock wave (SW), when one does not solve the equations of hydrodynamics but instead somehow approximates the temporal behavior of the temperature and density in shocked matter thereby adjusting the nucleosynthesis to the supernova mechanism. It became almost a standard practice to use a simple exponential approximation for the temperature: $T \sim \exp[-t/(3\tau)]$ where τ is the "hydrodynamic" time scale connected with the *local* density ρ by the expression

$$\tau = \frac{446}{\sqrt{\rho}} \text{ s.} \qquad (1)$$

We show below that such an approximation is far from to be satisfactory and present much more accurate approximation formulae based on the hydrodynamic calculation of the SW propagation in presupernovae.

The iteration of neutron and proton channels

Consider two sets of nuclear kinetic equations — one for the light and intermediate nuclides (the L-set) and another for the heavier nuclides (the H-set). The two sets are connected through the neutron and proton channels. The equations controlling the abundances of neutrons and protons in the L-set are given by

$$\frac{dY_{\rm n}}{dt} = S_{\rm n} - Y_{\rm n}F_{\rm n}\,, \qquad \frac{dY_{\rm p}}{dt} = S_{\rm p} - Y_{\rm p}F_{\rm p}\,, \tag{2}$$

where $S_{\rm n}$ and $S_{\rm p}$ are the sums over all the neutron and proton emitting or absorbing reactions among the species belonging to the L-set whereas $F_{\rm n}$ and $F_{\rm p}$ come from the neutron and proton interaction with the nuclides belonging to the H-set. To begin the iterations one has to specify some preliminary F-values: $F^0_{\rm n,p}$. Then integrating with these values the full L-set of nuclear kinetic equations (together with Eqs. (2)) in the time interval of interest ($0 < t < t_{\rm max}$) one obtains the functions $Y^0_{\rm n,p}(t)$ as the first guess. The next step is to integrate the H-set of equations using $Y^0_{\rm n,p}(t)$ as the input neutron and proton densities to obtain new trial F-values:

$$F^1_{\rm n} = -\frac{1}{Y^0_{\rm n}(t)}\left(\frac{dY_{\rm n}}{dt}\right)^0_{\rm H}\,, \qquad F^1_{\rm p} = -\frac{1}{Y^0_{\rm p}(t)}\left(\frac{dY_{\rm p}}{dt}\right)^0_{\rm H}\,, \tag{3}$$

where $\left(\frac{dY_{\rm n,p}}{dt}\right)^0_{\rm H}$ are the rates of the neutron and proton change required by all the nuclear reactions involving neutrons and protons in the H-set. Now one can begin the second iteration by solving the L-set of equations with the F-values given by Eqs. (3). The iterations are to be cycled this way until the neutron and proton densities converge to a prescribed accuracy, say $\left(Y^{k+1}_{\rm n,p} - Y^k_{\rm n,p}\right)/Y^{k+1}_{\rm n,p} < 0.01$. A word of caution should be added to such a procedure. Typically neutrons and protons are absorbed in the H-set and $F_{\rm n,p}$ prove to be positive. However, for some periods of time the F-values could be negative. For instance, in some cases during the after-shock-wave freezout $F_{\rm n}$ can become negative owing to the emission of beta-delayed neutrons. If this happens, in order to avoid a numerical instability one has to use in Eqs. (2) $\left(\frac{dY_{\rm n,p}}{dt}\right)_{\rm H}$ instead of $Y_{\rm n,p}F_{\rm n,p}$.

Figure 1 shows an example of the two-code method implementation in the case of the neutrino-induced nucleosynthesis in the helium shell. Free neutrons and protons come from the neutrino breakup of ^{4}He. The initial physical conditions in the helium shell are $T_9 = 0.8$, $\rho = 10^4\,{\rm g\,cm^{-3}}$. The helium shell is assumed to be located at radius $R = 1{\cdot}10^9$ cm that is by a factor of ~ 4 closer to stellar center than follows from presupernova evolutionary models of massive stars. Such a small value of R was chosen for the temperature to be high enough to ensure effective interaction of protons with the nuclides belonging both to the L-set and H-set. Astrophysically, the small R-values are of interest because of a possibility for helium shell matter to be brought down to the center by macroscopic advection expected either at the very last moments of presupernova evolution or during the origin of the shock wave at the boundary of the collapsing stellar core. The shock wave reaches the helium shell at $t = 0.26\,{\rm sec}$ and heats it up to $T_9 \approx 2.2$ causing an abrupt increase in $Y_{\rm n}$ (Fig. 1) due to the (γ,n) reactions.

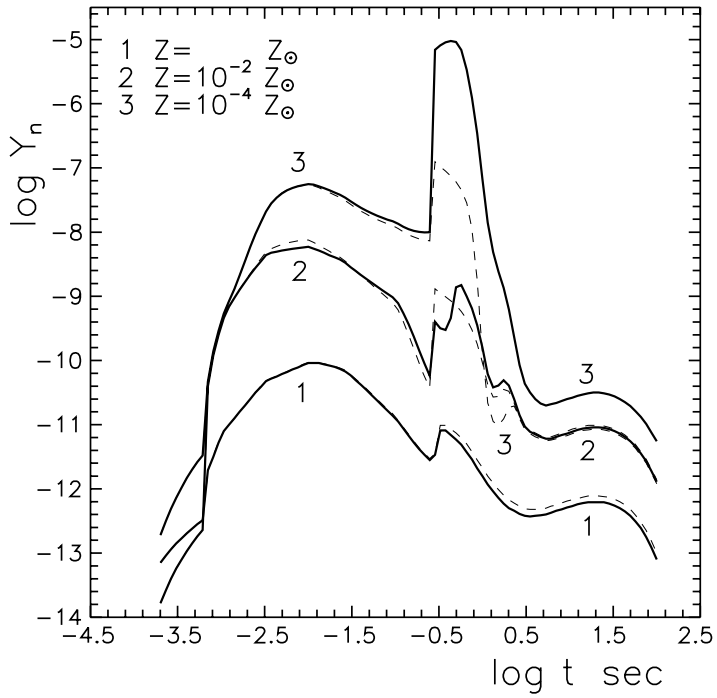

Figure 1: The temporal behavior of the neutron density resulting from the neutrino breakup of ^{4}He for different metallicities. The neutrino burst begins at $t = 0$; $N_n = 6{\cdot}10^{27}\, Y_{\rm n}\,{\rm cm}^{-3}$.

In this example, the L-set describes the nuclear kinetics of about 120 reactions among the light and intermediate nuclides (n, p, D, T, ^{3}He, ^{4}He ... ^{24}Mg) whereas the H-set deals with more than 4000 equations describing the processing of the initial ^{56}Fe seeds into heavier elements via copious n- and p-capture intermitted with β-decays (for details see [2]).

The dashed lines in Fig. 1 correspond to the first approximation for the F-values in Eqs. (2) which is given by

$$F_{\rm n} \,=\, Y_{\rm Fe56} N_A \,<\sigma_{n,\gamma} v>\,, \qquad F_{\rm p} \,=\, Y_{\rm Fe56} N_A \,<\sigma_{p,\gamma} v>\,, \tag{4}$$

where N_A is the Avogadro number and the ^{56}Fe abundance $Y_{\rm Fe56}$ remains constant and equal to its initial value during all the time interval of interest ($0 \le t \le 100$) sec. Thus, the (n,γ) and (p,γ) reactions on the ^{56}Fe seeds are used to evaluate the first approximation for $F_{\rm n,p}$. The full lines show the final selfconsistent solution. The iterations were terminated after 4–6 iterations when the accuracy better than 1% was achieved. One can see from Fig. 1 that for metallicities $Z \gtrsim 0.01\, Z_\odot$ the first approximation given by Eqs. (4) ensures a practically good accuracy for $Y_{\rm n}$.

The conclusion is that for not too low metallicities one can study the neutrino nucleosynthesis of the light and intermediate elements in the helium shell using a very simple procedure given by Eqs. (4) to take into account the absorption of neutrons and protons by the iron-peak elements. As for the H-set, a noticeable transformation of the iron seeds into heavier nuclides occurs only for very low metallicities ($Z \le 0.01\, Z_\odot$) — the number of neutrons captured per iron seed, n/Fe, turns out to be equal to 0.3, 34, 62 for $Z=Z_\odot$, $10^{-2}Z_\odot$, and $10^{-4}Z_\odot$, respectively.

The properties of supernova shock waves

In order to obtain the approximation of the supernova SW properties useful for exploring nucleosynthesis, we have fulfilled a series of supernova hydrodynamic simulations. The calculations were done with the hydrodynamic supernova code SNV used long ago at the ITEP (see, e.g. [3]). The results of these calculations for different supernova layers can be approximated by the following simple relations for the radius, temperature, and density of a Lagrangian layer:

$$r(t) \;=\; R\left(1+\xi_r\frac{t}{t_u}\right), \qquad T(t) \;=\; \frac{T_p}{1+\xi_T\,t/t_u}, \qquad \rho(t) \;=\; \rho_p\left(\frac{T}{T_p}\right)^3, \tag{5}$$

where R, T_p, ρ_p are the initial radius of the layer, and the peak temperature and density of shocked matter, respectively. We deal with a strong radiation dominated SW, therefore the initial temperature T does not enter Eqs. (5) while the peak density with a good accuracy can be expressed through the initial density ρ as $\rho_p \approx 7\rho$. Equations (5) imply that the SW reachs the layer at $t = 0$. In the case of the neutrino nucleosynthesis, to synchronize the neutrino flux with the post-shock nucleosynthesis one needs also to know the time interval Δt_s between the beginning of the neutrino burst and the SW arrival to the layer under consideration. We shall present the approximation for Δt_s elsewhere.

The peak temperature T_p and characteristic time t_u are given by

$$T_p \;=\; \xi_p\,T_{\rm WW} \equiv \xi_p\left(\frac{3E}{4\pi a R^3}\right)^{1/4} = 2.37{\cdot}10^9\xi_p\,E_{51}^{0.25}\left(R/10^9\ {\rm cm}\right)^{-0.75}\ {\rm K}\,, \tag{6}$$

$$t_u \;=\; 3.83{\cdot}10^{-3}\rho^{0.5}E_{51}^{-0.5}\left(R/10^9\ {\rm cm}\right)^{2.5}\ {\rm sec}\,, \tag{7}$$

where $T_{\rm WW}$ is the Weaver–Woosley temperature [4, 5] and E stands for the supernova explosion energy ($E_{51} = E/10^{51}$ erg).

The dependence of the characteristic time t_u on density turns out to be just opposite to that for τ from Eq. (1). The point is that first, the hydrodynamic time scale τ depends actually on the *mean* density in the sphere of radius r rather than on the local one ρ and second, the time scale of the post-shock expansion is controlled by the speed of sound, $v_{\rm sound}$, in shocked matter and by the order of magnitude is equal to $R/v_{\rm sound}$. Taking into account that $v_{\rm sound}^2 = \gamma P/\rho$, one can obtain that $v_{\rm sound} \sim 1/\sqrt{\rho}$ for the radiation dominated media when $\gamma = 4/3$, $P = aT^4/3$. Such is a correct way to estimate the time scale of the after-shock expansion realized in Eq. (7) and used earlier in ref. [6].

The above approximation formulae include the dimensionless structural coefficients ξ_r, ξ_p, and ξ_T. Their numerical values for a $15{\rm M}_\odot$ supernova [7] are presented in Table 1 for different layers (silicon, carbon-oxygen, helium) and were chosen to fit the hydrodynamic calculations as close as possible.

The coefficients give virtually a good accuracy for a wide range of the supernova explosion energies covered in our calculations: $0.13 \le E_{51} \le 21$. Our calculations for a $30{\rm M}_\odot$ supernova show that the coefficients are weakly dependent on the supernova mass. Thus in the first rough approximation, one may neglect this dependence.

Figure 2 demonstrates an excellent coincidence between the approximation formula for T from Eqs. (5–7) and hydrodynamic calculations — compare the thick line 1 with the thin lines giving the results of hydrodynamic calculations for different supernova explosion energies. In

Table 1: The structural coefficients for a $15M_{\odot}$ supernova.

Layer	ξ_p	ξ_T	ξ_r
Si-middle	1.0	1.9	1.1
Si-top, CO-bottom	0.97	1.6	1.1
CO-middle	0.82	1.1	1.25
CO-top, He-bottom	0.74	0.65	0.85
He-middle	0.90	1.5	1.38
He-top, HeH-bottom	0.73	1.3	1.1

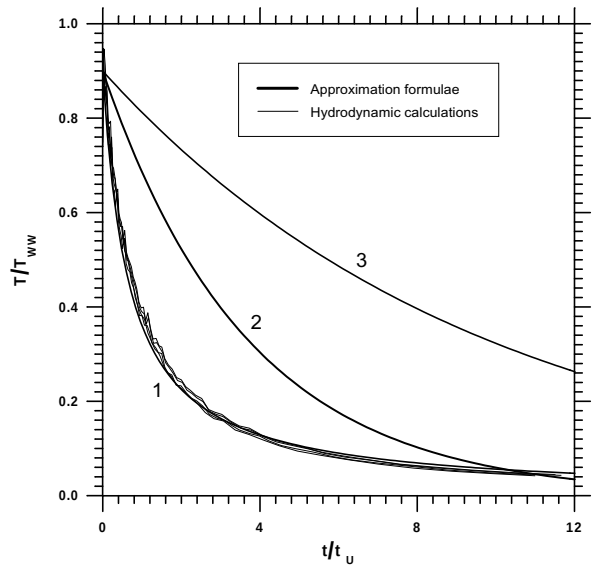

Figure 2: The post-shock temperature versus time for the middle of a $15M_{\odot}$ supernova helium shell.

the middle of a $15M_\odot$ supernova helium shell, the initial (pre-shock) radius, temperature, and density are $R = 1.6 \cdot 10^{10}$cm, $T_9 = 0.08$, and $\rho = 35\,\mathrm{g\,cm^3}$, respectively. The thick line 3 in Fig. 2 shows $T(t)$ for the exponential approximation when one inserts $\rho = 35\,\mathrm{g\,cm^3}$ in τ (Eq. 1). One can see that such approximation results in a much slower decrease in the post-shock temperature. Even for the post-shock density, which is by a factor of 7 larger ($\rho_p = 7\rho$), the exponential approximation is far from to be satisfactory (thick line 2).

Acknowledgements

It is a pleasure to express our deep gratitude to the Max-Planck-Institut für Astrophysik for hospitality and for giving possibility to attend the Ringberg Castle Workshop. The work was supported also by the Swiss Science National Foundation, the International Science and Technology Center (Project No 370-97) and the Russian Foundation for Basic Research.

References

[1] T. Rauscher, J.H. Applegate, J.J. Cowan, F.–K. Thielemann, and M. Wiescher, Ap. J. **429** (1994) 499.

[2] D.K. Nadyozhin, I.V. Panov, S.I. Blinnikov, A&A **335** (1998) 207.

[3] I.Yu. Litvinova, D.K. Nadyozhin, Ap. Sp. Sci. **89** (1983) 89.

[4] T.A. Weaver, S.E. Woosley, Ann. NY Acad. Sci. **336** (1980) 335.

[5] A.Yu. Deputovich, D.K. Nadyozhin, Pis'ma Astr. Zh. **25** (1999) 750 [Astron. Lett. **25** (1999) 649].

[6] F.–K. Thielemann, M. Arnold, W. Hillebrandt, A&A **74** (1979) 175.

[7] S.E. Woosley, T.A. Weaver, Ap. J. Suppl. **101** (1995) 181.

Nucleosynthesis in Massive Stars Including All Stable Isotopes

A. Heger[1], *R. D. Hoffman*[2], *T. Rauscher*[1,3], *& S. E. Woosley*[1]

[1] *Astronomy Department,*
University of California, Santa Cruz, CA 95064, U.S.A.
[2] *Nuclear Theory and Modeling Group, L-414,*
Lawrence Livermore National Lab, Livermore, CA 94551-9900, U.S.A.
[3] *Departement für Physik und Astronomie,*
Universität Basel, CH-4056 Basel, Switzerland

Abstract

We present the first calculations to follow the evolution of all stable isotopes (and their abundant radioactive progenitors) in a finely zoned stellar model computed from the onset of central hydrogen burning through explosion as a Type II supernova. The calculations were performed for a $15\,M_\odot$ Pop I star using the most recently available set of experimental and theoretical nuclear data, revised opacity tables, and taking into account mass loss due to stellar winds. We find the approximately solar production of proton-rich isotopes above a mass number of $A = 120$ due to the γ-process. We also find a weak s-process, which along with the γ-process and explosive helium and carbon burning, produces nearly solar abundances of almost all nuclei from $A = 60$ to 85. A few modifications of the abundances of heavy nuclei above mass 90 by the s-process are also noted and discussed. New weak rates lead to significant alteration of the properties of the presupernova core.

1.1 Introduction

Stars above $\sim 10\,M_\odot$ are responsible for producing most of the oxygen and heavier elements found in nature. Numerous studies of such stars and their detailed nucleosynthetic yields for various masses and metallicities, have been carried out previously, e.g., [32, 27]. However, our knowledge of both the input data and the physical processes affecting the evolution of these stars has improved dramatically in recent years. Updated opacity tables [12] have become available along with more accurate prescriptions for mass loss due to winds and new weak rates [16] that affect the evolutionary stages after central oxygen depletion. Perhaps most important for nucleosynthesis, new, accurate reaction rates for all the relevant strong and electromagnetic nuclear reactions above neon have been recently calculated by Rauscher and Thielemann [21]. Here we present the first results for a $15\,M_\odot$ supernova evolved with the new physics. Additional masses and metallicities will be explored in future papers. These future papers will also include rotationally induced mixing processes [9].

We also employ a nuclear reaction network of unprecedented size. The nuclear reaction network used by [32] (WW95), large in its day, was limited to 200 isotopes and extended only to to germanium (see also Chieffi and Limongi in these proceedings). Studies using nuclear reaction networks of over 5000 isotopes have been carried out for single zones or regions of stars, especially to obtain the r-process, e.g., [4, 5, 15], but "kilo-isotope" studies of nucleosynthesis in complete stellar models (typically of 1000 zones each) have been hitherto

Table 1: Properties of stellar models at the onset of core collapse (*first section*) and integrated stellar yields of some important radioactive nuclei (*second section*).

		this work			WW95 [32]		
initial mass	(10^{34} g)	3	4	5	3	4	5
	($M_\odot$)	15.08	20.11	25.14	15.08	20.11	25.14
final mass	($M_\odot$)	12.64	14.23	13.87	15.08	20.11	25.14
He core	($M_\odot$)	4.16	6.20	8.19	4.36	6.67	9.13
C/O core	($M_\odot$)	2.82	4.57	6.38	2.47	4.37	6.54
Ne/O core	($M_\odot$)	1.87	2.27	2.77	1.81	2.44	2.81
Si core	($M_\odot$)	1.75	2.07	2.11	1.77	2.02	2.06
"Fe" core	($M_\odot$)	1.55	1.47	1.74	1.32	1.74	1.78
delept. core	($M_\odot$)	1.29	1.47	1.59	1.29	1.74	1.78
central Y_e		0.436	0.439	0.444	0.422	0.430	0.430
Pist. location	($M_\odot$)	1.29	1.47	1.74	1.29	1.74	1.78
remnant mass	($M_\odot$)	1.72	1.76	2.31[a]	1.43	2.06	2.41[b]
		radioactive yields					
^{26}Al	($M_\odot$)	$4.66{\cdot}10^{-5}$	$4.89{\cdot}10^{-5}$	$1.45{\cdot}10^{-4}$	$4.30{\cdot}10^{-5}$	$3.47{\cdot}10^{-5}$	$1.27{\cdot}10^{-4}$
^{44}Ti	($M_\odot$)	$1.75{\cdot}10^{-5}$	$8.89{\cdot}10^{-6}$	$2.75{\cdot}10^{-6}$	$5.68{\cdot}10^{-5}$	$1.38{\cdot}10^{-5}$	$1.95{\cdot}10^{-6}$
^{56}Ni	($M_\odot$)	$9.08{\cdot}10^{-2}$	$7.67{\cdot}10^{-2}$	$5.07{\cdot}10^{-3}$	$1.15{\cdot}10^{-1}$	$8.80{\cdot}10^{-2}$	$7.26{\cdot}10^{-5}$
^{60}Fe	($M_\odot$)	$7.16{\cdot}10^{-5}$	$2.84{\cdot}10^{-5}$	$1.45{\cdot}10^{-4}$	$2.66{\cdot}10^{-5}$	$1.12{\cdot}10^{-5}$	$2.10{\cdot}10^{-5}$

[a] $1.5{\cdot}10^{51}$ erg explosion

[b] in [32] a remnant mass of $2.07\,M_\odot$ is given in error for the $1.2{\cdot}10^{51}$ erg explosion. This change decreases significantly the yields of ^{56}Ni and ^{44}Ti (WW95: $1.29{\cdot}10^{-1}\,M_\odot$ and $3.04{\cdot}10^{-5}\,M_\odot$, respectively).

lacking. We thus also present the first calculation to determine, self-consistently, the the complete synthesis of all stable isotopes in any model for a massive star. However, because its thermodynamic properties continue to be poorly determined (and for lack of space), we will ignore here the nucleosynthesis that occurs in the neutrino wind, which may be the principal site of the r-process [31].

1.2 Input Physics

Our calculations were performed using a modified version of the stellar evolution code KEPLER [33, 32] with the following modifications:

- updated neutrino loss rates [13]
- improved opacity tables (OPAL95) [12, 29]
- mass loss due to stellar wind [19]
- updated weak rates [16]
- updated strong and electromagnetic reaction rates [21]

As in WW95, nucleosynthesis was followed by co-processing the stellar model throughout its evolution using an extended nuclear reaction network. From hydrogen ignition through

central helium depletion a 617 isotope network was employed that included all elements up to polonium, adequate to follow the s-process. Just prior to central carbon ignition, we switched to a 1482 isotope network (also including astatine). This new network incorporated more neutron-rich isotopes to follow the high neutron fluxes in carbon (shell) burning. Five to ten isotopes were also added on the proton-rich side, in particular for the heavy elements, to follow the γ-process [30, 23, 24]. The nucleosynthesis during the supernova explosion itself was followed in each zone using a 2439 isotope network that included additional proton-rich isotopes to follow better the γ-process in the neon-oxygen core, and also many additional neutron-rich isotopes to follow the n-process expected during supernova shock front passage through the helium shell [3].

We implemented a new library of experimental and theoretical reaction rates. In particular, we used theoretical strong rates from [21] (using input from the FRDM [17]), experimental neutron capture rates (30 keV Maxwellian average) along the line of stability by [1], and experimental and theoretical rates for elements below neon as described in [11]. Experimental (α,γ) rates were implemented for ^{70}Ge [6] and ^{144}Sm [25]. The derived α+^{70}Ge and α+^{144}Sm potentials were also utilized to recalculate the transfer reactions involving these potentials.

Experimental β^-, β^+, and α-decay rates were taken from [20], experimental β^- rates from [14] and [26], and theoretical β^- and β^+ rates from [18]. As a special case, we implemented the temperature-dependent ^{180}Ta decay as described in [2].

The supernova explosion was simulated, as in [32], by a piston that first moved inward for 0.45 s down to a radius of 500 km and then moved outward to a radius of 10 000 km such that a total kinetic energy of the ejecta at infinity of $1.2{\cdot}10^{51}$ erg resulted (for the 25 $M_\odot$ stars we used a total kinetic energy of $1.5 \cdot 10^{51}$ erg). The final mass cut outside the piston was determined by the mass that had settled on the piston at $2.5{\cdot}10^4$ s after core collapse. Note that the amount of fallback resulting from this prescription depends on both the initial location of the piston used and the energy of the explosion. In particular, the yields of ^{44}Ti and ^{56}Ni are very sensitive to this "final mass cut" determined by the fall back. Multidimensional effects of the explosion are not considered here. The temperature of the μ and τ neutrinos emanating from the proto-neutron star and causing the ν-process nucleosynthesis [34] were assumed to be 6 MeV in contrast to WW95 who assumed 8 MeV. However, we do not follow the ν-process for isotopes with Z or N larger than 40.

1.3 Results and Discussion

1.3.1 Stellar Structure

Table 1 gives the presupernova properties of our new models and, for comparison, those of WW95. The helium, carbon-oxygen, and neon-oxygen cores were defined as the location where hydrogen, helium, and carbon, respectively, first drop below a mass fraction of 1 %, from the stellar surface going inward. The silicon core was defined by where silicon becomes more abundant than oxygen and the iron ("Fe") core by where the sum of the mass fractions of ^{48}Ca and heavier nuclei first exceeds 50 %. The deleptonized core was defined as the region where the number of electrons per baryon, Y_e, first drops below 0.49.

The lower helium core masses in the new models (Table 1) are due to both mass loss and the use of the OPAL opacities. In the 25 $M_\odot$ case a model using OPAL opacities but no mass loss resulted in a helium core of 8.69 $M_\odot$. As a result of the reduced helium core size our new models typically have lower helium-free and carbon-free cores. Due to the interaction of the

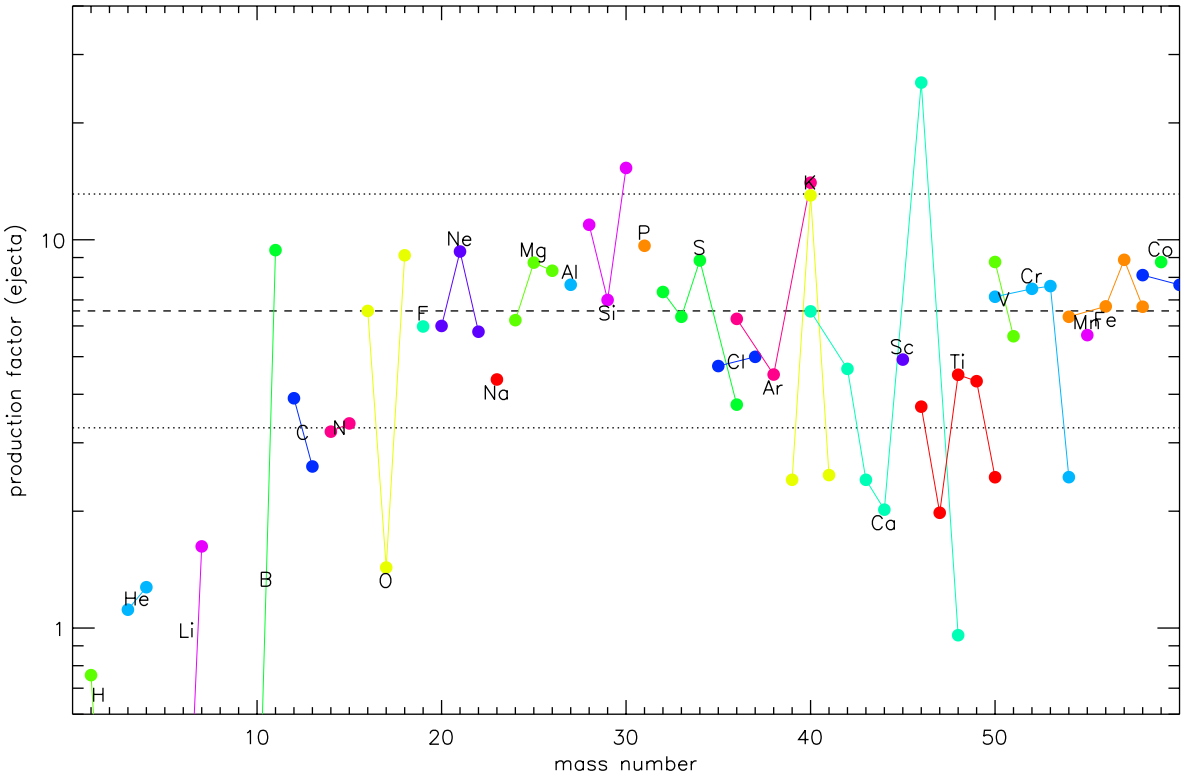

Figure 1: Production factors of iron group and lighter nuclei in a $15\,M_\odot$ star of solar metallicity. Shown here are the average integrated abundances in the ejecta (including mass loss by stellar winds) relative to solar[7] (production factors). The *dashed line* indicates the production factor of ^{16}O and the *dotted lines* span a band of ± 0.3 dex.

different phases of shells burning, the sizes of the "inner cores" do not always monotonically change with the size of the helium core. More details will be given elsewhere [22, 9].

Some important changes in the new models are due to the revised weak rates [16]. These rates become important during core silicon burning and thereafter. Typically, they lead to an increase of the central Y_e at the onset of core collapse by 2 to 3 % (Table 1), and this difference tends to increase with increasing stellar mass [8]. Perhaps more important for the explosion mechanism of core collapse supernovae is an increase of the density in the mass range of $m = 1.5\,M_\odot$ to $2\,M_\odot$ by $30 - 50$ % relative to the same models computed with the previous set of weak rates [32]. This may significantly affect the dynamics of the core collapse. For further details see [8].

1.3.2 Nucleosynthetic Production Factors

In Figs. 1 through 4 we show the production factors of all ejecta of the star after the explosion, including all the mass lost due to stellar winds, relative to solar [7] abundances. We assume that all radioactive nuclei have decayed to their stable products. As a gauge we provide the production factor of ^{16}O, the dominant "metal" produced in massive stars (*dashed line*), and a band of acceptable agreement of ± 0.3 dex relative to this values (*dotted lines*).

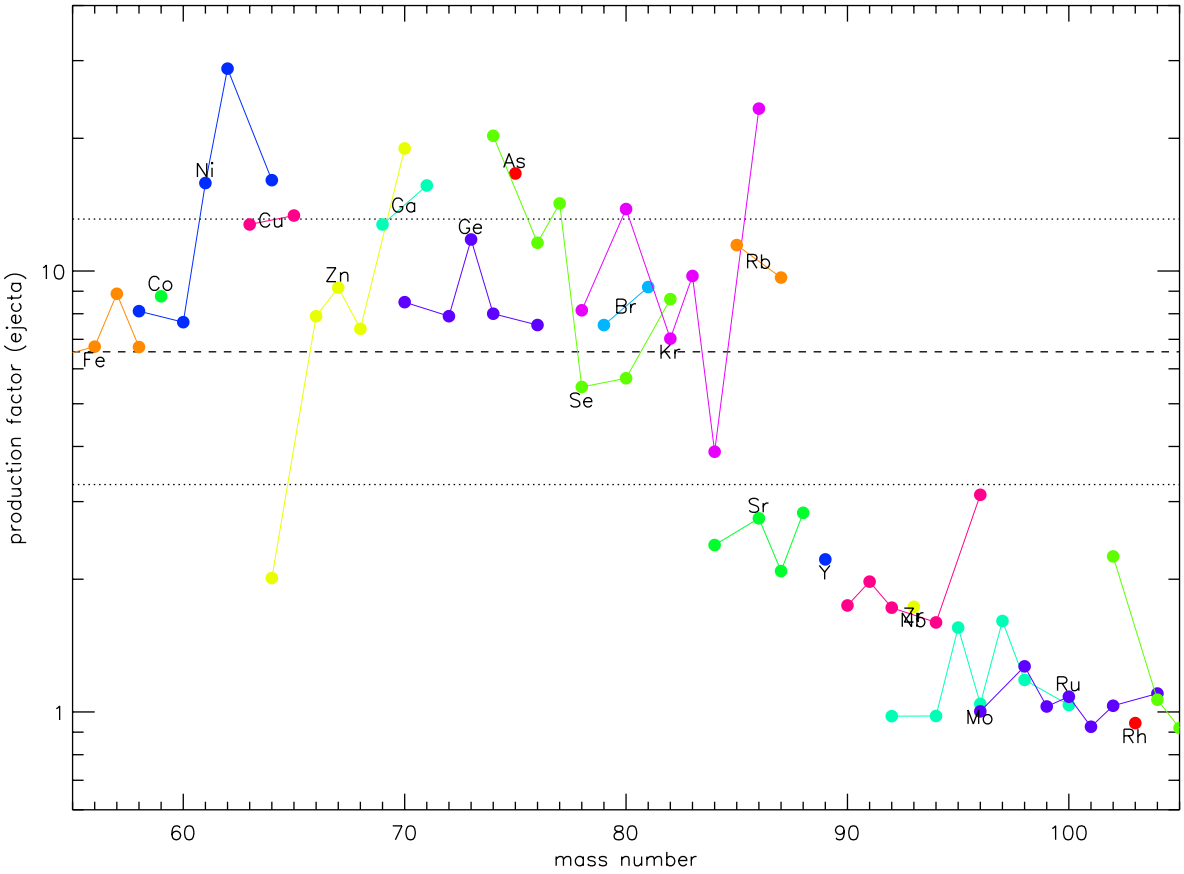

Figure 2: Production factors of trans-iron group nuclei (all isotopes are on scale)

1.3.3 Light Elements and the Iron Group

The species ^{2}H, ^{3}He, lithium, beryllium and boron were destroyed in the envelope of the star during central hydrogen burning. However, substantial ^{7}Li and ^{11}B were recreated by the ν-process during the explosion [34], as was ^{19}F (Fig. 1). ^{17}O was significantly underproduced as a result of the revised reaction rates for $^{17}\mathrm{O}(p,\alpha)^{14}\mathrm{N}$ and $^{17}\mathrm{O}(p,\gamma)^{18}\mathrm{F}$ [11].

The isotopes ^{18}O through ^{38}Ar are in good agreement with solar abundance ratios. ^{40}Ar and ^{40}K are both significantly higher while other potassium isotopes are lower. This signature for the potassium was also found in other stellar models. The under-abundance of ^{44}Ca was caused by the low yield of ^{44}Ti (Table 1) which beta-decays to calcium. The yield of this isotope strongly depends on the location of the final mass cut, i.e., the amount of fall back, and might also be affected by mixing processes during the supernova explosion. The same caveat also applies for other isotopes that mainly originate from regions close to the neutron star, like ^{56}Ni (see contribution of Kifonidis in these proceedings).

1.3.4 The s-Process

The nuclei above the iron group up to about $A = 90$ (Fig. 2) are produced as secondary isotopes by the s-process starting from iron. When considering galactic chemical evolution these yields are to be combined with those of metal-poor stars that contribute correspondingly

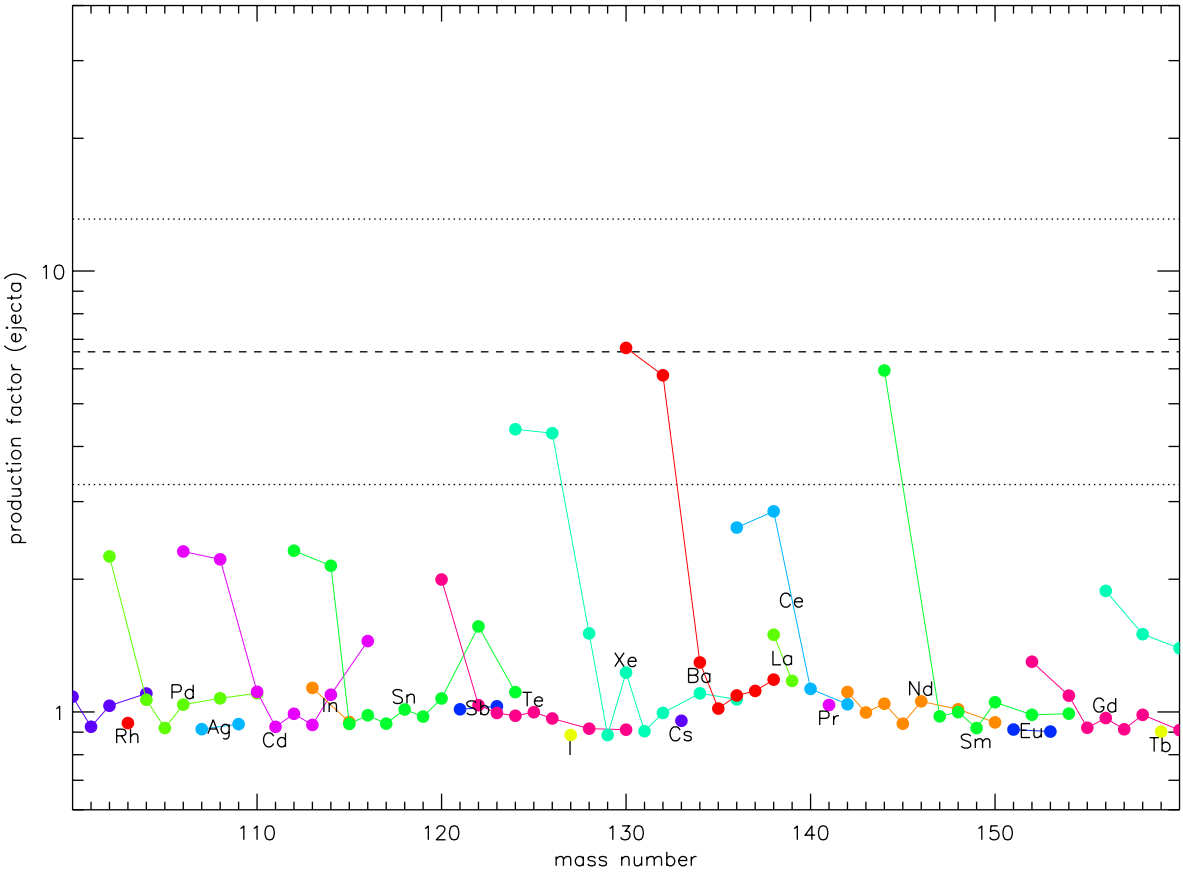

Figure 3: Post iron group nuclei

less of these isotopes, therefore a production factor of about twice that of ^{16}O is in good agreement with reproducing the solar abundance pattern. Note that the yields of these isotopes, by abundance, starting from iron decreases about exponentially. ^{64}Zn, which is underproduced as shown in Fig. 2, may be a product of the neutrino wind from the proto-neutron star [10]. The possible contributions due to this process are not included in the results presented here.

The overabundance of the neutron-rich nickel isotopes, ^{61,62,64}Ni, and other s-process products in the $A = 60 - 90$ mass range has been observed before [28, 11] and is still not well understood. It is even greater in stars of 20 and 25 $M_\odot$. Perhaps the problem will be alleviated by a more complete grid of supernovae of various metallicities and masses, perhaps the stellar structure will be altered by still uncertain physics (overshoot, $^{12}C(\alpha,\gamma)^{16}O$, rotation), or perhaps key reaction rates responsible for neutron production or absorption will change. For now, it remains problematic.

Above $A = 100$ (Figs. 3 and 4) the s-process had only minor effects in this 15 $M_\odot$ star, though there were important "redistributions" of some of the heavy isotopes. Most of the s-process above mass 90 is believed to come from AGB stars.

The "cutoff" towards lower values at a production factor of ~ 0.9 is due to the fact that most of the star does not become hot enough to affect the abundances of these nuclei, or is even lost in the wind. The supernova ejecta containing regions depleted by the s-process and

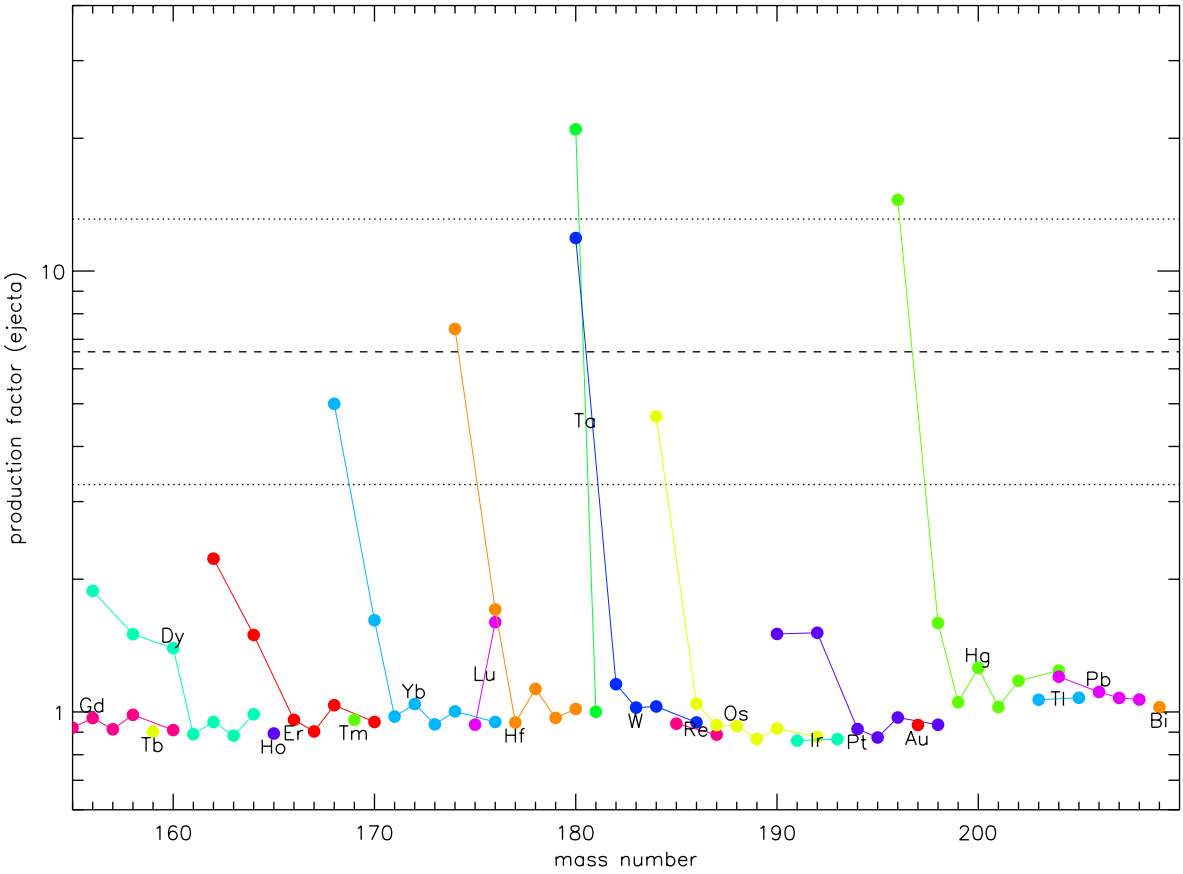

Figure 4: Heavy nuclei

other processes are then averaged with the dominating contribution of unaffected matter. In the $15\,M_\odot$ star presented here, this leads to the fact that 80 % of all *ejecta*, including winds, did not experience the s-process.

1.3.5 The γ-Process

The production of the proton-rich nuclei results from photo-disintegration of heavy nuclei during implosive and explosive oxygen and neon burning (γ-process [30, 23, 24]). Here we present the results of the first calculations that follow the γ-processes through the presupernova stages and the supernova explosion in the whole star. Fully self-consistent, the γ-process here operates in stellar regions that were exposed to previous episodes of s-processing.

Above $A = 123$ to $A = 150$ and between $A = 172$ and $A = 200$ the proton-rich heavy isotopes are produced in solar abundance ratios within about a factor of two relative to ^{16}O (Figs. 3 and 4). Below $A = 123$ and around $A = 160$ the production of the proton-rich isotopes is down by about a factor of three to four. The total production of the proton-rich isotopes increases for higher entropy in the oxygen shell, i.e., with increasing mass of the helium core, as we have seen in our $25\,M_\odot$ star, but also depends on details of stellar structure and the composition of the star at the time of core collapse. Therefore the contribution from more massive stars may well fill in the gaps of the low production factors seen in the $15\,M_\odot$ star.

The isotope ^{180}Ta, the rarest stable nuclear species in the solar abundance pattern, shows

a remarkable overproduction (Table 4) in all of our models, despite our taking into account its destruction by de-excitation into the short-lived ground state through thermal excitation into an intermediate state [2]. This may indicate that decay from other excited states could be important, which are not accounted for here. We cannot exclude, however, that our treatment of ^{180}Ta as a single species in the excited state only may cause, at least in part, the overproduction found here.

1.3.6 The r- and n-Process

The base of the helium shell is suspected to be a possible site for fast neutron capture processes as the supernova shock front passes these layers, especially in the less massive core collapse supernovae. Since current models of r-process sites have difficulties in reproducing the r-process peak around $A = 130$ when adjusted to fit the heavier nuclei (see the contribution of Truran in these proceedings), the base of the helium shell was considered as a possible environment for producing these isotopes.

In our present models a distinct redistribution of nuclei around $A = 123$ was found at the base of the helium shell, but the resulting yields were too small to constitute a significant contribution that would be visible in Fig. 3. We may speculate that less massive core collapse supernovae might have a stronger contribution though. More details on the present calculations will be given in [22].

1.4 Conclusions

We have presented the first calculation to follow the complete s-process through all phases of stellar evolution and the γ-process in the whole star through the presupernova stage and subsequent supernova explosion. Below, we summarize the important results for our $15\,M_\odot$ star. Note, however, that though this mass is a numerically typical case of a Type II or Ib supernova, the average nucleosynthetic yield of massive stars is the result of populations of different stars each of which has its own peculiar yields which must be combined to result in a solar-like abundance pattern. Some isotopes that are underproduced here may be strongly overproduced in other massive stars while isotopes overproduced here may be deficient in others.

The proton-rich heavy isotopes above $A = 123$ can be well produced by the γ-process occurring during implosive and explosive oxygen and neon burning. The proton-rich isotopes around $A = 160$ and those between $A = 100$ and $A = 123$, however, are underproduced by a factor of 3 to 4 with respect to ^{16}O. The isotope ^{180}Ta shows a strong overproduction by the γ-process. This may indicate that decay from excited states, of which we include only one, could be important.

A strong secondary s-process contribution appears between iron and a mass number of $A = 90$. Above $A = 100$ the s-process in our $15\,M_\odot$ star is very weak, but it becomes notably stronger in stars with more massive helium cores that perform helium burning at higher entropies.

The expected r- or n-process contribution due to the supernova shock front running through the base of the helium shell does not show a significant contribution in any of our preliminary model stars, not even at $A = 130$. We observed some redistribution of isotopes at the base of helium shell around $A = 123$, but this did not show the characteristics of a typical r-process nor was it important compared to the total yield of the star.

The revisions of opacity tables and the introduction of mass loss generally leads to smaller helium core sizes which tend to also decrease the mass of the carbon-oxygen and the silicon core (Table 1). Note, however, that the absolute values of these core masses depend on the uncertainties, in particular, of the mixing processes in the stellar interior, such as semiconvection, overshooting, and rotation.

The revision of the weak rates [16], important after central oxygen burning, leads to a $2-3\,\%$ higher electron fraction per nucleon, $Y_{\rm e}$, at the time of core collapse in the center of the star (Table 1) and the "deleptonized core" tends to comprise less mass [8]. More important for the core collapse supernova mechanism might be the $30-50\,\%$ higher densities of the new models between the region of $m = 1.5-2\,{\rm M}_\odot$ [8], which may result in a correspondingly higher ram-pressure of the infalling matter.

Acknowledgements

We thank Karlheinz Langanke and Gabriel Martínez-Pinedo for discussion and supplying their theoretical weak reaction rates [16] and are grateful to Frank Timmes for providing us with his implementation of the neutrino loss rates of [13] and the sparse matrix inverter we used for the large network. This research was supported, in part, by Prime Contract No. W-7405-ENG-48 between The Regents of the University of California and the United States Department of Energy, the National Science Foundation (AST 97-31569, INT-9726315), and the Alexander von Humboldt-Stiftung (FLF-1065004). T.R. acknowledges support by a PROFIL professorship from the Swiss National Science foundation (grant 2124-055832.98).

References

[1] Z.Y. Bao, H. Beer, F. Käppeler, F. Voss, K. Wisshak, and T. Rauscher, ADNDT **76** (2000) 1.

[2] D. Belic, et al., Phys. Rev. Lett. **83** (1999) 5242.

[3] J.B. Blake, S.E. Woosley, T.A. Weaver, and D.N. Schramm, ApJ **248** (1981) 315.

[4] J.J. Cowan, A.G.W. Cameron, and J.W. Truran, ApJ **294** (1985) 656.

[5] C. Freiburghaus, et al., ApJ **516** (1999) 381.

[6] Zs. Fülöp, et al., Z. Phys. A **355** (1996) 203.

[7] N. Grevesse and A. Noels, in Origin and Evolution of the Elements, ed. N. Prantzos, E. Vangioni-Flam, M. Casse, Cambridge, Cambridge Univ. Press (1993) p. 13.

[8] A. Heger, S.E. Woosley, G. Martínez-Pinedo, and K. Langanke, ApJ (2000) in prep.

[9] A. Heger, S.E. Woosley, R.D. Hoffman, and T. Rauscher, ApJS (2001) in prep.

[10] R.D. Hoffman, S.E. Woosley, G. Fuller, and B.S. Meyer, ApJ **460** (1996) 478.

[11] R.D. Hoffman, S.E. Woosley, and T.A. Weaver, ApJ (2000) in prep.

[12] C.A. Iglesias and F.J. Rogers, ApJ **464** (1996) 943.

[13] N. Itoh, H. Hayashi, A. Nishikawa, and Y. Kohyama, ApJS **102** (1996) 411.

[14] K.L. Kratz, et al., priv. com. (1996).

[15] K.L. Kratz, et al., ApJ **402** (1993) 216.

[16] K. Langanke and G. Martínez-Pinedo, Nucl. Phys. **A673** (2000) 481.

[17] P. Möller, J.R. Nix, W.D. Myers, and W.J. Swiatecki, ADNDT **59** (1995) 185.

[18] P. Möller, J.R. Nix, and K.L. Kratz, ADNDT **66** (1997) 131.

[19] H. Nieuwenhuijzen and C. de Jager, A&A **231** (1990) 134.

[20] J.K. Tuli, et al., Nuclear Wallet Charts, 5^{th} edition, Brookhaven National Laboratory, USA (1995).

[21] T. Rauscher and F.-K. Thielemann, ADNDT **75** (No. 1+2) (2000) 1.

[22] T. Rauscher, R.D. Hoffman, A. Heger, and S.E. Woosley, ApJ (2000) in prep.

[23] M. Rayet and M. Arnould, and N. Prantzos, A&A **227** (1990) 517.

[24] M. Rayet, M. Arnould, M. Hashimoto, N. Prantzos, and K. Nomoto, A&A **298** (1995) 517.

[25] E. Somorjai, et al., A&A **333** (1998) 1112.

[26] F.-K. Thielemann, priv. com. (1992).

[27] F.-K. Thielemann, K. Nomoto, and M.-A. Hashimoto, ApJ, **460** (1996) 408.

[28] F.X. Timmes, S.E. Woosley, T.A. Weaver, and S.E. Woosley, G. Fuller, and B.S. Meyer, ApJS **98** (1995) 617.

[29] A. Weiss, priv. com. (1996).

[30] S.E. Woosley and W.M. Howard, ApJS **36** (1978) 285.

[31] Woosley, S. E., Wilson, J. R., Mathews, G., Meyer, B., and Hoffman, R. D., ApJ, **433** (1994) 229.

[32] S.E. Woosley and T.A. Weaver, ApJS **101** (1995) 181.

[33] T.A. Weaver, G.B. Zimmermann, and S.E. Woosley, ApJ **225** (1978) 1021.

[34] S.E. Woosley, R.D. Hoffman, D. Hartmann, and W. Haxton, ApJ **356** (1990) 272.

The evolution of massive stars and the explosive yields

A. Chieffi [1] [2], *M. Limongi* [2], *O. Straniero* [3]

[1] *Istituto di Astrofisica Spaziale, CNR*
[2] *Osservatorio Astronomico di Roma*
[3] *Osservatorio Astronomico di Collurania*

1.1 Extended Abstract

The present discussion is based on a series of evolutionary tracks computed from the pre main sequence up to the break out of the shock wave at the surface of a massive star. All these models have been computed with our evolutionary code FRANEC (now at release 4.8) which is fully described in [3], [5] and [2]. In particular we have computed a set of 11 evolutionary tracks: 13, 15, 20 and 25 $M_{\odot}$ having Y=0.285 and Z=0.02, 13, 15, 20 and 25 $M_{\odot}$ having Y=0.23 and Z=0.001, and 15, 20 and 25 $M_{\odot}$ having Y=0.23 and Z=0. All these evolutionary tracks have been computed by adopting strictly the Schwarzschild criterion to fix the borders of the convective zones, apart from the central He burning phase where the induced overshooting and semiconvection have been taken into account. The adopted rate for the $^{12}C(\alpha,\gamma)^{16}O$ reaction is the one given by [1]. The explosive yields have been computed by adopting the "radiation dominated" approximation, firstly discussed by [7]. The comparison between the yields computed by means of this approximation and those computed by means of an Hydro-code shows that the "radiation dominated" approximation is very good if one is interested only in the computation of the yields. At variance with the choices made by the others groups involved in this kind of computations, we do not provide just one set of explosive yields but a variety of them for different choices of the mass cuts. The presupernova models and the relative explosive yields may be found in our evolutionary database ORFEO (Online Repository of Franec Evolutionary Output) at the address *www.mporzio.astro.it/∼mandrake/orfeo.html* All our models are extensively discussed in a series of papers ([2], [4] and [6]).

A star is usually defined as "massive" if its central part moves in the Log(ρ_c)-Log(T_c) plane outside the region characterized by a strong electron degeneracy. Hence, by definition, these are the stars which may freely raise the central temperature up to several billion degrees and the central density up to several times 10^9 gr/cm^3. These stars are thought to eventually form a dynamically unstable highly neutronized core which collapses up to nuclear densities and whose rebounce forms a shock front able to succesfully exit the star - soon (prompt) or later (delayed) - bringing in the interstellar medium at least part of the material synthetized during the lifetime of the star itself. During the hydrostatic part of their evolution, these stars pass through a number of central (and shell) nuclear "burnings" (H, He, C, Ne, O and Si) which correspond to episodes during which the nuclear energy is able to counterbalance the energy losses; these occur mainly from the surface (photons) until a central temperature of $T_c \simeq 8 \times 10^8 K$ (i.e. the C_{ign}) and mainly from the center (pair neutrinos) in the further evolutionary phases. Since these nuclear burnings often occur in a convective environment, the final stratification of the matter within a star at the moment of the core collapse will reflect the overlap of the various convective episodes experienced by the star during its hydrostatic lifetime. Moreover, since the various evolutionary phases depend on the initial mass and

chemical composition, it is clear that the final preexplosive structure of a star will depend on both these parameters.

The largest uncertainties connected to the computation of these presupernova models are certainly due to the fact that we can't reliably model the convective zones, i.e. both their extension in mass and the efficiency of the chemical mixing, and to the lack of a good knowledge of the cross section for the $^{12}C(\alpha,\gamma)^{16}O$ reaction. Also the mass loss may certainly play a significant role but probably only above 30-35 $M_{\odot}$ when it is supposed to become very efficient.

The final chemical composition attained ba a star at the moment of the explosion can not be considered as representative of the final yields which will be really ejected outward since the passage of the shock wave through the mantle significantly alters the final yields. Unfortunately, as it is well known, at present it is not possible to obtain a successful explosion in a natural and consistent way; hence one possibility to compute the explosive yields is simply to *assume* that a shock wave succesfully escapes the iron core (which is the only region where the shock wave may loose a significant fraction of its energy). It is clear that such an assumption implies that the energy of the shock wave, the possible time delay between the rebounce and the rejuvenation of the shock itself and the amount of fall back can not be reliably determined on first principles but, on the contrary, that they must be considered as the main uncertainty factors in the computation of the explosive yields.

However, once the explosion has been simulated (usually by means of a piston located at the border of the "Fe" core or a thermal or kinetic bomb) and the various unstable isotopes have fully decayed, one is left with a set of final yields which will vary with the initial mass and the metallicity. A detailed discussion of all the properties of these yields may be found in our papers mentioned above. Here we want to remind only some very general properties of these yields; in particular we want to stress that it is possible to define "groups" of elements depending on their location of production. In particular we identify the following groups.

The "hot" one is formed by Fe, Co and Ni: these elements are produced mainly in the region exposed to a peak temperature T larger than 5×10^9 K (usually referred to as "complete explosive Si burning") where the matter reaches the Nuclear Statistical Equilibrium. Hence the final abundances of these elements mainly depend on: the mass cut, the initial energy of the shock front, the time delay between the core bounce and the rejuvenation of the shock wave, the preexplosive mass-radius relation and the electron density (Ye) in this region.

The "semi-hot" one is formed by Cr, V and Mn: these elements are mainly produced in the region which experienced a peak temperature T between 5×10^9 K and 4×10^9 K (usually referred to as "incomplete explosive Si burning") where the matter reaches the Quasi Statistical Equilibrium (QSE). Also in this case the parameters which will influence the final yields of these elements are those mentioned above for the "hot" group.

The "golden" group is formed by Si, S, Ar and Ca: these elements are completely produced by both the "incomplete explosive Si burning" and the so called "explosive Oxygen burning", which is simply the region exposed to a peak temperature between 4×10^9 K and 3.3×10^9 K where two QSE clusters form. The production of these elements depends almost exclusively on the presupernova mass-radius relation and on the initial energy of the shock wave. Hence these are the elements whose theoretical prediction is less dependent on the uncertainties affecting the computation of both the presupernova evolution and the explosive phase.

There are three other elements, namely K, Sc and Ti which also form in regions exposed to peak temperatures larger than 3.3×10^9 K, like the other ones mentioned up to now, but they behave pecularly respect to the others. Scandium is mainly produced very close to the border

of the "Fe" core and hence it should remain almost completely locked in the remnant unless one assumes that a large amount of ^{56}Ni ($\geq 0.2 M_{\odot}$) is ejected outward. Potassium could pertain to the golden group but it differs from the other ones because it forms *exclusively* in the so called "explosive Oxygen burning" region. Titanium is simultaneously a "hot" and a "semi-hot" element since it forms in both these two regions.

The "volatile" group is formed by Ne, Na, Mg, Al, P and Cl: these elements are produced mainly in the convective C-burning shell and then partially modified by the passage of the shock wave (i.e. untill the peak temperature remains larger than, say, 1.9×10^9 K - the so called "Ne and C explosive burning") This means that the yields predicted for these elements largely rely on many details concerning both the hydrostatic evolution and the passage of the shock front.

The lighter elements He, C, N, O and F are essentially unaffected by the explosion and hence they will simply reflect the abundances of the presupernova models: actually the oxygen is partially destroyed by the passage of the shock wave and hence it depends at some extent also on the properties of the explosion.

Before closing this paper let us mention an interesting property of the elements forming the "golden" group. Though the absolute abundances of these elements depend on the total mass exposed to both the "explosive incomplete Si burning" and the "explosive O-burning", it happens that the abundance ratios between any two of these elements is almost **independent** on both the initial mass and chemical composition: the reason is that these ratios are just a property of the matter exposed to this peak temperature range and not on the amount of mass involved in this burning. By the way note that the degree of neutronization is in this region sufficiently small that it does not affect significantly the abundance ratios. It goes without saying that these ratios are also essentially not affected by the various uncertainties involved in the computation of the presupernova evolution first and of the explosion later. We therefore predict that the ratio between any two of the elements forming the "golden" group should remain fairly constant along the lifetime of our galaxy. A preliminary comparison with spectroscopic data of stars in the metallicity range $-3 \leq [Fe/H] \leq 0$ seems to show that such a constancy does exist.

References

[1] G.R. Caughlan, W.A. Fowler, M. Harris and B. Zimmerman, At. Data Nucl. Data Tab. **32** (1985) 197.

[2] A. Chieffi, M. Limongi and O. Straniero, ApJ **502** (1998) 737.

[3] A. Chieffi and O. Straniero, ApJS **71** (1989) 48.

[4] M. Limongi, O. Straniero and A. Chieffi, ApJS accepted (2000).

[5] O. Straniero, A. Chieffi and M. Limongi, ApJ **490** (1997) 425.

[6] O. Straniero, A. Chieffi and M. Limongi, in preparation

[7] T.A. Weaver and S.E. Woosley, Ann. NY Acad. Sci. **336** (1980) 335.

Study of the Nova-Produced ^{22}Na with COMPTEL

A.F. Iyudin[1]

[1] *Max-Planck Institut für Extraterrestrische Physik, Giessenbachstrasse, 85748 Garching, Germany*

Abstract

The COMPTEL telescope on board the Compton Gamma-Ray Observatory (CGRO) is capable of imaging γ-ray line sources, like classical novae, in the MeV regime at a level of sensitivity up to a few 10^{-5} photons cm^{-2}s^{-1}. At this level of sensitivity quite high expectations can be placed on the detection of the predicted ^{22}Na γ-ray line at 1.275 MeV from nearby novae.

We have used COMPTEL data collected during 9 years of the CGRO mission to study the sodium production by the old and the most recent novae. The derived results are discussed and compared with model predictions.

1.1 Introduction

The classical nova outburst has been modelled as a thermonuclear runaway in the accreted hydrogen-rich envelope of the white dwarf companion of a close binary system, e.g. [21, 23]. In general, observations of novae support such models [8, 9].

It is currently believed that neon novae, a distinct subclass of the classical novae associated with an underlying oxygen-neon-magnesium (ONeMg) white dwarf, may be an important source of Galactic ^{22}Na [5]. ^{22}Na decays with a 3.75 yrs life-time to a short lived excited state of ^{22}Ne at 1.275 MeV. An individual nova at 1 kpc from the Sun with a total ejected mass of the order of 10^{-4} M$_\odot$ and a ^{22}Na mass fraction of the order of 10^{-4} could have been seen at a flux value of 4×10^{-5} cm^{-2} s^{-1} [25].

In addition to the ^{22}Na line, both types of novae (CO and ONe) are prolific producers of 511 keV γ-ray line emission, which accompanies the decay of the β^+-unstable products of the nucleosynthesis in novae, as well as of 478 keV emission originating from the ^{7}Be decay to ^{7}Li. Until now, there have been no positive detections of any of these lines, at 1.275 MeV, 478 keV and 511 keV [12, 14, 16, 18]. Below we will discuss the results of a ^{22}Na line study with COMPTEL.

The latest predictions of the ^{22}Na mass ejected as the result of thermonuclear runaway on the white dwarf in a binary vary between $\leq 2.0\times10^{-9}$ M$_\odot$ and $\leq 1.4\times10^{-8}$ M$_\odot$ [11,13,15,22]. Unfortunately, these predictions were made using reaction flows that are still containing notable uncertainties in cross-sections of several key reactions [6]. **Additionally, none of the above models could reproduce high masses of the ejected nova shell** (see discussion in [22]). It appears to be quite plausible that in all models considered up to now the mixing of the accreted envelope material with that of the underlying core was not correctly treated. One has to find the way to prolong the accretion of the white dwarf envelope (and consequently to increase the ejecta mass) before the runway will start. The only (parametric) model that appears capable to reproduce high ejected masses of neon novae is that of Wanajo, Hashimoto and Nomoto (1999). Below we will compare measured ^{22}Na line fluxes (upper limits) from the group of old and recent neon novae with those that were predicted by this model [24].

Table 1: **Parameters of the Galactic novae discussed in this work.**

Nova name	Date, TJD	m_v	t_3, days	E(B-V)	d, kpc	M_{wd}, $M_\odot$	M_{ej} $M_\odot$
V693 CrA	4697	7.0	∼14	≥0.5	≤7.2	1.08±0.14	?
V1370 Aql	4995	5.0	∼10	0.6	4.2	1.14±0.18	$\geq 2\times10^{-4}$
QU Vul	6073	5.1	28±4	0.60±0.05	1.6±0.4	0.88±0.10	3×10^{-4}
V838 Her	8339	5.3	4	0.5±0.1	∼3.0±1.0	0.87±0.12	$1.2\text{-}6.7\times10^{-4}$
V1974 Cyg	8672	4.4	47	0.36±0.04	∼1.8	∼1.1	$2\text{-}5\times10^{-4}$

Table 2: **^{22}Na line flux and ejected mass as modelled and measured from novae.**

Nova	M_{wd} $M_\odot$	M_{ej} msol	^{22}Na line flux, $cm^{-2}s^{-1}$ predicted[a]	measured[b]	XM_{ej}, 10^{-8} $M_\odot$ predicted[a]	derived[b]
V693 CrA	1.05	10^{-3}	5.5×10^{-4}	$\leq 1.7\times10^{-5}$	2.0×10^{3}	≤170
V1370 Aql	1.1	10^{-3}	7.0×10^{-3}	$\leq 3.5\times10^{-5}$	3.1×10^{3}	≤360
QU Vul	1.05–1.1	$10^{-3.5}$–10^{-3}	4.4×10^{-4}	$\leq 3.05\times10^{-5}$	89	≤35
V838 Her	1.05	10^{-4}–$10^{-3.5}$	6.3×10^{-6}	$\leq 3.3\times10^{-5}$	1.9	≤12
V1974 Cyg	1.1	$10^{-4.5}$	3.0×10^{-5}	$\leq 2.1\times10^{-5}$	2.5	≤2.1

From the large number of Galactic novae observed by COMPTEL we will first consider novae with the well established Ne over-abundances (Table 1) and then will turn to the more recent novae (Table 3).

Instrument and Data Analysis

COMPTEL, due to its combination of imaging and spectroscopic capabilities [20], provides a unique opportunity to measure line emission from point-like sources or from extended regions (e.g. the Galactic bulge).

Generally, different viewing periods covering the position of the relevant nova (listed in Table 1) were combined to achieve the best possible sensitivity. In calculating the ^{22}Na mass in the ejected shell, the time delays between the nova maximum brightness and the time of the COMPTEL's measurements have been taken into account. Imaging and flux evaluation were done in a ± 2 σ energy window around the 1.275 MeV line, where σ is the instrumental energy resolution for this line. The results are given in Table 2. The background model used in this work is based on the similarity of event distributions in the (χ, ψ) data space in the adjacent energy bands, which is energy independent in first order aproximation, and on the event distribution in the $\bar{\varphi}$ coordinate of the line photons. Some smoothing is then applied in the (χ, ψ) coordinates to reduce statistical fluctuations. The background model derived in this way still contains systematic uncertainties due to the underlying continuum emission and small differences in the event distributions in the (χ, ψ) space.

[a] initial flux, or ^{22}Na ejected mass (XM_{ej}) as derived from [24];

[b] flux value, derived from COMPTEL measurements; XM_{ej} was calculated from the measured flux, time delay and nova parameters of Table 1 ([14], and this work).

Table 3: **Parameters of the more recent novae.**

Nova name	Date, TJD	m_v	t_2, t_3 days	Nova type	d, kpc	M_{wd}, $M_\odot$
NCas 1993	9328	5.8	t_2=65	CO	1.25±0.29	0.7
NCir 1995	9744	7.2	t_2=20	ONe	2.8-4.8?	1.14±0.18
NAql 1995	9755	5.9	t_2=11	ONe	∼1.9	?
NCen 1995	9771	7.2	t_2∼6	CO	1.4-8.3	?
NCas 1995	9953	7.1	n.a.	ONe?	2.95±0.70	0.58±0.07
NCru 1996	10323	7.2	t_2=5.2	ONe	∼1.3	1.19
V382 Vel	11321	2.60	$t_3 \leq 10$	ONe	∼1.5	1.12±0.13

Discussion

The derivation of ^{22}Na mass limits from the 1.275 MeV line flux measurements for a single nova is hampered by the fact that in many cases the distance to the nova is unknown. The extinction-based distances are not reliable due to the possible presence of circumstellar dust, or due to a wrong colour determination [26, 1]. Even relatively well studied novae are subject to uncertainties in the distance estimate and/or in the derived abundances. Examples of such uncertainties were addressed in recent publications [2, 9, 10]. These uncertainties have forced us to give a highest priority to the analysis of the ^{22}Na from the old (1981-1984) neon novae and from the more recent bright novae, like Nova Her 1991, and Nova Cyg 1992, where overabundance of Ne is firmly established ([17]; [9] and references therein). Table 2 summarises the COMPTEL-limits on the ejected masses from the old novae NCrA 1981, NAql 1982 and NVul 1984, and the more recent neon novae NHer 1991, NCyg 1992 in comparison with the predictions of the model by Wanajo et al. (1999). The new upper limit of the ^{22}Na yield from Nova Cyg 1992 is based on the improved flux upper limit of COMPTEL and a latest distance estimate of this nova [4]. It is a pity that no more exposure time of the CGRO was allocated in 1992-1993 to observe NCyg 1992 where we were close to the detection, according to the model prediction [24] and to the experimental upper limit (see Table 2 and [14]).

We have to state that the detection of the ^{22}Na gamma-ray line remains an elusive goal for CGRO. In this respect it is useful to reiterate that **until now, no firm detection of Na exists in the UV or infrared spectra of novae with the largest Ne over-abundances known** [10, 19, 27]. Therefore, an obvious question eventually arises: **Is the ^{22}Ne (neon-E) anomaly [3] related at all to the ^{22}Na production in novae?** All theoretical models of the nova runaway, as well as spectroscopic analysis of the novae abundances are pointing towards a large overproduction of Ne. However, there are no experimental results supporting the over-production of Na in novae!

In view of the Ne overproduction in the ONe type nova another problem for the detection of ^{22}Na in the nova ejecta is arising. Because of the low energy threshold, and of the relatively high cross section of the reaction $^{22}\mathrm{Ne}(p,p')^{22}\mathrm{Ne}^*$, it is quite possible to have in the nova environment a γ-ray emission in a line at the 1.275 MeV which is not related to the ^{22}Na. The obvious way out is to measure the decay curve of the nova produced ^{22}Na, which implies a necessity to follow the bright ONe nova for at least 2-3 years in the 1.275 MeV line emission.

Actually, it means, that in order to understand the explosive nucleosynthesis of the white

dwarf runaway in a binary system, one has to measure successfully the nova light-curve in the 1.275 MeV γ-ray line, ideally in the combination with high-resolution spectroscopy of the sodium and of the neon coronal lines. This potentially could be achieved with the deployment of the next generation of space-borne γ-ray line and infrared spectrometers like SPI (INTEGRAL) and IRS (SIRTF). Before this, the only possible undertaking is to restrict ourself to the γ-ray line emission follow-ups with the COMPTEL γ-ray telescope.

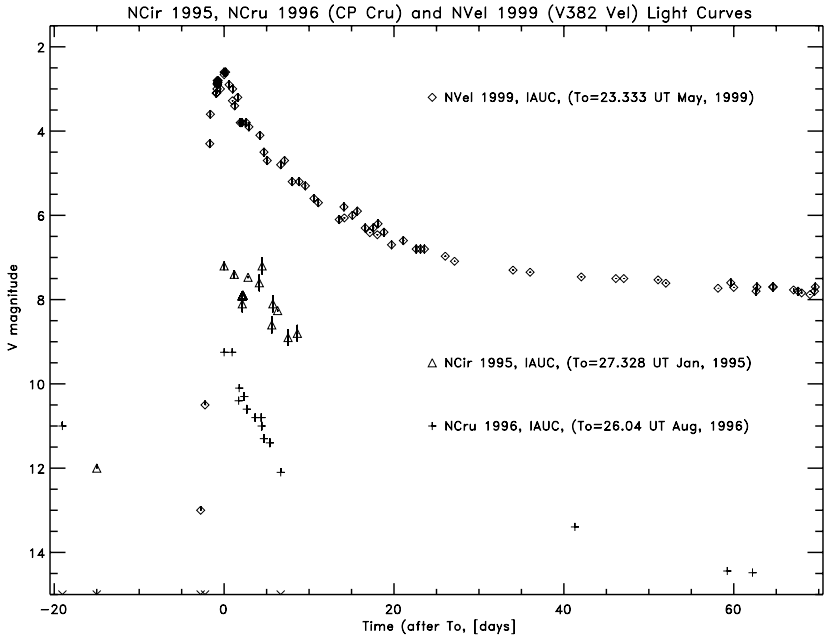

Fig. 1. Light curves of the NCir 1995, NCru 1996 and V382 Vel in V-band.

Luckily, quite a few of the more recent novae that have flared in 1994-1999 were recognised as ONe-type novae and were in the field of view of COMPTEL (see Table 3). We have followed emission of these recent novae in the 1.275 MeV line for 1 to 4.5 years, depending on the date of their optical discovery. Table 3 presents some of the known or calculated parameters of recent novae. For example, to derive the distance of $d\sim$1.5 kpc to NVel 1999, we have used the standard relation between M_v, m_v, d and A_v=3.3×E(B-V). Here m_v=2.6 (IAUC No. 7177) and E(B-V)=0.2 (IAUC No. 7192) were used. M_v=–8.89±0.02 was evaluated from the relation between t_2 and M_v, as was proposed in [7].

In Figure 1 are shown optical light curves for the cases of the very fast nova NCru 1996, of the definitely fast nova NVel 1999 and of the probably fast nova NCir 1995. Figure 2 shows 1.275 MeV emission data points taken at the different times for two interesting novae, none of which is significant by itself. Only in the boundaries of the expanding shell model those points taken as a light curve for the particular nova could be discussed as a hint for the detection of the 1.275 MeV line emission, that may be related to the nova produced ^{22}Na, namely that of the very fast nova NCru 1996 and of the very slow nova NCas 1995. Note, that the 1.275 MeV light curves of the NCru 1996 and of the NCas 1995 are very different. The difference in our opinion is related to the speed classes of novae. It is expected that the opaqueness of the envelope to the 1.275 MeV emission of the NCas 1995 become $\leq$1 at the time of $\leq$400 days after the optical detection. Detailed discussion of the ^{22}Na abundances in all novae of the Table 3 will be presented elsewhere, as well as results of the data analyses of the most bright recent nova NVel 1999, which is not yet completed at the time of the writing.

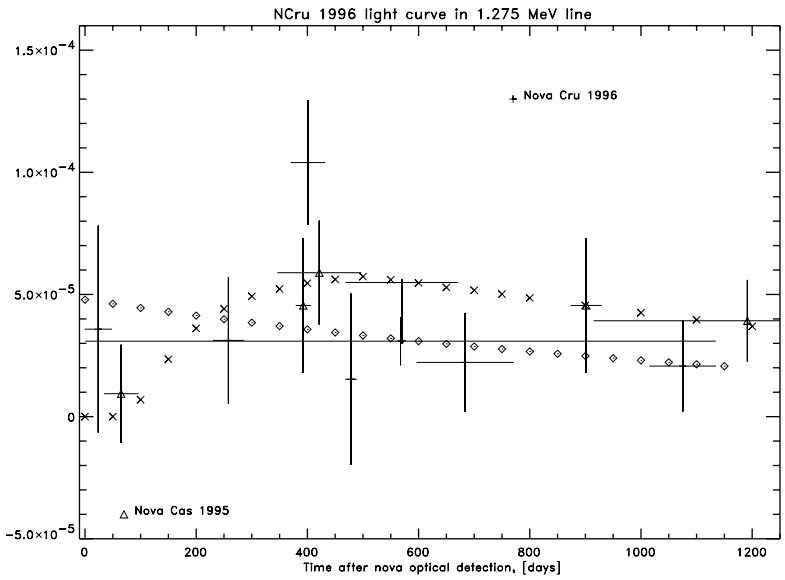

Fig. 2. Light curves of the NCas 1995 and NCru 1996 in the γ-ray line emission at 1.275 MeV. By diamonds is shown decay of the ^{22}Na in ejecta of the very fast nova NCru 1996, and asterisks represent a model for the decaying ^{22}Na embedded in the NCas 1995 ejecta (M_{ej}=10^{-3} $M_\odot$) that expands with the velocity of 100 km/s.

Acknowledgements

The COMPTEL project is supported by the German government through DARA grant 50 QV 90968, by NASA under contract NAS5-266645, and by the Netherlands Organization for Scientific Research. AFI acknowledges financial support from the German Bundesministerium für Bildung, Wissenschaft, Forschung und Technologien.

References

[1] Andreä, J., Drechsel, H., & Starrfield, S., *A&A* **291**, 869 (1994).

[2] Arkhipova, V.P., Esipov, V.F., Sokol, G.V., *Astr. Let.* **23**, No. 6, 819 (1997).

[3] Black, D.C., *Geochim. Cosmochim. Acta* **36**, 377 (1972).

[4] Chochol, D., et al., *A&A* **318**, 908 (1997).

[5] Clayton, D.D., & Hoyle, F., *ApJ* **187**, L101 (1974).

[6] Coc, A., et al., *A&A* **299**, 479 (1995).

[7] Della Valle, M., & Livio, M., *ApJ* **452**, 704 (1995).

[8] Gallagher, J.S. & Starrfield, S., *ARAA* **16**, 171 (1978).

[9] Gehrz, R.D., Truran, J.W., Williams, R.E. and Starrfield, S., *PASP* **100**, 3 (1998).

[10] Gehrz, R.D., Woodward, C.E., Greenhouse, M.A., et al. *ApJ* **421**, 762 (1994).

[11] Gomez-Gomar, J., Hernanz, M., Jose, J. & Isern, J., *MNRAS* **296**, 913 (1998).

[12] Harris, M.D., et al., astro-ph/0004164, (2000).

[13] Hernanz, M., Gomez-Gomar, J., Jose, J., Coc, A., Isern, J., *Astrophysical Letters and Communications* **38**, 407 (1999).

[14] Iyudin, A.F., Bennett, K., Bloemen, H., et al., *A&A* **300**, 422 (1995).

[15] Jose, J., Hernanz, M., *ApJ* **494**, 680 (1998).

[16] Leising, M.D., Share, G.H., Chupp, E.L. & Kanbach, G., *ApJ* **328**, 755 (1988).

[17] Livio, M., & Truran, J.W. *ApJ* **425**, 797 (1994).

[18] Mahoney, W.A., et al., *ApJ* **262**, 742 (1982).

[19] Salama, A., Evans, A., Eyres, S.P.S., et al., *A&A* **315**, L209 (1996).

[20] Schönfelder, V., Aarts, H., Bennett, K., et al., *ApJS* **86**, 657 (1993).

[21] Starrfield, S., Sparks, W.M. & Truran, J.W., *ApJS* **28**, 247 (1974).

[22] Starrfield, S., et al., *MNRAS* **296**, 502 (1998).

[23] Truran, J.W., in Essays in Nuclear Astrophysics, ed. C.A. Barnes, D.D. Clayton, & D.N. Schramm (Cambridge: Cambridge Univ. Press), 467 (1982).

[24] Wanajo, S., Hashimoto, M.-A., & Nomoto, K., astro-ph/9905279 (1999).

[25] Weiss, A., & Truran, J.W., *A&A* **238**, 178 (1990).

[26] Williams, R.E., *ApJ* **426**, 279 (1992).

[27] Williams, R.E., et al. *MNRAS* **212**, 753 (1985).

Results from Gamma-Ray Line Astronomy

Roland Diehl

Max Planck Institut für extraterrestrische Physik, D-85741 Garching, Germany

Introduction

Observations of radioactivity gamma-ray lines have advanced constraints from direct measurements of cosmic nucleosynthesis in recent years. Cosmic-ray activation of such telescopes, operated in near-Earth orbits, generates a large background of instrumental radioactivity lines, so that measurements extend over weeks and face signal-to-background ratios below the percent level only. Yet, from about a dozen of gamma-ray lines observable with current instruments, a handful have been detected, and measured fluxes turn out significant for a few astrophysical cases. Here we discuss specific nucleosnthesis objects (supernovae, WR stars) mainly, but also adress constraints from diffuse nucleosynthesis (see also [3] for an extended review).

Thermonuclear Supernovae

Thermonuclear supernovae produce $\sim$0.5 $M_\odot$ of ^{56}Ni , and are observable with present gamma-ray telescopes out to distances of 10–15 Mpc, which includes the Virgo cluster of galaxies. Supernova search projects of recent years have increased the indentification rate of candidate gamma-ray sources, and indicate a prospect of $\sim$1-2 SNae y^{-1} for ESA's INTEGRAL observatory, due for launch in April 2002. The NASA Compton Observatory experienced during its mission (April 1991 - June 2000) three sufficiently nearby SNIa, two of which actually could be targetted with the COMPTEL and OSSE telescopes: SN1991T and SN1998bu.

For SN1991T an initially-reported upper limit [16] evolved into a marginal ($\sim 3\ \sigma$) detection of the 847 and 1238 keV lines from ^{56}Co decay [18, 19]. The ^{56}Ni mass inferred from the measured gamma-ray line fluxes spans a wide range, from 0.6 to 3.3 $M_\odot$; with this uncertainty, the nominal 2 $M_\odot$ result should not be interpreted as support for a merger scenario, though SN1991T is peculiar in many aspects.

SN1998bu occurred most likely on May 1-2 of 1998 within a dusty region of M96. In spite of more than 14 observation-weeks invested by the Compton Observatory community, neither COMPTEL[7] nor OSSE[15] can report detection of the expected ^{56}Co decay lines. The observations started too late (on 19 May) for the early ^{56}Ni lines, unfortunately. Upper limits on the 847 and 1238 keV lines of $\sim 2\ 10^{-5}$ ph $cm^{-1}s^{-1}$ end up below the expectations from predictions according to the brighter model classes which have some of the radioactive ^{56}Ni in the outer parts of the supernova, such as delayed-detonation and in particular Helium cap (sub-Ch) models (see Figure 1).

Core Collapse Supernovae

SN1987A and Cas A are the prime study objects for core collapse nucleosynthesis. While SN1987A is our unique chance for concurrent tracing of early evolution, Cas A is the remnant with favorable distance (3.4 kpc) and age (330 y) to provide us with detailed measurements

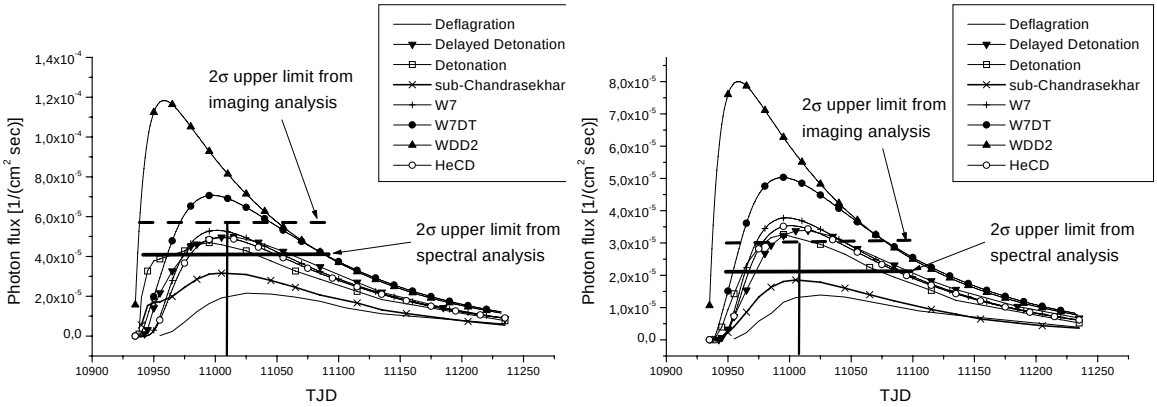

Figure 1: The COMPTEL upper limits on ^{56}Co decay gamma-ray lines from SN1998bu seem to favour models which have ^{56}Ni embedded deeper within the supernova[7]. (Left: 847 keV; right:1238 keV line; both for a SN distance of 9.9 Mpc)

over many frequency domains of the electromagnetic spectrum. Other core collapse supernovae or their remnants have not been seen in gamma-ray lines, not surprising when instrumental sensitivities ($\sim 10^{-5}$ ph cm^{-1}s^{-1}) are considered (Ni and Co line detections demand measurement of a core collapse supernova in the Galaxy or LMC within the first year, ^{44}Ti sup Galaxy, and ^{26}Al from a cor the past few million years.)

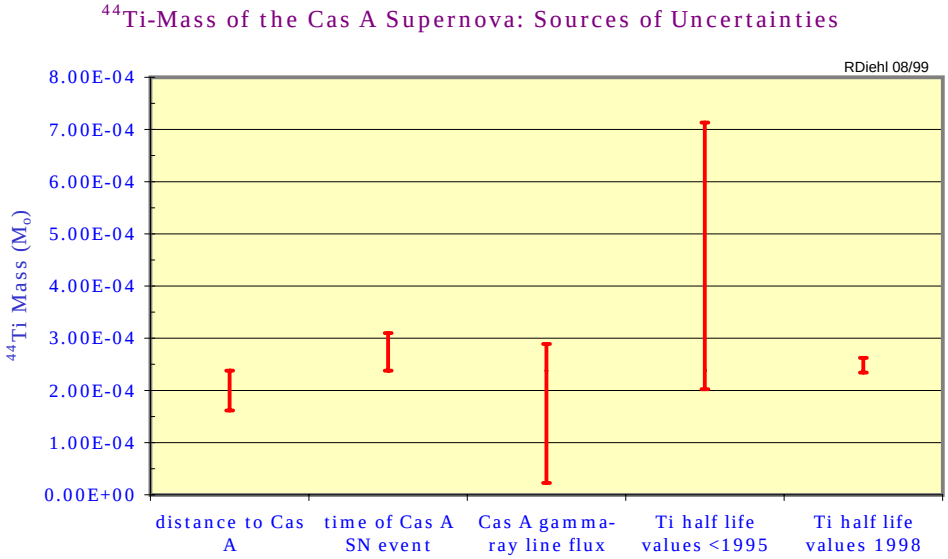

Figure 2: The COMPTEL ^{44}Ti flux derived for Cas A depends on various parameters: Accuracy of the gamma-ray line flux measurement, distance and age of the supernova, and ^{44}Ti decay time. Before 1997, the latter dominated the uncertainty, while presently underlying continuum from cosmic rays accelerated in the SNR needs better assessment.

The ^{44}Ti -(^{44}Sc-)^{44}Ca 1.157 MeV gamma-ray line measurement with COMPTEL from Cas A[8] appears well established ($> 6\sigma$), although no other instrument could provide an independent confirmation. Measurements in the 68 and 78 keV lines (from the ^{44}Ti to ^{44}Sc

decay) have been attempted with the OSSE[25], RXTE[23], and BeppoSax[27] instruments, ASCA K_α X-ray measurements from ^{44}Sc may add yet another potential window. In all cases, uncertainties about possible underlying continuum emission makes the ^{44}Ti decay line measurements largely uncertain. The COMPTEL 1.157 MeV line could be thought to be unaffected by such problems, since MeV emission from young supernova remnants seems unlikely. With OSSE/ASCA and TeV experiments' measurements on Cas A, SN1006, and IC433, however, the acceleration of cosmic rays in young supernova remnants received attention again also from theorists. Models of Fermi acceleration in the magnetic field irregularities characteristic for supernova shocks now predict that electron Bremsstrahlung may become significant at MeV energies[6], provided the TeV energies of accelerated electrons as inferred from hard-X and TeV measurements indeed are obtained. In this case, the COMPTEL line measurement may be reduced in flux down to ranges of 10^{-5} ph cm^{-1}s^{-1}, in comfortable agreement with all current models for ^{44}Ti nucleosynthesis and the other measurements (see Figure 2).

We note that care must be taken when measurements of Cas A in different spectral windows are interpreted and compared: The radioactivity seen in gamma-rays relates directly to the supernova (transparency to gamma-rays is achieved within months, $\ll \tau_{44Ti}$), while radio emission reflects electron velocities and the magnetic-field strength (and configuration) both early-on in the supernova and later in the shock region of the remnant. Optical and X-ray emission early-on (from the supernova itself) is a by-product of the initial supernova radioactivity. Much more prominent, bright, and structured emission in IR, optical, and X-ray bands arises however in the remnant phase from interaction of the supernova blast wave with material. In the case of Cas A, the morphology of emission in these different bands has been interpreted to reflect the spatial distribution of supernova ejecta, to allow indirect inferences on the structure of the supernova explosion. Such inferences are complex, not only because vastly different density regimes from 10^4 cm^{-1} (optical) down to 10^{-3} cm^{-3} (X-rays) are responsible for the main emission, but also because non-equilibrium line excitation of species in different ionization stages has to be considered. Overall, Cas A remnant images seem to support both the presence of large-scale mixing of different supernova regions, and significant deviations from a spherically-symmetric explosion. It remains to be seen how this may affect the ejection of ^{44}Ti from the very inner part of a supernova, quite close to the edge of the compact remnant that formed and probably burried the bulk of the heavier nucleosynthesis products.

The penetration power of gamma-rays suggests the possibility to detect supernovae from otherwise occulted dense regions through ^{44}Ti radioactivity. Searches from the COMPTEL sky survey have not shown a convincing detection, however, contrary to expectations[5]. The reported detection of a new remnant in the Vela region[10], although now assessed as somewhat optimistic[24], still is the most promising candidate source. ^{44}Ti survey maps are characterized by the Cas A source, and a few candidate sources in regions of the outer Galaxy, but a marked absence of any signals in the inner Galaxy[11]. This is in clear contrast to expectations, if supernovae are assumed to be responsible for ^{44}Ti production: from current massive star distributions such as reflected in the ^{26}Al distribution (see below) one would expect a 'few-event-sample' from a parent distribution with a center of gravity in a ridge covering Galactic longitudes $\sim$-60° $\leq l \leq$40°. A more quantitative assessment of this inconsisteny has been made, using supernova brightness and ^{44}Ti yield distributions together with a Galactic extinction model in a Monte Carlo simulation analysis, to compare optical supernova records over the past millenium with COMPTEL's ^{44}Ti data [26]. This confirms

that ^{44}Ti -producing supernovae appear to be a rarer subclass of all supernovae.

Diffuse Radioactivities and Stellar Nucleosynthesis

The gamma-ray image of the sky in the 1.809 MeV line from radioactive ^{26}Al ($\tau \sim 10^6$y) reflects recent nucleosynthesis sources in the Galaxy[22]. Imaging MeV gamma-rays is difficult, therefore different methods are applied and compared[13, 2] (see Figure 3). It has been assessed now that all along the plane of the Galaxy ^{26}Al is produced, with a fairly flat level of emission all across the inner Galaxy, and remarkable emission arising from the Cygnus, Carina, and Vela regions. Comparison with tracers of different candidate sources has identified massive stars as the dominating sources, from close similarities to the maps of dust heated by young stars and to the free-free emission indicating material which has been ionized by intense UV emission[12]. This makes the visibility of recently-active star forming regions in Cygnus, Carina, and Vela quite plausible, also the appearance of emission maxima at tangential views to spiral arms. A total amount of ~2.4 $M_\odot$ appears consistent with both nucleosynthetic yields and ionization power, if the stellar population across the Galaxy is taken from the nearby stellar census, from the Galactic metallicity trend, and from plausible assumptions about the (largely invisible) massive-star content of the inner Galaxy. From these comparisons, it is suggested that the Wolf-Rayet phase ejection of hydrostatically-produced ^{26}Al dominates over the ^{26}Al ejection from supernovae[14]. Generally, we suggest that one even may reverse this argument, and use the gamma-ray map from ^{26}Al to complement our knowledge about the massive-star distribution across the Galaxy.

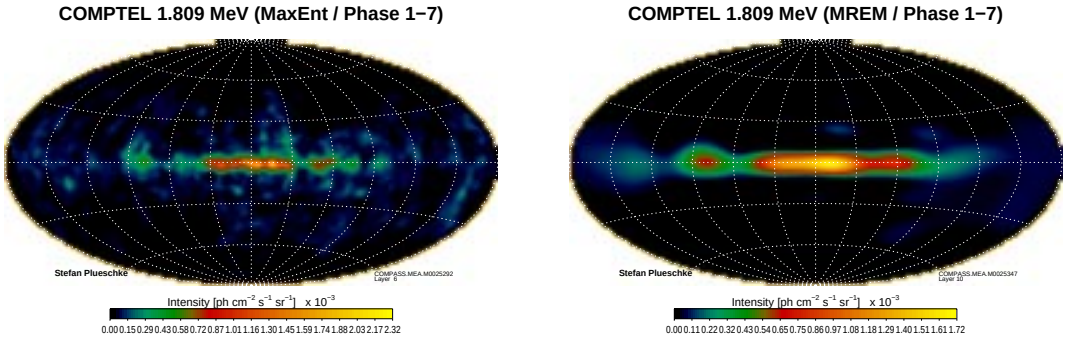

Figure 3: The COMPTEL ^{26}Al maps must be compared for alternaive imaging and background methods. A ridge of emission in the inner Galaxy and excesses in the Cygnus and Vela regions appear as consolidated characteristics. The maps from seven years of data are shown for a Maximum-Entropy method, and a Multi-Resolution Expectation Maximization method[21, 13]

Specific studies have been initiated to decompose and understand the ^{26}Al gamma-ray emission in nearby regions where we can deduce the stellar population from other astronomical data with best confidence.

In the Cygnus region, emission from the Cyg OB2 association appears to dominate the ^{26}Al brightness, other OB associations and the Cygnus superbubble consistently add to the observed gamma-ray morphology[21]. Stellar population-synthesis modeling of the time variation of ^{26}Al gamma-ray brightness with association age is consistent with these findings.

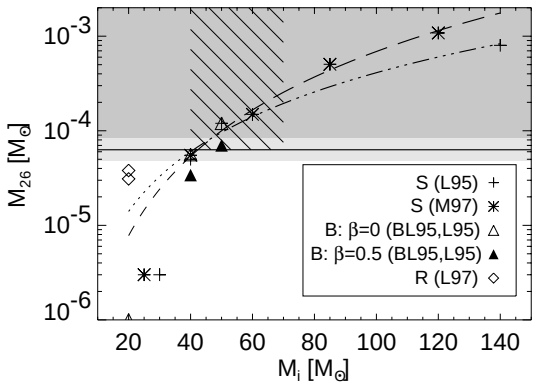

Figure 4: The absence of 1.809 MeV emission from the nearby Wolf-Rayet star WR11 appears inconsistent with present-day models for WR nucleosynthesis[20, 17]

In the Vela region, different tracers show that the Vela molecular ridge appears to generate the observed emission morphology[4]. From the relatively-increased brightness in dust emission and free-free radiation as compared to molecular gas density (in CO), indications are that this region experienced somewhat increased star formation activity in the recent past. Possibly individual nearby candidate sources contribute, although this could not (yet?) be proven. The Vela supernova remnant, now found to be located at 250 pc distance, cannot be detected individually, consistent with core-collapse nucleosynthesis predictions. Another supernova remnant found recently in X-ray emission (RXJ 0852-4622[1]) could be at similarly nearby distance, if the ^{44}Ti excess apparent in COMPTEL measurements is consolidated and can be assigned to this source. Its directional coincidence with the Vela Molecular Ridge peak emission does not allow a deconvolution from ^{26}Al imaging data alone[4]. The absence of any ^{26}Al signal from the nearby Wolf-Rayet star in the γ^2Velorum binary system is surprising, in view of current models of WR star nucleosynthesis yield[20] (see Figure 4). It is possible, that the binarity reduces the ejection of envelope material, or else that the recently-concluded proximity of the source is incorrect. Alternatively, the nucleosynthetic yield models for Wolf Rayet stars would have to be revised.

Summary

Astronomical measurements with gamma-ray lines from radioactivity have resulted in interesting constraints on nucleosynthesis, and offer the prospect of finding otherwise occulted massive-star regions or young supernova remnants. Among the prominent results are the gamma-ray lines from SN1987A, the ^{44}Ti measurement from Cas A, and the map of the Galaxy in recently-produced ^{26}Al . Absence of gamma-ray line signals is a significant surprise for SN1998bu Ni/Co decay lines, for ^{44}Ti from core-collapse supernovae expected to occur in the inner Galaxy, and from ^{26}Al emission from the nearby $\gamma^2 Velorum$ system.

Acknowledgements

It is a pleasure to thank my colleagues Hans Bloemen, Robert Georgii, Dieter Hartmann, Wim Hermsen, Anatoli Iyudin, Hans-Thomas Janka, Jürgen Knödlseder, Mark Leising, Georges Meynet, Uwe Oberlack, Stefan Plüschke, Nikos Prantzos, Volker Schönfelder, and Ulf Wes-

solowski, and the entire COMPTEL Team for helping to obtain the results and insights reported in this paper.

References

[1] Aschenbach B., (1998), Nat. **369**, 140

[2] Bloemen H., et al., (1999), Astroph. Letters and Communications **39**, 205-208

[3] Diehl, R., & Timmes F.X., (1998), PASP **110**, 748, 637

[4] Diehl R., et al., (1999) Astroph. Letters and Communications **38**, 357-362

[5] Dupraz, C., et al., (1997), A&A **324**, 683

[6] Ellison D.C., et al., (1999), ICRC 26, OG2.2.09

[7] Georgii R., et al., (2000), AIP **510**, ed. M.L. McConnell and J.M. Ryan, in press

[8] Iyudin, A. F., et al., (1994), A&A **284**, L1

[9] Iyudin, A. F., et al., (1997), in Proc. 2nd INTEGRAL Workshop, eds. C. Winkler, T. J. -L. Courvoisier, P. Durouchoux, ESA SP-382, 37

[10] Iyudin A.F., et al., (1998), Nat. **369**, 142

[11] Iyudin A.F., et al., (1998), Astroph. Letters and Communications, **38**, 383

[12] Knödlseder J., et al., (2000), A&A **344**, 68

[13] Knödlseder J., et al., (2000), A&A **345**, 813

[14] Knödlseder J., (2000), ApJ **510**, 915

[15] Leising M.D., et al., (2000), AIP **510**, ed. M.L. McConnell and J.M. Ryan, in press

[16] Lichti G., et al., (1994), A&A **292**, 569

[17] Meynet, G., et al., (1997), A&A **320**, 460

[18] Morris, D. J., et al., (1995), 17th Texas Symposium, N.Y. Acad. Sci., **759**, 397

[19] Morris, D. J., et al., (1997), AIP, **410**, eds. C. Dermer, J. Kurfess, & M. Strickman,p 1084

[20] Oberlack, U., et al, (2000), A&A **353**, 715

[21] Plüschke S., et al., (2000), AIP **510**, ed. M.L. McConnell & J.M. Ryan, in press

[22] Prantzos, N. & Diehl, R., (1996), Phys. Rep. **267**, 1

[23] Rothschild R.E., et al., (1997), AIP **410**, ed. C. Dermer, M. Strickman, & J. Kurfess, 1089

[24] Schönfelder V., et al., (2000), AIP **510**, ed. M.L. McConnell & J.M. Ryan, in press

[25] The, L.-S., et al, (1995), ApJ **444**, 244

[26] The L.-S., et al., (2000), AIP **510**, ed. M.L. McConnell & J.M. Ryan, in press

[27] Vink J., et al., (2000), Adv.Sp.Res. **25**, 689

Gamma–ray emission from Type Ia supernovae

J. Isern[1,2], *E. Bravo*[1,3], *J. Gómez–Gomar* [1], *D. García–Senz*[1,3]

[1] *Catalonia Space Studies Institute (IEEC/CSIC/UPC)*
[2] *Space Science Institute (CSIC)*
[3] *Department of Physics & Nuclear Engineering (UPC)*

Type Ia supernovae are considered good distance indicators because they are intrinsecally bright events and there is an empirical relationship between the absolute magnitude at maximum and the shape of the light curve that allows to estimate with enough accuracy the intrinsic brightness of the event. The reliability of the method depends on the assumption that this relationship is not afected by evolutionary effects. Since it is not possible to separate the cosmological effects from the evolutionary ones [1], it is necessay to acquire a deep understanding of the explosion mechanism in order to connect the observed properties of the light curve with the initial conditions of the exploding star. This is not an easy task since terrestrial experiments indicate that minute changes in the initial conditions can lead to changes in the burning mode which, in turn, introduces dramatic effects in the photometric properties of the light curve [2].

The physics of stellar (and also terrestrial) deflagrations is not well understood. Since conductive flames are too slow to account for the observations [3], the burning front must accelerate as a consequence of the existence of wrinkling instabilities like those of Landau and Rayleigh–Taylor ([4], [5], [6], [7]). However, recent studies indicate that these instabilities are not enough and additional instabilities have to be found to account for the observations [8]. Since full 3–D (or even 1–D) modelling is not possible for the moment due to the length scales involved (they go from the with of the flame, 10^{-5} cm, to the full size of the star, 10^{9} cm) and the intrinsically chaotic nature of the burning front, the must useful approach is to observe the most direct outcome of the process: the freshly synthesized radioactive ashes.

Recently, Gomez–Gomar et al (1998) [9] have simulated the γ–ray spectra emitted by SNIa with arbitrary composition, velocity and density profiles assuming a pure detonation (DET), a pure deflagration (DEF),a delayed detonation (DEL) or a Sub–Chandrasekhar detonation (SUB). If a SNIa explodes at a distance of $\sim$ 1 Mpc or less, a high quality γ-ray spectrum could be obtained with INTEGRAL and a detailed comparison between observation and theoretical models would be possible. However, if more realistic distances ($>$ 5 Mpc) are considered the effect of background on observations becomes important and only some outstanding features can be distinguished. These features are: the intensities and widths of the strongest γ-ray lines and the intensity of the low energy continuum. The table shows the distances at which these features could be measured by INTEGRAL instruments. Since the maximum distance at which the strongest feature can be determined is $\sim$ 15 Mpc, the probability to detect a SNIa by INTEGRAL is $\sim$ 1/8 yr^{-1}, which implies that any event occuring at a smaller distance has to be considered as a high priority target of oportunity.

Supernova explosions could depart somewhat from spherical symmetry, particularly in the case of sub-Chandrasekhar models where only a rather unphysical synchronous ignition of the complete He envelope would lead to a 1D explosion. In order to test the impact of three dimensional effects on the γ-ray emission of these models we have performed several simulations. They correspond to two sub-Chandrasekhar mass models SUB1P (single point ignition) and SUBMP (multiple point ignition) whose gross properties resemble those of model

Model	847 keV line inten.	Continuum inten.	847 keV line width
DEF	11.2	5	6
DEL	16.2	10	7
DET	15.2	11	7
SUB	13.2	8	5

SUB. The models were computed with a SPH code [10] and the γ-ray spectra and light curves of these models with a 3D Monte Carlo code developed by [11].

In both cases the γ-ray emission presents appreciable symmetry around the axis passing through the centre of the WD and the initial ignition point. In all cases the light curves display fluctuations due to the presence of inhomogeneities in the ejecta. Both, SUB1P and SUBMP show a clear relative maximum $\sim$ 10 days after the explosion. Later than 150 days differences between 1D and 3D models become negligible. Weak differences appear for line profiles observed from different visuals in SUBMP model. Conversely, in SUB1P peculiar profiles are observed from visuals close to Z axis which reveal asymmetric distribution of ^{56}Ni at the centre. Both models show during the first months noisy profiles due to the presence of inhomogeneities. The characteristic line wings displayed by 1D subchandrasekhar models become much weaker for SUB1P and SUBMP indicating a smaller size of the ^{56}Ni void region obtained in 3D computations [12].

It is clear that the scarcity of SNIa events demands the use of extremely sensitive gamma-ray detectors able to explore a large volume of space. A tunable crystal diffraction lens on a stabilized space craft able to focuse γ–rays could fullfil such requirements. For instance, the MAX mission consists of a 140 cm diameter lens with a total geometric area of 7600 cm^2 that can provide a sensitivity of $\sim 5 \times 10^{-7}$ ph s^{-1} cm^{-2}. This sensitivity could allow to obtain useful measurements of the 847 keV line up to distances of $\sim$ 75 Mpc which implies the detection of 3 to 5 SNIa per year, opening a window of performing γ-ray diagnostics of SNIa on a regular basis [13].

Acknowledgements

This work has been funded by the CIRIT and by the CICYT (ESP98-1348).

References

[1] P.S. Drell and T.J. Loredo and I. Wasserman, Astro-Ph/9905027 (1999).

[2] E.I. Sorokin and S.I. Blinnikov and O.S. Bartunov, Astro-Ph/9906494 (1999).

[3] F.X. Timmes and S.E. Woosley, ApJ **396** (1992) 649.

[4] S.I. Blinnikov and P.V. Sasorov and S.E. Woosley, Space Sci. Rev. **74** (1995) 299.

[5] J.C. Niemmeyer and W. Hillebrandt, ApJ **452** (1995) 769.

[6] S.I. Blinnikov and P.V. Sasorov, Phys. Rev. E **53** (1996) 4827.

[7] E. Muller and D. Arnett, ApJ **307** (1986) 619.

[8] J.C. Niemmeyer, Astro-Ph/9906142 (1999).

[9] J. Gomez-Gomar and J. Isern and P. Jean, MNRAS **295** (1998) 1.

[10] D. Garcia-Senz and E. Bravo and S.E. Woosley, Thermonuclear Supernovae, Ed P.Ruiz-Lapuente, R.Canal, J.Isern (1997) 389.

[11] J. Gomez-Gomar, Thesis (2000).

[12] J. Isern and E. Bravo and J. Gomez-Gomar and P. Jean, Astro. Lett. and Communications **38** (1999) 411.

[13] P. VonBallmoss et al, MAX Report (2000).

Limitations and possible Extensions of the first Post-Newtonian Approximation in the context of neutron star dynamics

R. Oechslin[1], *S.K. Rosswog*[2]

[1] *Departement für Physik und Astronomie, Universität Basel, Klingelbergstr. 82, CH-4056 Basel, Switzerland*
[2] *Center for parallel computing/applied informatics ZPR/ZAIK, Universität zu Köln, Weyertal 80, D-50931 Köln, Germany*

1.1 Introduction

Modelling dynamical processes involving neutron stars (NS) is a challenging task. On the one hand a large variety of microphysical processes has to be considered (nuclear equation of state (EoS), nuclear reactions, neutrino emission and transport, magnetic fields....) and on the other hand the highly relativistic, self-gravitating fluid has to be treated correctly. Since general relativistic (GR) calulations in 3D (for a review see [1] and references therein) still have limited sucess, a reasonable first step beyond Newtonian fluid dynamics is the so-called first Post-Newtonian (1PN) approximation (Chandrasekhar 1965, [2]), where the GR equations are expanded in terms of a parameter

$$\epsilon := \frac{U}{c^2} \approx \frac{v^2}{c^2} \tag{1}$$

and only first order terms are taken into account. Here U and v are typical values of the Newtonian potential and the velocity in the system under consideration.
However, for a typical NS with values of 10 km and 1.4 $M_\odot$ for radius and mass, the expansion parameter ϵ takes values of up to 0.4 in the center. This indicates that the expansion is converging very slowly and thus higher order terms might substantially influence the results.

1.2 A Modified 1PN-Approach

The aim of this work is to modify the standard 1PN approach of BDS in a way that results known from GR can closely be approximated, but without sacrificing the first order consistency in ϵ. We start out from the formulation of Blanchet, Damour and Schäfer (1990, [3]; hereafter BDS), which is very close to the Newtonian one and thus especially suited for the implementation in existing hydrodynamic codes.
The magnitude of the corrective terms is determined by three parameters α, β and δ which are functions of the 1PN gravitational potential, thermodynamic quantities and the momentum per unit rest mass (for details we refer to BDS). We modify α, β and δ in a way that energy, linear and angular momentum are conserved. This modification is to some extent arbitrary, but the results for the investigated case (see below) are closer to the solutions of GR than standard 1PN while still preserving the pseudo-Newtonian form of the equations.
The results discussed below are obtained using (with $c = 1$)

$$1 + \alpha = \frac{1 + w^2/2 + 3U_*}{1 + w^2/2 + U_*} \tag{2}$$

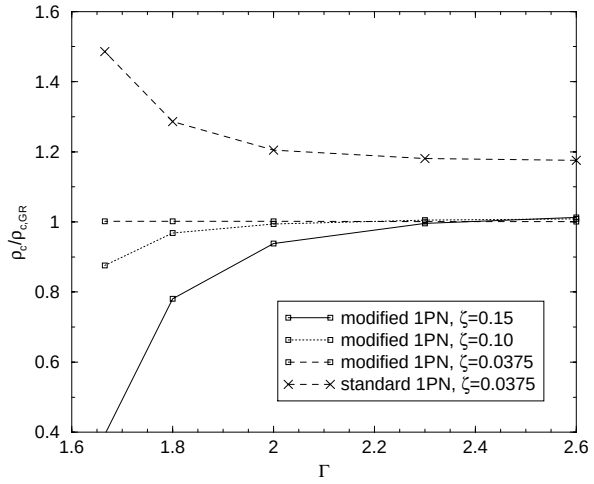

Figure 1: Ratio of 1PN central density to GR central density as a function of the adiabatic index Γ. The curves represent different compactness parameters $\zeta = GM/R$

$$\frac{1}{1+\beta} = 1 - \frac{e/\rho(1+\alpha)^2 + p/\rho}{(1+3U_* + w^2/2)^2} - \frac{3U_*}{1+3U_*} - \frac{w^2}{2} \tag{3}$$

$$\delta = \frac{e/\rho(1+\alpha)^2 + 3p/\rho}{(1+3U_* + w^2/2)^2} + \frac{3}{2}\frac{w^2}{(1+3U_*)^2} - \frac{U_*}{(1+3U_*)^{3/2}} \tag{4}$$

where U_* is the Newtonian potential obtained from the coordinate conserved density ρ_* (see BDS), w the momentum per unit rest mass and ρ is the usual physical density.

In addition the Newtonian pressure p and the internal energy e are used in the hydrodynamic equations rather than their Post-Newtonian counterparts p^* and e^*.
For details on the formalism, we refer to BDS.

1.3 Results

As a first test of the described approach we examine the structure of an isolated 1.4 $M_\odot$ NS governed by a polytropic EoS. In Fig. 1 the ratios of the central densities obtained once with the modified 1PN approach and once with the Oppenheimer-Volkoff-equation for different adiabatic exponents Γ and compactness parameters $\zeta = GM/R$ are shown and compared to the standard 1PN solutions. The modified 1PN approximation is poor for a very soft EoS, but for the stiffness expected from realistic NS EoS ($2 \leq \Gamma \leq 3$) the results are in agreement with the exact relativistic solutions to better about 5 %, for $\Gamma > 2.4$ solutions match to about 1% for all investigated compactness parameters. In contrast, the standard 1PN approximation overestimates the density by about 20% for $\zeta = 0.0375$ and a stiff EoS. For higher compactness parameters than $\zeta \approx 0.045$, no stable solution of the stellar structure equations can be found.

In Fig. 2 a sample profile for the case M=1.4 $M_\odot$, $\Gamma = 2.6, \zeta = 0.15$ is shown. To compare the different cases in a meaningful way, the radial coordinate has been rescaled by a metric factor $d^3r_{res} = (1 + 3U_*(r))d^3r$ in the modified PN and $d^3r_{res} = d^3r/(1 - 2m(r)/r)$ in the Oppenheimer-Volkoff case.

It has to be stated clearly that the described formalism is not based on first principles, but is rather oriented at the comparison with known general relativistic solutions. At the current

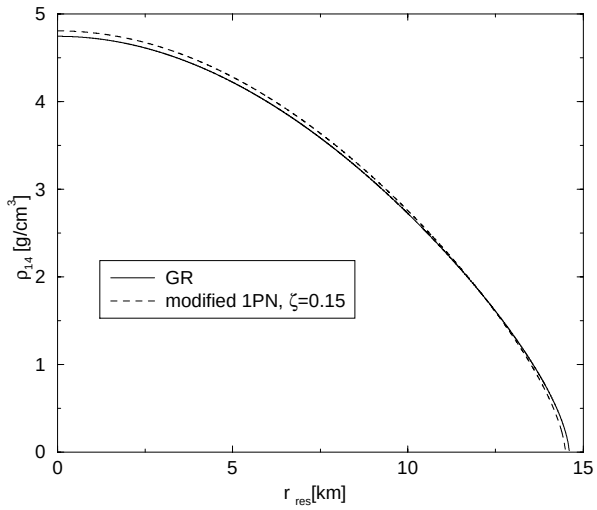

Figure 2: GR and modified 1PN profiles for a $\Gamma = 2.6, \zeta = 0.15$ star. ρ_{14} is the density measured in units of 10^{14} g/cm^3.

stage it is tested only for the static case described above. The general applicability remains to be explored in future work. To this end careful comparisons to other fully relativistic calculations, e.g. rotating relativistic stars as described by Cook et al. (1992, [4]), have to be performed.

References

[1] J. A. Font, gr-qc/0003101

[2] S. Chandrasekhar, ApJ, **142** (1965) 1488.

[3] L. Blanchet, D. Damour, G. Schäfer, MNRAS, **242** (1990) 289.

[4] G.B. Cook, S.L. Shapiro, S.A. Teukolsky, ApJ, **398** (1992) 203.

Simulations of binary neutron star and neutron star black hole merging

H.-Thomas Janka[1], *Maximilian Ruffert*[2]

[1] *Max-Planck-Institut für Astrophysik, Postfach 1317, 85741 Garching, Germany*
[2] *Department of Mathematics & Statistics, University of Edinburgh, Edinburgh, EH9 3JZ, Scotland, U.K.*

In the past years we have performed a large number of three-dimensional simulations of the merging of binary neutron stars and of neutron stars with companion black holes. We used a grid-based Eulerian hydrodynamics code, which is basically Newtonian, but includes the terms which describe the emission of gravitational waves and the corresponding back-reaction on the hydrodynamic flow according to the formalism of Blanchet et al. (1990). The use of a physical nuclear equation of state (Lattimer & Swesty 1991) allows us to calculate the energy and lepton number loss by neutrino emission with an elaborate trapping scheme.

The simulations yield information about gravitational-wave signals, neutrino emission, and dynamical processes during the merging, e.g., the ejection of neutron-rich matter which is speculated to provide the conditions for r-processing. Our models are post-processed for the annihilation of neutrinos and antineutrinos into electron-positron pairs in the surroundings of the merger remnant. This has implications for the discussion of the origin of cosmic gamma-ray bursts from such binary mergings.

Acknowledgements

HTJ was supported by DFG grant SFB 375 für Astro-Teilchenphysik, MR by a PPARC Advanced Fellowship.

References

[1] Blanchet L., Damour T., Schäfer G., 1990, MNRAS 242, 289

[2] Janka H.-Th., Ruffert M., 1996, A&A 307, L33

[3] Janka H.-Th., Eberl T., Ruffert M., Fryer C.L., 1999, ApJ 527, L39

[4] Lattimer J.M., Swesty F.D., 1991, Nucl. Phys. A535, 331

[5] Ruffert M., Janka H.-Th., 1998, A&A 338, 535

[6] Ruffert M., Janka H.-Th., 1999, A&A 344, 573

[7] Ruffert M., Janka H.-Th., Schäfer G., 1996, A&A, 311, 532

[8] Ruffert M., Janka H.-Th., Takahashi K., Schäfer G., 1997, A&A 319, 122

Tracing Cosmic Chemical Evolution

D. H. Hartmann[1], *T. M. Kneiske*[2], *K. Mannheim*[2], *K. Watanabe*[3]

[1] *Department of Physics and Astronomy, Clemson University, Clemson, SC 29634*
[2] *Universitäts-Sternwarte Göttingen, Geismarlandstrasse 11, Göttingen, D 37083*
[3] *USRA/LHEA, NASA, Goddard Space Flight Center, Greenbelt, MD 20771*

The chemical enrichment history of the Milky Way is determined by the yields of various sources of nucleosynthesis (AGB/WR stars, novae/supernovae, cosmic rays, etc.) and the star formation rate (SFR), whose present-day value is $\sim 3-6$ $M_\odot$/yr (e.g., [1] and references therein). This SFR produces a supernova rate of a few events per century. The SFR was larger in the past, but not by much more than a factor two to three, and the disk began forming stars about 10 ± 2 Grys ago (inferred from the white dwarf luminosity function, e.g., [13][25]). Well developed models of Galactic chemical evolution [14] describe the increasing metal content of the ISM and the evolving abundance pattern recorded in stars. But how can one apply the concepts of chemical evolution to the universe as a whole, and what kind of tracers should be used to constrain the models?

The task of building a cosmic chemical evolution (CCE) model would be straigthforward if we could use the Galaxy as a template, and relate time to redshift through a cosmological model. Unfortunately, the SFR history of the Galaxy is not representative of the cosmic star formation rate [4][18], because the cosmic rate was larger by more than a factor ten at a redshift of order unity (when the universe was about 40% its present age). Still, we can estimate the present rate density by using the Galaxy as a standard and multiplying with an effective local galaxy number density ($\sim 10^{-2}$ Mpc^{-3}). This gives a rate density of a few 10^{-2} $M_\odot$ year^{-1} Mpc^{-3}, which is indeed close to (although somewhat higher than) the value obtained from H_α emission surveys of local galaxies [6]. The evolution of this rate with lookback time (or redshift) is dramatic. From [OII] emission line surveys and studies of the UV continuum luminosity density Madau et al. [11] [12] demonstrated a rapid increase (factor ten for $z = 0 \rightarrow 1$) of the cosmic SFR density. Flores et al. [5] provide a recent update on this crucial function. The rate at redshifts past one is not yet reliably determined, but the rapid rise (or decline from the point of view of the evolving universe) has been confirmed with many studies. Here we draw attention to two complementary tracers of the cosmic SFR and thus the driver of CCE; the optical/IR background light produced by the stars with a fraction that is reprocessed by dust in the ISM, and the gamma-ray background produced by the decay of radioactive ^{56}Ni in supernovae. Figure 1 shows the evolution of the opt/IR background, and Figure 2 shows the MeV background due to photons from the decay chain $^{56}\mathrm{Ni} \rightarrow {}^{56}\mathrm{Co} \rightarrow {}^{56}\mathrm{Fe}$ escaping the expanding ejecta from (predominantly) Type Ia supernovae [19][20] [22]. The MeV background observations were carried out with SMM [22] and COMPTEL [7][23]. That these distinct backgrounds can be explained with the same cosmic star formation history suggests that we will be able to develop reliable models of "cosmic chemical evolution". Future supernova surveys, from the ground and space with the NGST, will directly probe the rate density of SNIa and even SNII to large redshifts. This information will provide a powerful consistency check on the two background light tracers emphasized here.

In a simple CCE model one ignores detailed evolutionary histories of galaxies due to mergers and applies a global ensemble average. Consider a comoving box, large enough to ensure a meaningful ensemble average. The mass fraction of baryonic matter locked in galaxies

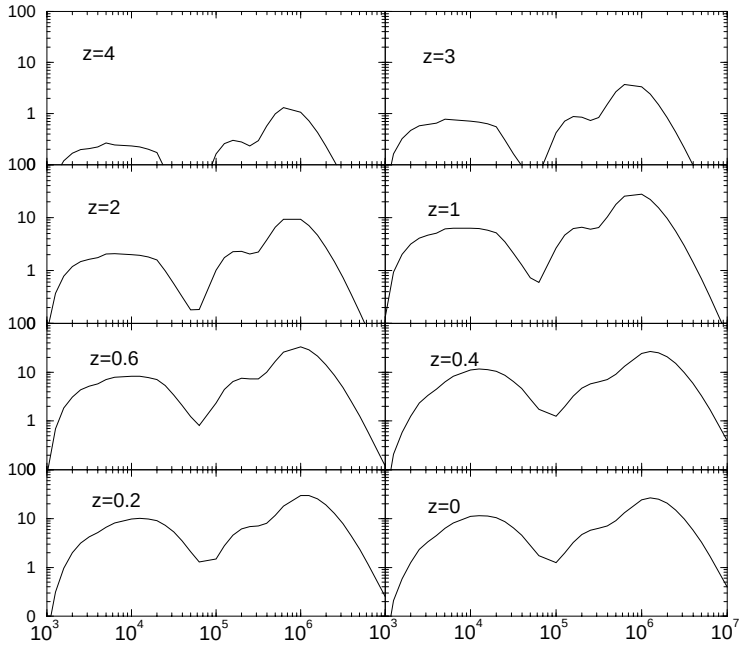

Figure 1: Cosmic chemical evolution is driven by the global star formation rate. The light produced by these stars adds to the present-day optical/IR background. Shown is the power spectrum (nW m^{-2} sr^{-1}) as a function of wavelength (A). The redshift-sequence demonstrates how the diffuse flux builds in time.

is $\Omega = \Omega_g(\mathrm{gas}) + \Omega_s(\mathrm{stars})$, and the mass fraction of "metals" in the galactic gas is $\Omega_m = \mathrm{Z}\ \Omega_g$, where Z is the mean metallicity of the gas. In the CCE formalism developed by Lanzetta *et al.* [10] and Pei & Fall [15] the comoving rate equations are

$$\dot{\Omega}_g + \dot{\Omega}_s = \dot{\Omega}_f \tag{1}$$

$$\Omega_g \dot{\mathrm{Z}} - \mathrm{Y}\dot{\Omega}_s = (\mathrm{Z}_f - \mathrm{Z})\dot{\Omega}_f \tag{2}$$

where the subscript f denotes infall or outflow, i.e. the exchange of matter between galaxies and the IGM. The parameter Y is an "effective" yield (see [16]) of heavy elements, which depends on assumtions about the universality of the IMF. The solution of these equations is straightforward if one uses as input the observed cosmic SFR, $\dot{\Omega}_s(z)$, and the gas mass fraction $\Omega_g(z)$ [16]. The latter quantity can be obtained from observations of damped Lyα systems (DLAs), which are absorbing clouds in front of distant quasars that are charaterized by HI column densities in excess of 2×10^{20} cm^{-2} (e.g., [9][21][24]. About 150 DLAs are currently known, and they are considered the primary tracer of neutral hydrogen throughout the universe. DLAs account for more than $\sim 80\%$ of the total neutral hydrogen content [9], but the total mass budget is dominated by diffuse, highly ionized gas. The distribution of DLAs with redshift thus provides a direct measure of $\Omega_g(\mathrm{z})$. The second function that can be obtained directly from observations is the SFR(z), i.e., $\dot{\Omega}_s$ in the above equations. Pei et al. [16] also include dust, which is important for questions related to hidden star formation at large redshifts and the reprocessing of star light.

The CCE equations can be integrated with the initial conditions $\Omega_g = \Omega_s = \Omega_m = 0$. In other words, galaxies grew from primordial gas through the infall terms in eqs. (1) and (2). To constrain the solution one uses the star formation history to construct spectral population

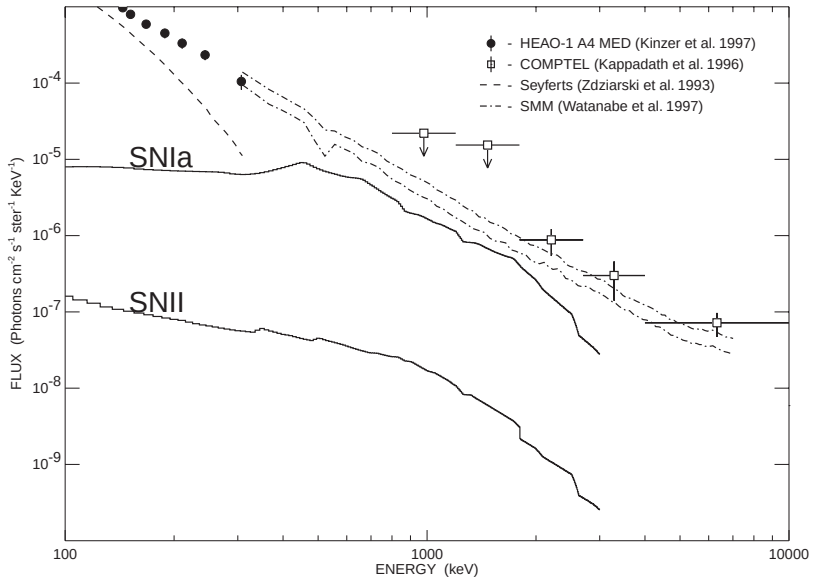

Figure 2: The gamma-ray background in the MeV regime observed with SMM and COMPTEL can be explained as cumulative gamma-ray emission from Type Ia supernovae.

synthesis models (see [8][16] for details) to determine the specific emissivity as a function of redshift. Some of the light emitted by stars is absorbed by dust and transformed to IR emission by means of a multi-component dust model. The combined optical/IR emissivity is then integrated in time and redshifted according to the adopted cosmological model, and then compared to the present-day background. The evolution of this background is shown in Figure 1. In addition, a given star formation rate produces a supernova rate according to the IMF, and a selection of the mass limit above which stars generate core collapse supernovae ($8-10\ M_\odot$). For Type Ia supernovae one must also include a possibly large delay (~ 1 Gyr) between star formation and the supernova event. This causes the Ia/II ratio to increase towards small redshifts, which has a large effect on the gamma-ray background. As discussed in [19] and [22], the large ^{56}Ni yield of SNIa and their much smaller envelope masses more than compensates for their lower rate, making SNIa the dominant source of background photons in the MeV regime (Fig. 2). Again, the background light provides a constraint on $\dot{\Omega}_s$, and thus CCE.

In addition to the background constraints the evolution of the gas metallicity can be probed directly with DLA systems. Metal absorption lines in DLAs provide abundances for a variety of heavy elements (Ar, N, O, P, S, Zn,...). Because of its small correction for depletion onto dust the most often used tracer of metallicity is Zn. The average [Zn/H] ratio as a function of redshift exhibits only a modest increase (factor 2−3) between z = 3 and z $\sim$ 1 [17] (there are too few DLAs at lower redshifts). This cosmic age-metallicity relation (AMR) can be compared against the Z(z) solution of the CCE equations. Pei, Fall, &Hauser [16] show that a satifactory match can be accomplished for an effective yield of $Y = 0.45\ Z_\odot$. The DLA data together with the optical/IR and the gamma-ray background in the MeV range thus support the notion of a consistent model of cosmic chemical evolution, at least in an average sense. Detailed simulations of the evolution of galaxies inside merging dark matter halos (e.g.,

[2][3] and references therein) have now reached a level of sophistication that allows one to go beyond averaged quantities discussed here, and begin to investigate inhomogeneous CCE. We are getting close to the answer to the question of where and when the heavy elements formed.

Acknowledgement:

It is a pleasure to thank the organizers and the staff at Ringberg castl e for a very stimulating meeting and for providing outstanding hospitality.

References

[1] Boissier, S., & Prantzos, N. 1999, MNRAS 307, 857

[2] Cen, R., & Ostriker, J. P. 1999, ApJ 514, 1

[3] Cen, R., & Ostriker, J. P. 1999, ApJ 519, L109

[4] Fields, B. 1999, ApJ 515, 603

[5] Flores, H., et al. 1999, ApJ 517, 148

[6] Gallego, J., et al. 1995, ApJ 455, 1

[7] Kappadath, S. C., et al. 1996, A&AS 120, 619

[8] Kneiske, T., Mannheim, K., & Hartmann, D. H. 2000, in preparation

[9] Lanzetta, K. M. et al. 1991, ApJ Suppl. 77, 1

[10] Lanzetta, K. M. et al. 1995, ApJ 440, 435

[11] Madau, P., et al. 1996, MNRAS 283, 1388

[12] Madau, P., Pozzetti, L, & Dickinson, M. 1998, ApJ 498, 106

[13] Oswalt, T. D., Smith, J. A., Wood, M. A., & Hintzen, P. 1995, Nature 382, 692

[14] Pagel, B. E. J. 1997, *Nucleosynthesis and Chemical Evolution of Galaxies*, (CUP)

[15] Pei, Y. C. & Fall, S. M. 1995, ApJ 454, 69

[16] Pei, Y. C., Fall, S. M., & Hauser M. G. 1999, ApJ 522, 604

[17] Pettini, M., *et al.* 1999, ApJ 510, 576

[18] Prantzos, N., & Silk, J. 1998, ApJ 507, 229

[19] Ruiz-Lapuente, P., Casse, M., & Vangioni-Flam, E. 2000, ApJ, in press

[20] The, L.-S., Leising, M. D., & Clayton, D. D. 1993, ApJ 403, 32

[21] Turnshek, D. A., *et al.* 1989, ApJ 344, 567

[22] Watanabe, K., Leising, M., Hartmann, D. H., & The, L.-S. 1999, ApJ 516, 285

[23] Weidenspointner, G. 1999, Ph.D. Thesis, Technische Universität München

[24] Wolfe, A. M., *et al.* 1995, ApJ 454, 698

[25] Wood, M. A., & Oswalt, T. D. 1989. ApJ 497, 870